Master's thesis

NTNU
Norwegian University of Science and Technology
Faculty of Natural Sciences
Department of Biotechnology and Food Science

Celine Oanæs

Functional Impact of the Ubiquitin Proteasomal System in Neurodevelopment and Neuroprotection

Master's thesis in Biotechnology
Supervisor: Mirta Mittelstedt Leal de Sousa
Co-supervisor: Wei Wang and Magnar Bjørås
May 2021

NTNU
Norwegian University of
Science and Technology

Celine Oanæs

Functional Impact of the Ubiquitin Proteasomal System in Neurodevelopment and Neuroprotection

Master's thesis in Biotechnology
Supervisor: Mirta Mittelstedt Leal de Sousa
Co-supervisor: Wei Wang and Magnar Bjørås
May 2021

Norwegian University of Science and Technology
Faculty of Natural Sciences
Department of Biotechnology and Food Science

NTNU
Norwegian University of
Science and Technology

Acknowledgements

This master thesis was performed at the Department of Clinical and Molecular Medicine (IKOM) for the completion of a degree in Master of Science within biotechnology at the Norwegian University of Science and Technology (NTNU).

The last one and a half year has been a journey full of learning, growing and development both on a personal and professional level. For that, I would like to start thanking Prof. Magnar Bjørås for accepting me into his group as one of his students, thereby giving me the opportunity to be part of a prominent research group at NTNU. Further, I would like to thank my supervisor, Dr. Mirta Mittelstedt Leal de Sousa, for giving me endlessly support and guidance throughout this year. Thank you for sharing all your incredible proteomics knowledge with me. It has been educational, and together with your positive attitude and great humor it has been an honor having you as my supervisor. Dr. Wei Wang, my co-supervisor, has also provided me with excellent expertise and guidance within stem cell technology, that has been highly appreciated. He constantly challenged me and encouraged me to think critically, giving me a steep learning curve from the beginning. Thank you to my internal supervisor Prof. Per Bruheim for helpful advice.

Also, I would like to give a huge thanks to senior engineer Animesh Sharma for helping me in processing my MS findings in a more suitable manner and senior engineer Nina-Beate Liabakk for her assistance with flow cytometry. Lastly, I would like to express my gratitude to the fellow students Erlend, Vanessa, Vilde and Jørn at the lab for being helpful and supportive. And a special thanks to my lab partner Ingvild, for her patience and insightful perspectives, leading to a good collaboration. In the very end I would like to thank all the other researchers and associates for giving me advice and keeping me in good company, and my friends and family for motivating and supporting me through this year.

Trondheim, 31st of May, 2021

Celine Oanæs

Index

List of figures

List of Tables

Abstract

Ubiquitin is a small molecule that regulates a plethora of vital molecular processes in our cells via binding to protein targets. It can be removed from substrates by ubiquitinases. Among a 100 ubiqutinases identified in humans, there is the Ubiquitin C-terminal Hydrolase L1 (UCHL1) enzyme. Although UCHL1 is highly abundant in the brain, its precise functions remain unknown. In 2016, Rydning *et al*. (1) described a Norwegian monozygotic twin pair with UCHL1 mutations suffering from severe motor function impairment. In this study, we aim at investigating the impact of UCHL1 dysfunction in neurodevelopment and neuroprotection via alterations on the major protein degradation system regulated by ubiquitin, namely, the Ubiquitin Proteasomal System (UPS). By using induced pluripotent stem cells (iPSC) reprogramed from cells derived from the described UCHL1- patients, we aimed at generating monolayer neuronal cells: Neural Progenitor Cells (NPC) and Mature Forebrain Neurons (FB); as well as brain organoids as human models to recapitulate neurodevelopment and pathological features related to UCHL1 dysfunction. Our data shows that iPSC and NPCs were successful generated, as well as brain organoids from healthy controls. Challenges in culturing NPCs hindered further differentiation to FB. Several attempts including different protocols and clones were performed without success. Nevertheless, viability assays were performed with NPCs using proteasome inhibitors. Based on the response of control NPCs, suitable doses as well as appropriated incubation time points were determined for further investigations of responses of control and patient-derived NPC upon proteasome inhibition. Moreover, proteasome 20S activity assays revealed no differences in basal level proteasomal activities between control and patient-derived cells in iPSC. Due to interfering signals in culture media, proteasomal activities in NPC were not determined. Alternative culturing conditions were identified to overcome this issue. Furthermore, quantitative mass spectrometry analysis was employed for the comparison of global protein expression profiles of healthy control- and patient-derived cells at two distinct developmental stages: iPSC and NPC. Notably, a 2-fold increase in the large amino transporter 2 (LAT2) was detected in patient iPSC. LAT2 has shown to be involved in retinal phototransduction and enhanced cognition. In UCHL1-patient NPCs, the proteomics data revealed downregulation of UCHL1, also reported in UCHL1-patient's fibroblasts; Calcineurin B homologous protein 1 (CHP1), which is associated with ataxia; and the neuronal marker Doublecortin (DcX). Up-regulation of Neurofilament medium polypeptide (NFM), a suggested marker of neurodegenerative diseases was also detected in UCHL1-deficient NPCs. It would be quite valuable to investigate the protein profiles of mature neurons and verify whether the levels of the mentioned proteins would be further altered, along with identification of novel protein targets associated with the clinical features of the disease. We cannot rule out that the UCHL1 mutations may be a major contributor for the lack of success in growing patient-derived brain organoid. However, development of more robust and reliable protocols for the generation of organoids, as well as NPCs, are necessary for further investigation of potential alterations in UPS associated to UCHL1 dysfunction in mature neurons and 3D brain models. Moreover, protocols that is based on direct differentiation of iPSCs to neurons could also serve as an alternative approach to obtain mature neurons.

Sammendrag

Ubiquitin er et lite molekyl som regulerer en mengde vitale molekylære prosesser i cellene våre ved å binde seg til diverse målproteiner. Ubiquitinaser kan fjerne dette molekylet fra substrat. Blant 100 ubiquitinaser som er identifisert i mennesket, finnes UCHL1. Selv om dette proteinet er svært rikelig i hjernen, er dets nøyaktige funksjon ikke kjent. I 2016, beskrev Rydning et al (1) et norsk enegget tvillingpar med UCHL1-mutasjoner med alvorlig nedsatt motorisk funksjon. I denne studien vil vi undersøke effekten av UCHL1-dysfunksjon i nevrologisk utvikling og beskyttelse via endringer i det viktigste nedbrytningssystemet for proteiner, UPS. Ved å benytte iPS celler reprogrammert fra somatiske celler fra de nevnte UCHL1-pasientene, er målet å generere et monolag av NPC og FB; så vel som hjerneorganoider som menneskelige modeller for å rekapitulere nevrologisk utvikling og patologiske trekk knyttet til UCHL1-dysfunksjon. Generering av iPS celler og NPCer viste seg å være vellykket, samt generering av hjerneorganoider fra de friske kontrollcellene. Utfordringer med NPC-kultivering hindret videre differensiering til FB. Flere forsøk ble gjort, inkludert utprøvelse av ulike protokoller og kloner, uten å lykkes. Det ble uansett utført levedyktighetsanalyser på NPC i respons mot proteasom-hemmere. Basert på responsen fra kontroll-cellene, ble det bestemt passende doser og inkubasjonstidspunkt for videre analyser av kontroll og pasient-celler i respons mot proteasom-hemming. Videre avslørte enzym-aktivitetsanalyser at det ikke var noen forskjell i proteasom 20S aktivitet mellom pasient og kontroll iPS celler. På grunn av forstyrrende signal i kultiveringsmediumet til NPC ble ikke proteasomaktivitet i NPC bestemt. For å sammenligne den globale proteinprofilen av UCHL1-pasientceller med friske kontrollceller ble det utført en kvantitativ masse-spektrometrisk analyse på iPS celler og NPCer. Merkbart hadde LAT2 en to ganger økning i pasient iPS cellene. Dette proteinet har vist seg å være involvert i netthinnens fototransduksjon og er assosiert med forbedret kognitive evner. I pasient-NPC avslørte den proteomiske analysen en nedregulering av UCHL1 proteinet sammenlignet med de friske kontroll NPCene, noe som også er rapportert i pasientens fibroblaster. CHP1, assosiert med ataksi, og nervecelle-markøren DcX var også nedregulert i pasient-derivert NPC. NFM var oppregulert i pasient-NPCene, som er en utpekt markør for nevrodegenerative sykdommer. Det vil være verdifullt å undersøke proteinprofilene til modne nevroner og å verifisere om nivået av de nevnte proteinene endres ytterligere, og samtidig identifisere nye proteiner assosiert med de kliniske egenskapene til UCHL1-pasientene. Det kan ikke utelukkes at UCHL1-mutasjonene har bidratt til manglende suksess ved generering av hjerneorganoider på pasient-cellene, men utvikling av mer robuste og pålitelige protokoller for generering av organoider og differensiering til NPCer er nødvendig for videre investigering av potensielle endringer i UPS, assosiert med UCHL1-dysfunksjon i modne nevroner og hjernemodeller. Samtidig kan protokoller med direkte differensiering fra iPS celler til nevroner stille som et alternativ.

Abbreviations

7-AAD	7-Aminoactinomycin D
AD	Alzheimer's disease
ARCA	Autosomal recessive cerebellar ataxia
BH	Benjamini-Hochberg
BSA	Bovine serum albumin
c-Myc	Myc proto-oncogene protein
Chr	Chromosome
CNS	Central nervous system
CT	Chamber Temperature
Ct	Cycle threshold
D-PBS	Dulbecco´s phosphate-buffered saline
DcX	Doublecortin
DE	Differentially-expressed
DM-/+A	Differentiation Medium without/with Vitamin A
DMEM	Dulbecco's Modified Eagle Medium: Nutrient Mixture
DUB	Deubiquitinating enzyme
E1	Ubiquitin-activating enzyme
E2	Ubiquitin-conjugating enzymes
E3	Ubiquitin ligases
EB	Embryoid body
EDTA	Ethylenediaminetetraacetic acid
Em	Emission
ESC	Embryoid stem cell
Ex	Excitation
FB	Forebrain neurons
FDR	False discovery rate
FOXG1	Forkhead Box G1
GABA	Gamma-aminobutyric acid
HD	Huntington´s disease
hiPSC	Human induced pluripotent stem cell
i	Inhibition
IAM	Iodoacetamide
ICC	Immunocytochemistry
IHC	Immunohistochemistry
Klf4	Krüppel-like factor 4
LC	Liquid chromatography
LFQ	Label-free quantification
m/z	Mass-to-charge
MEF	Mouse embryoid fibroblast
MS	Mass spectrometry
MSI1	Musashi-1
MSN	Medium spiny neuron
NDM	Neural Differentiation Medium
NEM	Neural Progenitor Medium
NIM	Neural Induction Medium
NO	Nitric oxide
NPC	Neural progenitor cell
NSC	Neural stem cell
OCT	Optimal cutting temperature
Oct4	Octamer-binding transcription factor
OT	Object Temperature
Pax6	Paired box protein 6
PCV	Packed cell volume
PD	Parkinson's disease
PLO	Poly-L-ornithine
qPCR	Quantitative polymerase chain reaction
RG	Radial glia's
ROCK	Rho-associated protein kinase
RT	Reverse transcriptase
Sox	SRY-box
SRY	Sex determining region Y
SSEA4	Stage-specific embryonic antigen-4
TCEP	Tris-(2-carboxyethyl) phosphine
Tuj1	Beta-III tubulin
Ub	Ubiquitin
UCHL1	Ubiquitin C-terminal hydrolase L1
UPS	Ubiquitin Proteasome System
VZ	Ventricular zone
w/w	Weight-to-weight
Y27632	ROCK inhibitor

1 Introduction

1.1 The Interplay Between Ubiquitin, the Ubiquitin Proteasome System and Ubiquitin C-terminal Hydrolase L1

This introduction summarizes the link between the Ubiquitin Proteasome System (UPS) and Ubiquitin C-terminal hydrolase L1 (UCHL1), as well as the current status on stem cell technology and mass spectrometry-based protein quantification.

1.1.1 Ubiquitin

Ubiquitin (Ub) is a highly conserved, small eukaryotic protein that induces posttranslational modification of target substrates through a process known as ubiquitination. Ubiquitination involves three main steps: activation, conjugation, and ligation, performed by Ub-activating enzymes (E1s), Ub-conjugating enzymes (E2s), and Ub ligases (E3s) (2), as illustrated in figure 1. In general, the modification results in either mono- or poly-ubiquitination of target substrates. While monoubiquitination has been shown to regulate receptor endocytosis and histone modification, polyubiquitination plays diverse functions that are dependent on the type of Ub chain linkages, including degradation of the substrate by the UPS, DNA repair, and activation of signal transduction pathways (3).

1.1.2 The Ubiquitin-Proteasome System

The UPS is the major intracellular proteolytic system responsible for maintaining rapid protein turnover in the cytosol and nuclei of cells, including the selective removal of abnormal and misfolded proteins (3-5). A properly functioning UPS is essential for many cellular processes, such as cell repair, signal transduction, stress response (6) and cell survival (7). The protein degradation occurs in a two-step process involving ubiquitination and the degradation of tagged proteins by the downstream 26S proteasome complex (figure 1.1). The 26S proteasome contains one 20S core particle and two 19S regulatory cap subunits. The core is hollow and provides an enclosed cavity in which proteins are degraded. Openings at the two ends of the core allow the target protein to enter. Each end of the core particle associates with a 19S regulatory subunit that contains multiple ATPase active sites and ubiquitin binding sites that recognizes polyubiquitinated proteins and transfers them to the catalytic core. Alteration of the UPS has been linked to many human diseases including cancers, cardiovascular diseases and neurodegenerative diseases (3-5).

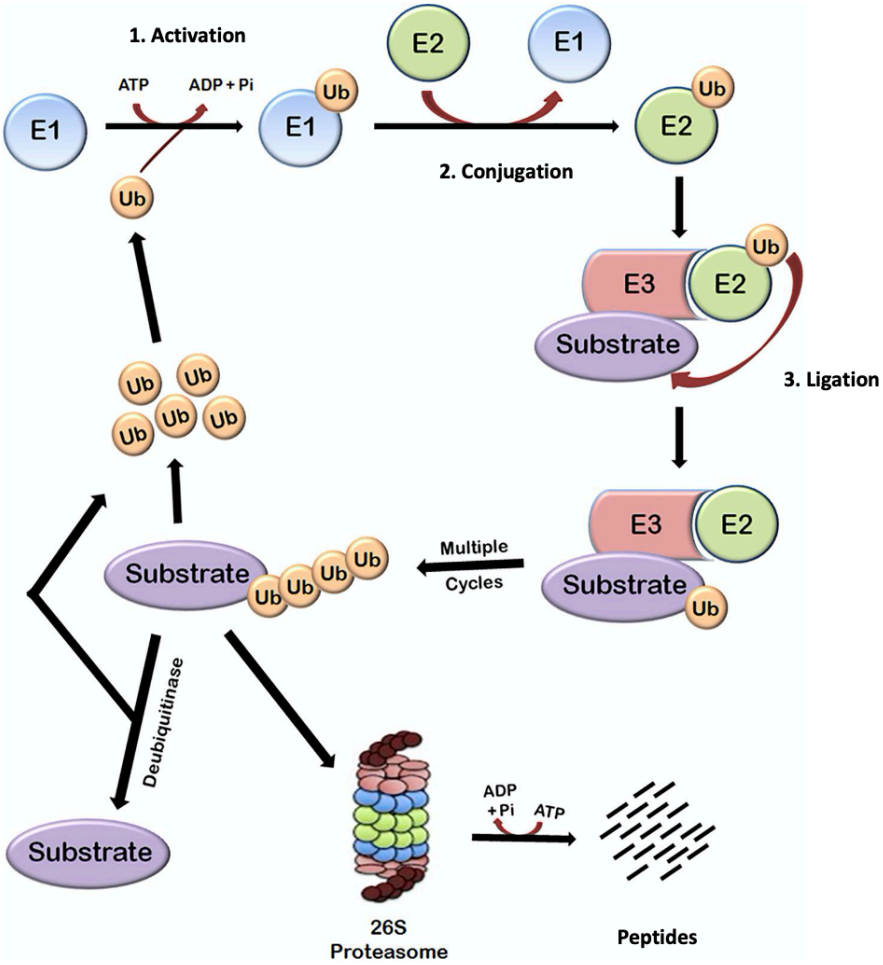

Figure 1.1. A simplified overview of protein ubiquitination and degradation via the ubiquitin-proteasome system (UPS). *First, through an ATP-dependent process, Ub becomes activated by an Ub-activating enzyme (E1). Secondly, the Ub is transferred to the Ub-conjugating enzyme (E2). Finally, the Ub forms a bond with a lysine residue on a specific target substrate, which is already bound by the Ub ligase (E3). The Ub itself carries lysine residues that can bind to another Ub molecules, resulting in polyubiquitin chains. The polyubiquitinated substrate will then be recognized by the 26S Proteasome and degraded. Deubiquitinates can reverse this process by removing ubiquitin groups from the substrate. The Ub molecules can then be re-used in a new ubiquitination process (8). Figure is modified from Lata et. al (9).*

1.1.3 Ubiquitin C-terminal Hydrolase L1

Structure & function

Ubiquitin can be removed from its substrates or trimmed from ubiquitin chains by deubiquitinating enzymes (DUBs). The human genome encodes approximately 100 deubiquitinates. Among them, there is the UCHL1 enzyme, which belongs to the Ub C-terminal hydrolases (UCHs) sub-family of DUBs (10, 11). In contrast to other UCHs, UCHL1 has a very short loop that prevents proteins to access its active site, only permitting access to short peptides fused to ubiquitin (11).

UCHL1 is a globular protein with a knot (figure 1.2), representing the most complicated structure of eukaryotic proteins. The knotted backbone is thought to protect the UCH proteins from proteasomal unfolding, degradation (10, 11) and protein aggregation. UCHL1 unfolding exposes the hydrophobic core of the protein, which can lead to unintended interactions with other proteins (11). Notably, UCHL1 is one of the most abundant proteins in brain comprising up to 2% of total neuronal protein (10, 11). It is also found to be highly expressed in many cancerous cells (11). Despite its high levels on neurons, the precise roles of this protein remain largely unknown (10, 11).

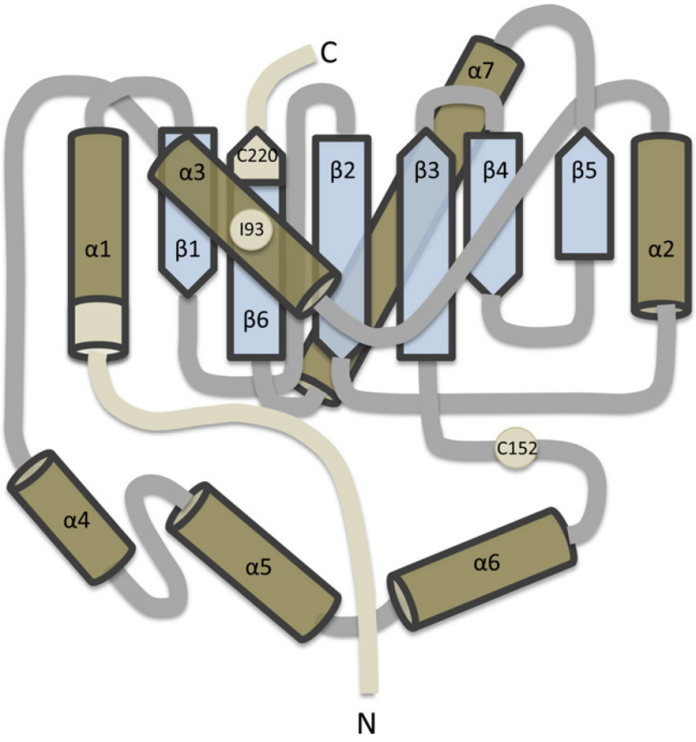

Figure 1.2. The UCHL1 structure illustrating its α-helical and β-strand structure. *Residues 1-11 at the N-terminus, 220-223 at the C-terminus, Ile93 and Cys152 are highlighted, as modifications on these areas can potentially disturb the hydrophobic core of β-strands, which is otherwise protected.*

UCHL1 has hydrolase activities in the UPS, and *in vitro* studies have also shown ubiquitin ligase activity for UCHL1 (12), linking ubiquitin molecules together to tag proteins for degradation (6). Recent studies have suggested that UCHL1 plays a role in cellular homeostasis by stabilizing ubiquitin monomers or as a neuronal antioxidant, reacting with and chelating free radicals during acute damage, thereby protecting cells from extensive damage. Notably, UCHL1 knockout mice displayed a phenotype of paralysis and death after seven months, suggesting that UCHL1 is not critical for development, but rather for the maintenance of axonal integrity (11).

Ubiquitin C-terminal Hydrolase L1 and human Disease

The importance of UCHL1 becomes evident by its impact in neurodegenerative disorders (13). Its dysfunction has been associated with Parkinson's disease (PD) and Alzheimer's disease (AD) and recent reports show that UCHL1 is directly implicated with severe clinical features, including early-onset neurodegeneration with optic atrophy, spasticity paraplegia and ataxia (1, 14, 15). In 2017, Rydning *et al*. described a Norwegian monozygotic twin pair and their sister suffering from recessive loss of UCHL1 function with mentioned clinical features. The twins are heterozygous for UCHL1 with the Arg178Gln and Ala216Asp variants. By studying biochemical characteristics of recombinant proteins, Rydning *et al*. showed that the Arg178Gln mutant protein had a 4-fold increase in hydrolytic activity compared to the wild type protein, while the Ala216Asp was insoluble. Based on structural analysis, the Arg178 residue is thought to restrict the catalytic activity rate of UCHL1, and this restriction is likely abolished by the Arg178Gln mutation. Considering the monozygotic twins have an IQ and memory functions above average, Rydning *et al*. proposed that the Arg178Gln variation may have a protective cognitive function. Moreover, the Ala216 is found in the hydrophobic core of the protein, and the Ala216Asp mutation destabilizes the protein causing protein aggregation.

Elucidation of UCHL1 functions is of utmost importance for the development of clinically useful therapies for patients harboring mutations on the UCHL1 gene, and for patients suffering from common neurodegenerative diseases associated with abnormal ubiquitin processing, such as AD and PD, which may also be connected with UCHL1 dysfunction (1, 13).

1.2 Stem Cell Technology

Patients harboring the newly identified UCHL1 mutations (R178Q and A216D) suffer from severe motor function impairment (1). Thus, in this study, we expected to investigate the impact of UCHL1 dysfunction and UPS alterations in cells associated with motor functions. To understand disease progression, three different stages of neuronal development were selected: induced pluripotent stem cells (iPSC), neural progenitor cells (NPCs) and forebrain neurons (FB). Accordingly, iPSCs previously reprogrammed from fibroblasts obtained from skin biopsies of UCHL1-patients and healthy controls were used as the starting point for the generation of NPCs, which would then be further differentiated into FB. In addition to

monolayer cells, brain organoids were also generated from iPSC as models to recapitulate disease progression and study key aspects of brain morphology and development. Due to the importance of these 2D and 3D models for this project, a brief introduction on stem cell technology, including the generation of iPSC, NPC, FB and brain organoids will be provided in this section.

1.2.1 Human Induced Pluripotent Stem Cells

Embryoid stem cells (ESCs) are derived from a mammalian blastocyst and have the ability to proliferate indefinitely. ESCs are pluripotent, i.e., they are capable of generating any cell type from the three germ layers: ectoderm, mesoderm and endoderm (16). This property makes them a valuable tool in regenerative medicine (17). However, it raises ethical issues concerning the use of human embryos. Therefore, there was an urgent need for the development of alternative strategies that did not include destructing human embryos. A way to circumvent this issue was to generate pluripotent stem cells from a patient's own somatic cells (16).

Late in the 90's, Wilmut *et al*. succeeded in reprogramming somatic cells to an embryoid stem cell (ESC)-like state by transferring their nuclei into an enucleated oocyte (18). In 2001, Tada *et al*. reprogrammed somatic cells into a pluripotent state through the hybridization of an adult thymocyte and an ESC (19). This implied that oocytes and ESCs contain specific factors that make somatic cells totipotent or pluripotent. In 2006, Takahashi and Yamanaka hypothesized that the same factors playing important roles in maintaining ESC identity also had a role in induction of pluripotency. Thus, Takahashi and Yamanaka identified 24 candidate genes for pluripotency in somatic cells and introduced them in different combinations and numbers in mouse embryoid fibroblasts (MEF) by retroviral transduction. Among the candidate genes, octamer-binding transcription factor (Oct)3/4, SRY (sex determining region Y)-box 2 (Sox2), Krüppel-like factor 4 (Klf4) and Myc proto-oncogene protein (c-Myc) (16), later collectively denoted as the OSKM factors (20), were shown to be essential for the generation of MEF iPSCs (16). The OSKM factors are master transcription regulators (20), involved in regulation of cell metabolism (21), gene expression and epigenetics (22). A major breakthrough in the stem cell technology field occurred in 2007, when Takahashi *et al*. successfully reprogrammed human fibroblasts to human iPSCs (hiPSCs) through the expression of the OSKM factors (23).

Conversion of differentiated cells to iPSC is slow and inefficient process, where only a few cells that receive the OSKM factors succeed. It takes about 10 days until the OSKM factors induce the expression of iPSC markers, which indicates that the successful conversion of

differentiated cells into iPSC requires a long cascade of changes. This cascade starts with c-Myc-induced cell proliferation and chromatin structure loosening to promote binding of the other three master transcription regulators to hundreds of different binding sites on the DNA. Oct4, Sox2 and Klf4 create a positive feedback loop to regulate themselves and also activate or repress genes encoding proteins involved in chromatin modifications and genes encoding noncoding RNAs (20).

The iPSCs can be characterized through evaluation of its morphology and presence of specific marker genes (table 1.1). iPSCs without any sign of differentiation are supposed be an ESC-like colony, which is described as a colony with distinct borders and well-defined edges, consisting of cells with a large nucleus and less cytoplasm (figure 1.4a) (24). The OSKM factors Oct4 and Sox2 are usually used to characterize iPSCs, as they are associated with pluripotency (16). Nanog is a transcription factor associated with self-renewal in ES cells, and therefore, can also be used for iPSC characterization (25). Furthermore, Stage-specific embryonic antigen-4 (SSEA4), an ES cell glycolipid epitope, is also considered an iPSCs marker (26).

Table 1.1. Some of the markers for pluripotency and self-renewal that can be used to characterize iPSCs.

Marker	**Type**	**Gene ID**
Nanog	TF	79923
Oct4	TF	18999
Sox2	TF	20674
SSEA4	Cell surface protein	330401

iPSCs are able to differentiate to the three germ layers, and this can be confirmed by immunocytochemistry (ICC) using specific endoderm, mesoderm and ectoderm markers (table 1.2). Brachyury is a transcription factor required for mesoderm formation and differentiation (27). The transcription factor Sox17 is associated with the formation and maintenance of the endoderm layer (28). Nestin is an intermediate filament protein expressed in undifferentiated central nervous system (CNS) cells (29). Paired box protein 6 (Pax6) is a transcription factor expressed in embryonic neurogenesis of the brain and CNS and is essential for the CNS development (30). Thus, both Nestin and Pax6 are associated with the ectoderm layer.

Table 1.2. Markers for trilineage differentiation of iPSCs.

Trilineage Layer	Marker	Type	Gene ID
Endoderm	Brachyury	TF	6862
Mesoderm	Sox17	TF	64321
Ectoderm	Nestin	Intermediate filament protein	10763
	Pax6	TF	5080

* *TF=Transcription Factor*

The revolutionary iPSC reprogramming technology led to an enhanced focus on the development of hiPSC-based clinical applications and novel strategies to exploit its full potential. iPSCs are now used to investigate pathological processes and for drug screening through the generation of a large homogeneous population of specialized cells of any preferred type. Multiple studies have been conducted isolating somatic cells, such as skin fibroblasts from patients, and reprogramming them to iPSCs. The iPSCs are further differentiated into the cell type where malfunction of the disease is observed. The cell type of interest is compared to the same cell type from healthy patients, and irregularities between the two can reveal pathological aspects of the disease on a molecular level. These findings provide the basis for the design and test of drugs that can potentially correct the misbehavior of the affected cells (20, 31). This process is summarized in figure 1.3.

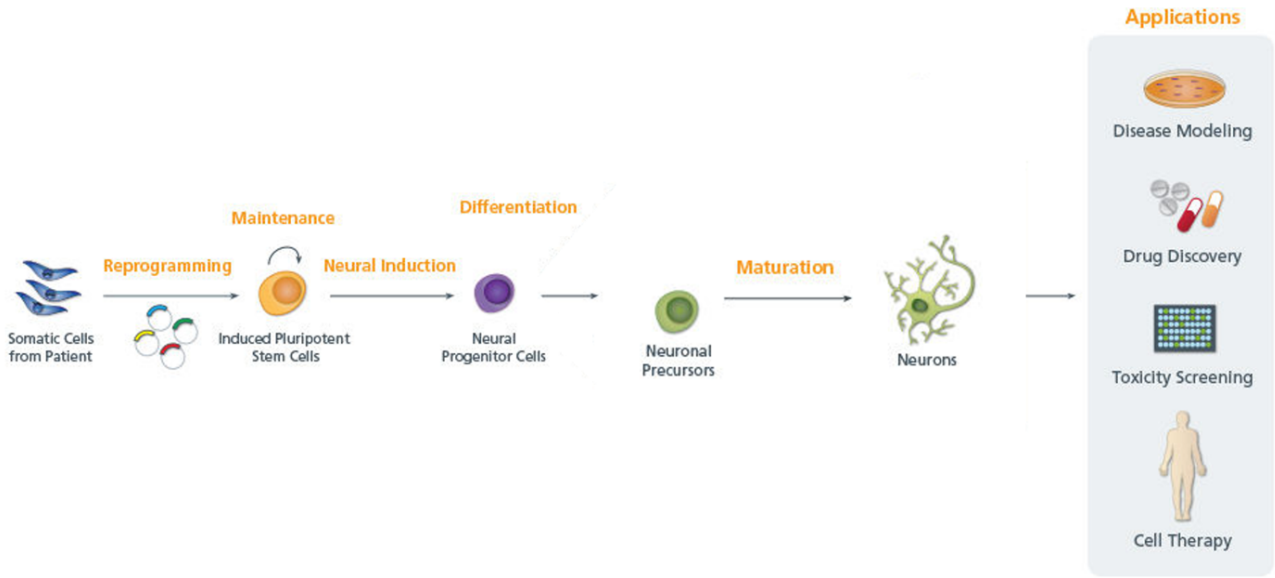

Figure 1.3. Pipeline from patient-specific cells to the discovery of treatment and molecular insights of a disease. *By isolating somatic cells from a patient with a disease, it is possible to reprogram the cells into iPSCs and further differentiate them to specialized cell types of interest, such as NPCs and neurons, relevant for this particular study. Through disease-modelling, toxicity, and drug screening, it is possible to uncover molecular mechanisms of the disease and identify promising treatments. Figure is modified from Stemcell Technologies (32).*

1.2.2 Differentiation of Induced Pluripotent Stem Cells to Neural Progenitor Cells

Since iPSCs are pluripotent, they are able to generate any type of cell, including neural progenitor cells (NPC). NPCs are multipotent (33), meaning they are capable of proliferating and differentiating into more than one cell type (34). They function as precursors for several cell types of the CNS, such as neurons and astrocytes (35).

These cells can be used for a plethora of applications including investigation of diseases such as AD and PD. Obtaining diseased cells directly from a patient, especially brain cells, comes with great difficulties. Thus, neurons derived from patient-specific iPSCs with NPCs as intermediate progenitors is beneficial (36). The first step in generating NPCs from iPSCs is neural induction. A number of activators and inhibitors of cell signaling pathways must act in order to form neural epithelial cell-like neural stem cells (NSCs), and further NPCs, which correspond to the embryonic development (37). This process needs to be solid and efficient to generate NPCs of high quality for downstream applications (35).

Two main approaches can be used for neural induction to generate NPCs. The first approach allows formation of embryoid bodies (EB) with morphology shown in figure 1.4B, which generates neural rosettes when exposed to neural induction conditions. These neural rosettes contain NPCs and are recognized with a characteristic morphological structure (figure 1.4C). They are thought to represent the neural tube, which in mammalian embryogenesis, folds from the neural plate that arises from the neuroectoderm layer. The neural rosettes are isolated and will build a monolayer of NPCs (34). By using this approach, the process from iPSCs to NPCs usually requires 16 to 19 days. Alternatively, NPCs can be generated in only six days according to a methodology described by Stem Cell Technologies (38). In this approach, iPSCs are plated on a defined matrix exposed to inductive factors in a monolayer culture system. The matrix can consist of poly-L-ornithine, laminin, or fibronectin to allow attachment of an adherent monolayer (figure 1.4D), that becomes confluent in 5-10 days. When NPCs are confluent, they are passaged and replated under the same initial conditions. NPCs can be differentiated to neurons using both approaches, by using a low-serum medium and mitogen removal (34).

Characterization of NPCs and neurons derived from iPSCs is usually performed by functional studies or assessing the morphology and expression of specific markers (tables 1.2 and 1.3). Nestin, Pax6, Sox1 and Musashi-1 (MSI1) are protein markers, known to be highly expressed in NPCs (39). Sox1 is a transcription factor involved in the maintenance of the NPC status, therefore, highly expressed in this stage. In contrast, Sox1 is downregulated in neurons (40). Another protein thought to be associated with proliferation and maintenance of NPCs is

the RNA-binding protein, MSI1 (41). The microtubule-associated phosphoprotein, doublecortin (DcX), is expressed in newly born neurons as well as in mature neurons (42). Furthermore, the Beta-III tubulin (Tuj1), a subunit of microtubules, is also highly expressed in neurons (43).

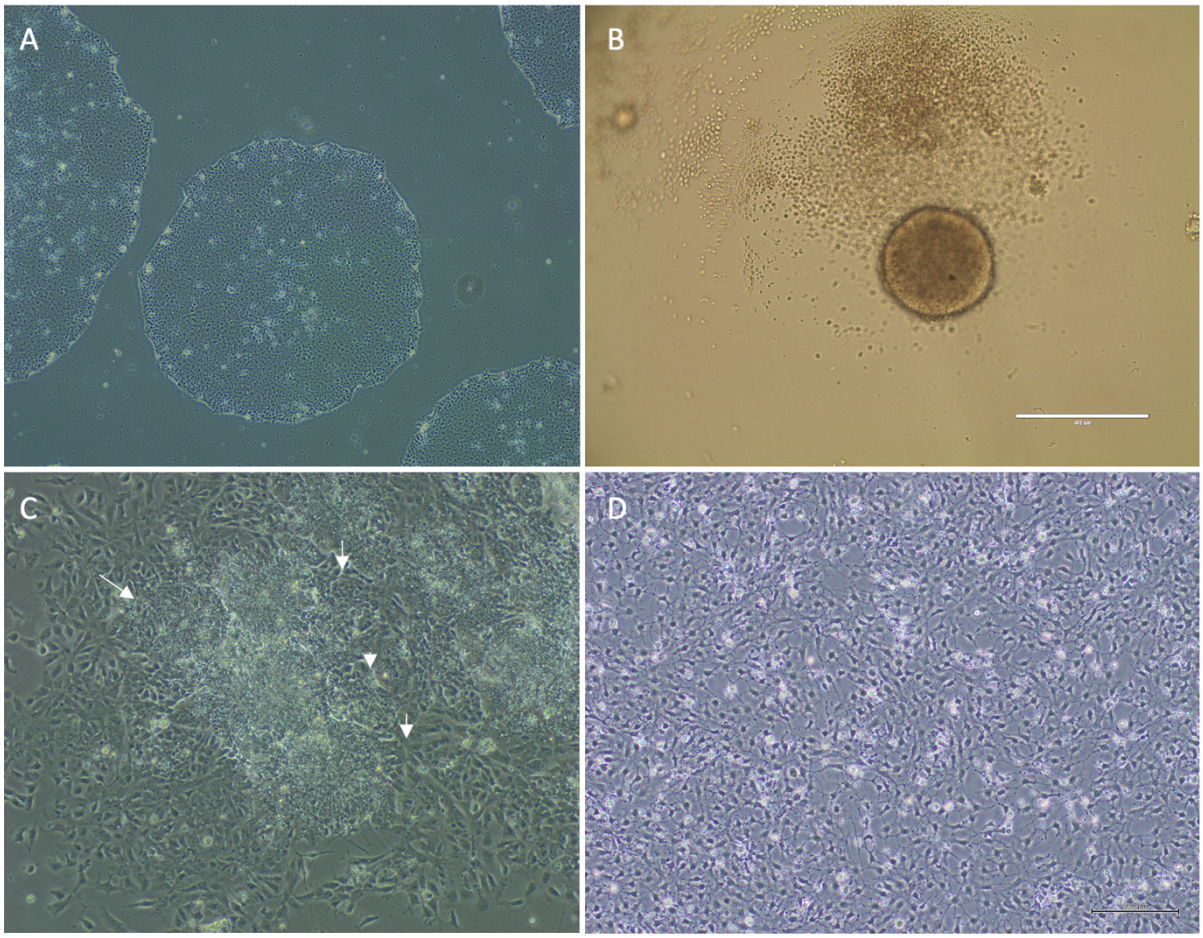

Figure 1.4. Morphology of cells from iPSCs through the differentiation to NPCs. *(**A**) Human induced pluripotent stem cells (hiPSCs) with clear edges. (**B**) Aggregated hiPSCs forming an embryoid body (EB). (**C**) Rosette-like structure (arrows). (**D**) Neural progenitor cells (NPCs).*

1.2.3 Differentiation of Induced Pluripotent Stem Cells to Forebrain Neurons

The forebrain region is an important part of the CNS. Dysfunctional forebrain neurons are associated with several neurological disorders, such as Huntington´s disease (HD) (44) and AD (45). Thus, it is relevant to generate forebrain neurons for investigating molecular mechanisms underlying the UCHL1-patients. The three main types of neurons in the forebrain are the cortical excitatory glutamatergic neurons, inhibitory striatal medium spiny neurons (MSNs) and gamma-aminobutyric acid (GABA) interneurons. In this study we aim at generating a combination of excitatory and inhibitory forebrain neurons. The goal is to generate the neurons from iPSCs through an intermediate stage with NPCs (46).

Characterization of forebrain neurons can be done by assessing its morphology and staining for forebrain-specific neuronal markers (table 1.3). The forebrain neurons morphology exhibits clear polarized axons and dendrites, as seen in figure 1.5 (47). The neurons can be characterized by positive staining of the Forkhead box G1 (FOXG1) (48), a TF involved in brain development, specifically in maintenance and survival of mature neurons in specific regions of the forebrain (49).

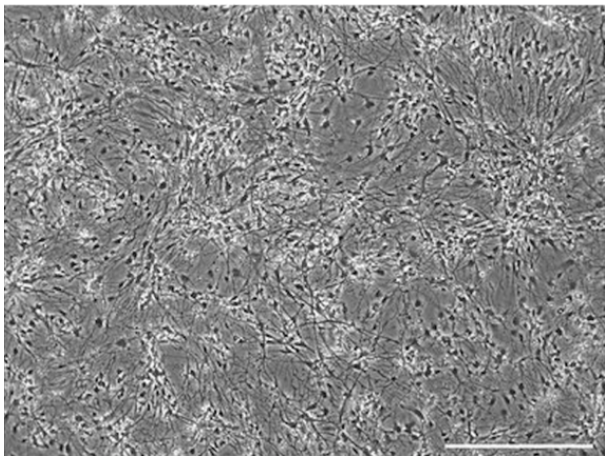

***Figure 1.5**. Morphology of forebrain neurons derived from NPCs at day 15. Scale bar = 130 µm. Figure modified from Bell et al (47).*

Table 1.3. Markers for progenitor- and differentiated cells of the CNS.

Marker	Location	Type	Gene ID
DcX	Neuron	Microtubule-associated protein	1641
FOXG1	Forebrain neuron	TF	
MSI1	NPC	RNA-binding protein	4440
Sox1	NPC	TF	6656
Tuj1	Neuron	B-III-tubulin ab	10381

1.2.4 Generation of Cerebral Organoids from Induced Pluripotent Stem Cells

Animal models have been used to study diseases for over a century, with mice as the predominant mammalian model. Mice and humans have shown to have similar genes and development, thus, mutations in mice often mimic the effects of the corresponding mutation in humans (20). Even though mice and humans share many genetic features (20), there are dramatic differences between these species (50). The human brain development is unique due to its high complexity, exhibiting large expansion of neuronal output. In fact, a number of human biological processes are absent or only partially represented in animals. Therefore, it is

challenging to study animal models to better understand the human brain. In addition, extrapolation of data from animal models to humans has become a major concern in the drug discovery field, as animals have limited value as simulators of human development, metabolism, drug efficacy and toxicity (51, 52). Thus, a humanized *in vitro* approach is highly needed for the study of human brain development and disease (53).

iPSCs can differentiate to specific cell types by exposure to defined signal proteins and growth factors in a timing that represents a normal developmental pathway (20). By careful manipulation of culture conditions, iPSCs connect with each other to construct entire organs on a small scale, called organoids (20). This field is rapidly expanding and provides more precise *in vitro* models for *in vivo* events (53). The recent advances within 3D organoid technology show great promise in translational and personalized medicine, through the discovery of diagnostic biomarkers for early disease and drug screening for potential therapies (54).

Presently, protocols to construct organoids for multiple different human organ systems have been established (53). In 2014, Lancaster *et al*. described a protocol for generating cerebral organoids from hiPSCs (53) based on methods describing the generation of neural identity and differentiation and 3D tissue-organization. *In vivo*, brain structures are developed from expanded neuroepithelia derived from the neural ectoderm layer. Thus, to generate cerebral organoids from iPSCs, it is essential to induce the development of ectoderm germ layer cells, from which neural tissue is generated *in vivo*. To achieve this, the first step is to generate embryoid bodies (EBs) through aggregation of iPSCs, enabling the formation of the three germ layers. Further, the EBs are directed to ectoderm formation and promoted to induce primitive neuroepithelia, resembling the neural tissue development *in vivo*. The neural tissue is embedded in a hydrogel with extracellular matrix proteins, and neuroepithelial buds with fluid-filled cavities protrude from the EBs, representing the brain ventricles. After 2-3 weeks, the neural tissue has expanded to become a cerebral organoid and expanding neuroepithelium can be identified through the detection of Sox2 or Pax6 expression. This type of tissue is usually observed next to the ventricle-like cavities. After a month, neuronal differentiation can be observed via Tuj1 or DcX expression. When the cerebral organoid has been growing for 2 months, different brain regions, such as the forebrain and hippocampus, can be identified using specific regional markers. The ventricular zone (VZ) (53), a pseudostratified epithelium layer, consists of multipotent neural stem cells (55), which can be identified by Sox2 expression (53).

In principle, it is possible to generate any type of organoid from EBs. After embedding EBs in Matrigel to ensure correct structural orientation, EBs can be cultured in medium containing specific grow factors, to mimic the developmental steps that lead to the organ of

interest, illustrated in figure 1.6. During this process, generated organoids are kept in suspension to allow evenly distributed endoderm, ectoderm or mesoderm formation along the surface, and to promote further development (53).

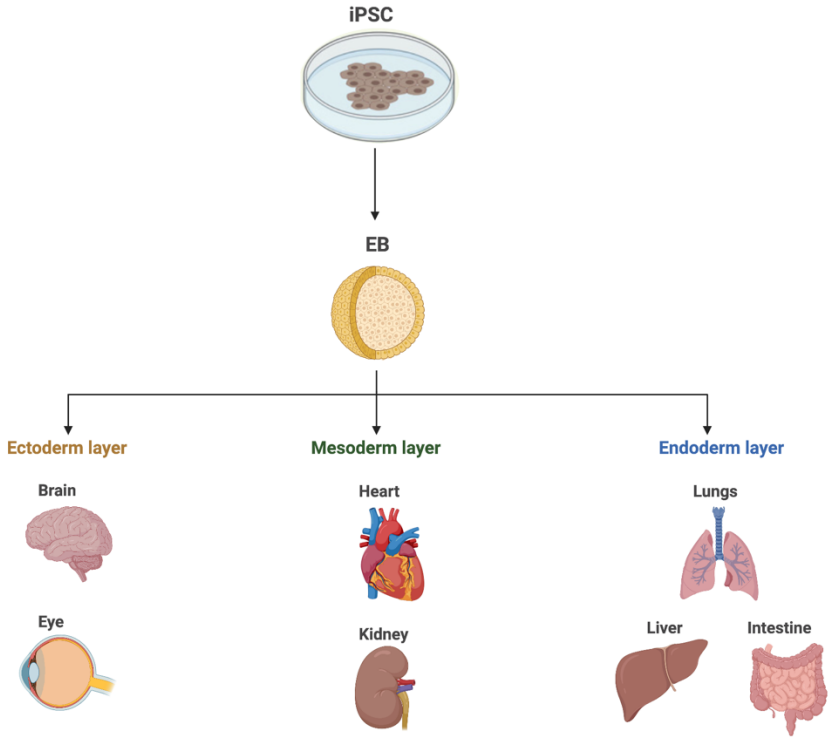

Figure 1.6. *Schematic diagram illustrating the differentiation potential of EBs generated from iPSCs. The EBs can be stimulated to go into any of the three germ layers to generate organoids of associated lineage. Figure created using BioRender (https://biorender.com/).*

1.3 Quantitative Protein Profiling by Mass Spectrometry

Proteins are the key players in a plethora of cellular processes. They exert major roles in fundamental processes such as gene expression, cell proliferation, trafficking of molecules, degradation of proteins and cellular organelles, response against toxic agents, regulation of cell metabolism and homeostasis, among many others. Importantly, protein malfunction is frequently associated with disease. Therefore, it is critically important to understand how biological processes are regulated at protein level. Unraveling the molecular mechanisms underlying diseases is paramount for the development of novel strategies for disease prevention, diagnosis and therapies (56).

Since the late of 1990s, mass spectrometry (MS) emerged as a powerful tool for the identification, characterization and quantification of macromolecules, especially proteins. The rapid advances in instrumentation and methodologies have enabled in-depth proteome analysis leading to identification and accurate quantification of thousands of proteins isolated from

complex mixtures, such as cells or tissues. The mainstream MS-based technology employed to compare alterations in protein levels between different samples is named shotgun proteomics. In this strategy, proteins isolated from complex mixtures are digested by a site-specific enzyme, such as trypsin. The resulting peptides are separated by liquid chromatography (LC) and analyzed by a high-throughput tandem mass spectrometer. The information on mass-to-charge (m/z) ratios of the peptides and their fragments is then used for identification through searches against databases of protein sequences (57) (figure 1.7).

There are many strategies to compare relative levels of different proteins across samples. Labeling proteins or peptides by the use of isotopes is a common approach in quantitative shotgun proteomics and offer a universal quantitative reference within samples (58). It is based on labeling individual samples differently, and then combining the samples into one mixture that are prepared together before analyzing it by a single MS run (59). However, this strategy is usually cost-prohibited and offers limited tag versions which only allows a small number of different samples to be combined (58). In this study, another commonly used approach for proteome wide-quantification that does not involve the use of labels was adopted: label-free quantification (LFQ). LFQ is based on preparing individual samples separately and subjecting them to individual MS runs prior to data analysis (60). This strategy allows a large number of replicates to be analyzed and provides a simplified sample preparation process as the labeling step is unrequired, but then, a more careful optimization and evaluation of the data analysis is needed (58).

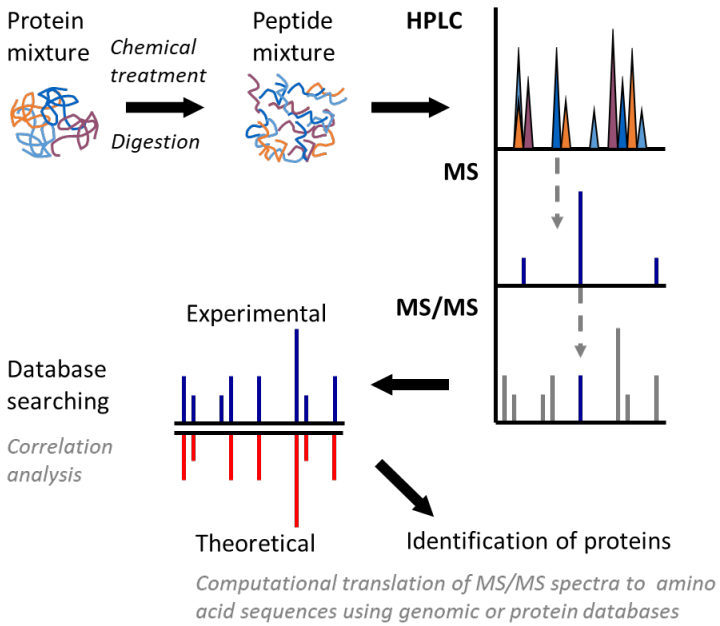

Figure 1.7. *Workflow of protein identification by mass-spectrometry. Figure taken from Edith Cowan University (61).*

MS-based proteomics has become an essential tool for elucidating biological processes at protein level. Over the past decade, the application of MS-based proteomic technologies has led to many exciting discoveries, particularly in the biomedical field where it has been employed to characterize disease-related proteomes and interactomes, as well as the identification of biomarkers and targets for clinical diagnosis and treatment of disease (56). Recently, the combination of proteomics and iPSCs has revolutionized the field of biological sciences, leading to the identification of key regulatory factors implicated in maintenance of the pluripotent state and the differentiation process to the diverse cell types and organoids (62).

1.4 Aim

This project is based on the hypothesis that UCHL1 alteration leads to dysregulation of the UPS in the brain and consequently neurodegeneration. Thus, the major aim is to investigate the functional roles of UCHL1 in neurodevelopment and neuroprotection. To meet this goal, this research project was divided into four parts:

1. Generation and characterization of iPSCs, NPCs, forebrain neurons (FB) and cerebral organoids from healthy controls and patients harboring mutations in the UCHL1 gene.

2. Investigating the response of NPCs and FB to drugs that modulate the UPS.

3. Determining global alterations in protein expression profiles at different stages of neural differentiation by shotgun mass spectrometry.

4. Identifying alterations in levels of ubiquitinated proteins and proteins associated with the ubiquitin proteasome system.

2 Materials and Methods

This study is based on experiments performed on cells derived from a monozygotic twin pair carrying UCHL1 mutations (1) referred as patient B an T, and cells derived from two healthy individuals used as controls. Prior to this project, healthy control- and patient-derived fibroblasts were reprogrammed to iPSCs using CytoTune®-iPS 2.0 Sendai Reprogramming Kit (Thermo Fisher Scientific) containing the four well-described OSKM reprogramming factors: Oct3/4, Sox2, Klf4 and L-Myc, carried out by Dr. Wei Wang. The clones used for experiments in this study is listed in table 2.1. All mediums used for cell culture are listed in Appendix 1.

The experimental procedures were conducted in accordance with the Health Research Act (2008, no. 44).

Table 2.1. The iPSC clones cultured for experiments in this study and their origin.

Sample type (origin)	**Clones**
Control 1	AGc1, AGc6
Control 2	ATc2
Patient B	Bc4, Bc6, Bc9
Patient T	Tc3, Tc9, Tc18

2.1 Human Induced Pluripotent Stem Cell Culture

All live cells were cultured in an incubator with 37 °C and 5% CO_2. The iPSCs were cultured in a 6-well plate (SARSTEDT) with Essential 8 (E8) medium and old medium was replaced every day to provide nutrients and growth factors. The cells were passaged after four to seven days, when reaching 70-80% confluence. Experiments on the iPSCs were not performed before they reached passage 10, to ensure that the exogenous genes from the iPSC reprogramming were silenced. Furthermore, iPSC clones were not cultured to more than passage 60 to avoid genetic and epigenetic instability (53). As iPSCs are more sensitive compared to other cell lines used in laboratories, extra care was taken when handling the cells to minimize cell death, maintain stem cell properties and prevent unintended differentiation. Areas showing any sign of differentiation prior to passage were removed manually by scraping with a pipette tip. All handling of live cells was done in sterile conditions in a hood.

2.1.1 Preparing Culture Plates with Extracellular Matrix

The plates used for iPSC culture were prepared with an extracellular matrix coating prior to adding the cells, to achieve proper attachment and maintenance. Geltrex (Thermo Fisher Scientific) stocks stored in -20 ºC were thawed on ice for 1-2 hours. The stock was diluted 1:100 in Dulbecco's Modified Eagle Medium: Nutrient Mixture F-12 (DMEM/F12) (Thermo Fisher Scientific) with 1% Penicillin Streptomycin (Thermo Fisher Scientific) to prevent contamination. The volume used for coating the different plates is listed in table 2.2. After adding the Geltrex, the plates were incubated for 1-2 hours at 37 ºC. Subsequently, the plates were used immediately or stored at 4 ºC for maximum one week. One hour before use, coated plates were kept in room temperature. The extracellular matrix was aspirated immediately before adding the cells.

Table 2.2. Volumes used for coating the different plates (SARSTEDT) and for culturing the cells according to the surface area of the wells.

Cultureware	**Approximate surface area (cm^2)**	**Volume/well (µl) for coating**	**Volume/well (µl) for culturing**
6-well plate	8.87	1000	2000
12-well plate	3.65	500	1000
24-well plate	1.82	500	1000
48-well plate	0.64	150	300
96-well plate	0.29	60	150

2.1.2 Passage of Induced Pluripotent Stem Cells

iPSCs at 70-80% confluence were passaged by washing once with 1-2 ml Dulbecco´s phosphate-buffered saline (without Ca^{2+} and Mg^{2+}) (D-PBS) (Thermo Fisher Scientific) and then adding 1 ml of 0.5 mM ethylenediaminetetraacetic acid (EDTA) (Thermo Fisher Scientific) to dissociate the cells. After incubating at room temperature for approximately 3-4 minutes, 4.5 ml of E8 medium was added in the wells with force to separate the colonies into smaller pieces. The cells from each well were distributed equally to three new wells, therefore, diluted in a 1:3 ratio. The newly passaged cells were incubated at 37 ºC and the plate was moved with small, rapid movements back and forth, side-to-side, to evenly distribute the colonies in the wells. After 24 hours, cells were washed once with 1-2 ml D-PBS and 1.5 ml of E8 medium was added. The medium was changed every day with fresh E8 medium.

2.1.3 Storing Pellet of Induced Pluripotent Stem Cells

iPSCs were stored as pellets to use in further experiments, such as karyotyping, qPCR and mass spectrometry analysis. When cells were confluent and ready to be passaged, they were washed once with D-PBS and detached from the bottom using a cell scraper. Further, cells were transferred to Eppendorf tubes and centrifuged for 3.5 minutes at 8.000 rpm. The supernatant was aspirated, and the pellets were stored in -80 °C. The pellets were thawed on ice before use in further experiments.

2.2 Trilineage Differentiation

To confirm that the iPSCs are in fact pluripotent, a trilineage differentiation was performed on two control clones (AGc1, ATc2) and four patient clones (Bc4, Bc6, Tc3, Tc18). An overview of the experiment is shown in figure 2.1.

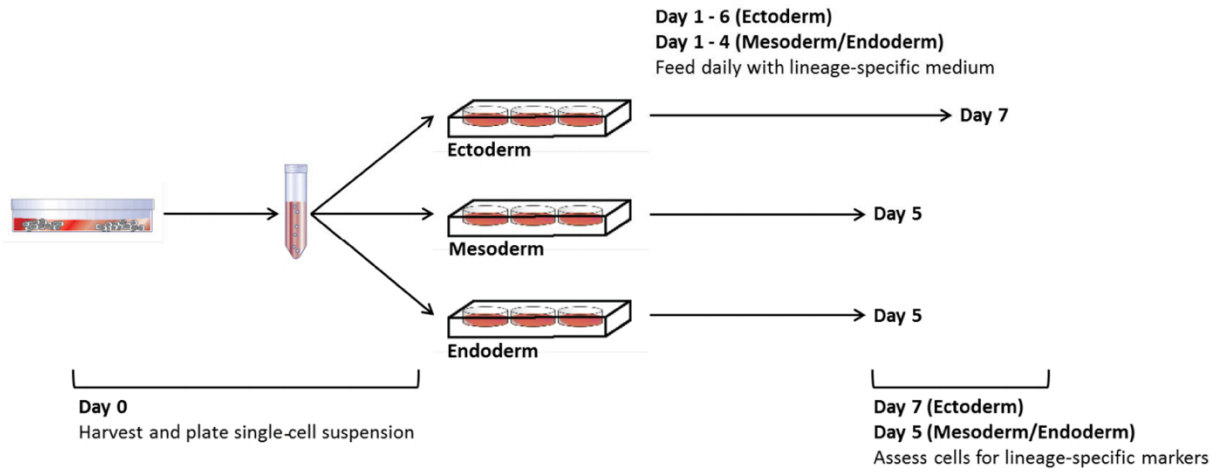

Figure 2.1. An overview of the trilineage differentiation experiment. Figure taken from Stemcell Technologies (63).

2.2.1 Coating Plates with Extracellular Matrix

Before seeding cells, two 24-well plates were coated with Matrigel (Corning). Matrigel aliquots were thawed on ice for 2 hours and diluted 1:50 in DMEM/F12. The volume used for each well is described in table 2.2.

2.2.2 Passaging the Induced Pluripotent Stem Cells to Generate the Three Germ Layers

When the iPSCs were ready to passage at 70-80% confluence, they were washed once with 1.5 ml D-PBS and dissociated into single cells by adding 1 ml Accutase (Stemcell Technologies). After 6-8 minutes incubation at 37 °C, the Accutase from the wells were pipetted

up and sprayed back into the wells 1-3 times to detach the cells from the plate. Further, the cells were transferred to a 15-ml Falcon tube with pre-filled 4 ml DMEM/F12. Additionally, 1 ml DMEM/F12 was added to the wells collect residual cells from the plate. The tubes were centrifuged for 5 minutes at 1.000 rpm, supernatant was discarded, and pellets were resuspended in E8 medium with 10 µM Rho-associated protein kinase (ROCK) inhibitor (Y-27632, Stemcell Technologies) to promote cell survival. The cells were quantified using Countess™ II automated cell counter (Invitrogen) and trypan blue stain (Invitrogen).

The coating from the 24-well plate was aspirated and 500 µl of E8 medium with 10 µM Y-27632 was added to the wells. 400.000 cells (for ectoderm and endoderm) or 100.000 cells (for mesoderm) per well in 500 µl medium were loaded. The plates were placed in an incubator at 37 °C moving the plate in quick movements back-and-forth and side-to-side.

After 24 hours, medium was aspirated, and 1 ml of appropriate medium (see table 2.3) was added to each well. This was repeated every day until day 5 for endoderm and mesoderm differentiation and day 7 for ectoderm differentiation.

Table 2.3. Media (Stemcell Technologies) used for different germ layer differentiation of iPSC.

Medium	**Germ layer differentiation**
STEMdiff™ Trilineage Ectoderm Medium	Ectoderm layer
STEMdiff™ Trilineage Mesoderm Medium	Mesoderm layer
STEMdiff™ Trilineage Endoderm Medium	Endoderm layer

2.3 Karyotyping

A genetic analysis was performed on the on two iPSC control clones (AGc1, ATc2) and all of the six iPSC patient clones (Bc4, Bc6, Bc9, Tc3, Tc9, Tc18) to check for karyotypic abnormalities, by the use of hPSC Genetic Analysis Kit (Stemcell Technologies). This works by performing quantitative polymerase chain reaction (qPCR) using nine primer probes that target the most common karyotypic abnormalities reported in iPSCs (64).

First, DNA was extracted from cell pellets of cultured iPSCs using DNeasy® Blood & Tissue Kit (Qiagen), according to the manufacturer's recommendations. The DNA was quantified using NanoDrop OneC spectrophotometer (Thermo Fisher Scientific).

120 µl of ROX Reference Dye (Stemcell Technologies) was added to the qPCR Master Mix (2X) (Stemcell Technologies) to make it complete, and pulse-vortexed for 3-5 seconds, kept on ice, protected from light. Then, 300 ng DNA extracted from iPSC samples or 1.5 µl of

the Genomic DNA Control (Stemcell Technologies) was added to 1.5 ml Eppendorf tubes. Nuclease-Free Water (Nalgene) was then added to the tubes with DNA to make a total volume of 90 µl. 150 µl of the master mix prepared in the beginning was added to each tube.

Primer probes were prepared in separate tubes by centrifuging the Genetic Assay Tubes (Stemcell Technologies) at 750 x *g* for 10 seconds and resuspended in 33 µl of TE Buffer (Stemcell Technologies). After the tubes were once again centrifuged. 45 µl of Nuclease-Free Water and 15 µl of each primer probe was added to separate PCR tubes.

The DNA samples with the qPCR master mix and the primer probes were briefly centrifuged. 8 µl of the DNA samples and 2 µl of the primer probes were added to each well in a 96-well PCR plate (Thermo Fisher Scientific). The plate was sealed with MicroAmp™ Optical Adhesive Film (Thermo Fisher Scientific) and centrifuged before being loaded in the StepOnePlus™ Real-Time PCR Systems (Applied Biosystems). A standard 40-cycle program was performed. Data was analyzed using the ΔΔCt method, see Appendix 2.

2.4 Differentiation of Induced Pluripotent Stem Cells to Neural Progenitor Cells using the Standard Protocol

The "Standard Protocol" is modified from two papers published by Li *et al*. (35) and Perriot *et al*. (65). The iPSCs used to generate NPCs with this protocol are listed in table 2.4.

Table 2.4. *The iPSC clones used for the different NPC protocols.*

NPC Protocol	Clones
The Standard Protocol	AGc1, AGc6, Bc4, Bc9, Tc3
Stemcell Technologies´ NPC Monolayer/EB Protocol	AGc1, ATc2, Bc4, Bc6, Tc3, Tc18

2.4.1 Preparing plates with extracellular matrix

1 ml of 15 µg/ml poly-L-ornithine (PLO) in 1X PBS was added to each well on a 6-well plate. After incubating for 2 hours at room temperature or overnight at 4 °C the wells were washed twice with 1X PBS and once with DMEM/F12. 1 ml of 5 µg/ml laminin diluted in DMEM/F12 was then added to each well and incubated at room temperature for 2 hours or overnight at 4 °C. The coated 6-well plate was ready for use and stored for a maximum of one week at 4 °C for future experiments.

2.4.2 Generating and Passaging the Neural Progenitor Cells

When the iPSCs reached 70-80% confluence, they were dissociated to single cells and quantified as described in subchapter 2.2.2, except the pellet was resuspended in NPC(+) medium with 10 µM Y-27632. 500.000 cells were added to each well of a PLO/Laminin-coated 6-well plate and incubated at 37 °C for one week in NPC (+) medium supplemented with 10 µM Y-27632. Half of the medium was changed with fresh NPC(+) medium every day. After 7 days the cells were passaged as described in subsection 2.2.2, except the pellet was resuspended in NEM this time. Dissociated cells were added to each well of a PLO/Laminin-coated 6-well plate with a density of 100.000 cells/cm^2 and cultured in NEM. The cells were passaged every 3-5 days.

2.4.3 Storing Neural Progenitor Cells

Following passage, remaining NPCs were stored at every passage. Aliquots of 2 million cells were transferred to an Eppendorf tube and centrifuged at 8.000 rpm for 3.5 minutes. Supernatant was removed and the pellet was washed once with 1X PBS, centrifuged again and the pellet was stored in -80 °C for further experiments.

At the same time, 6 million cells were transferred to a 15-ml Falcon tube, centrifuged at 1.000 rpm for 5 minutes and resuspended in 1 ml NEM with 10% DMSO. The cell suspension was transferred to a cryotube (Thermo Fisher Scientific) and stored in a nitrogen tank to ´pause´ the differentiation. This enables the option to thaw NPCs at different passages at a later time point to continue culturing them.

2.4.4 Thawing Stored Neural Progenitor Cells

NPCs stored in a nitrogen tank were thawed to resume culturing the cells, aiming at performing further experiments on live cells. The cryotubes were put in a 37 °C water bath until the cells were almost thawed, before getting transferred to a 15-ml Falcon tube containing 5 ml DMEM/F12. The tubes were centrifuged at 1.000 rpm for 5 minutes and the pellet was resuspended in NEM with 10 µM Y-27632. The cells were plated on a coated 6-well plate at 100.000 cells/cm^2 and cultured as described in subsection 2.4.2.

2.5 Differentiation of Induced Pluripotent Stem Cells to Neural Progenitor Cells using Stemcell Technologies´ NPC Monolayer Protocol

The technical manual: "Generation and Culture of Neural Progenitor Cells Using the STEMdiff™ Neural System" from Stemcell Technologies (56) was tested to generate NPCs from iPSCs and determine whether NPCs would then survive until later passages, compared to the standard protocol described in 2.4. See figure 2.2 for a simplified timeline of the protocol. A 6-well plate was coated as described in subsection 2.4.1, but with a laminin concentration of 10 µg/ml. The iPSCs used to generate NPCs with this protocol are listed in table 2.4.

2.5.1 Preparing Medium for Stemcell Technologies´ NPC Monolayer Protocol

STEMdiff™ Neural Induction Medium (Stemcell Technologies) and STEMdiff™ SMADi Neural Induction Supplement (Stemcell Technologies) were thawed according to the instruction and mixed as working medium, STEMdiff™ NIM. Subsequently, the medium was aliquoted into 50-ml tubes and stored at -20 °C. One aliquot was thawed at a time at 4 °C and kept in 4 °C for a maximum of one week.

2.5.2 Generating and Passaging the Neural Progenitor Cells

An aliquot of STEMdiff™ NIM and Accutase (Stemcell Technologies) were warmed up to 37 °C in a water bath before use. The iPSCs were dissociated to single cells and quantified as described in subsection 2.2.2, except the pellet was resuspended in DMEM/F12. Also, an additional step was added; to ensure that all cells were collected, 1 ml of DMEM/F12 was added to each well to transfer any remaining cells. 4 million cells were transferred to a new 15-ml Falcon tube and centrifuged at 1.000 rpm for 5 minutes. The cells were resuspended in 4 ml STEMdiff™ NIM with 10 µM Y-27632 and plated into 2 wells of a PLO/Laminin-coated 6-well plate at a density of 200.000 cells/cm^2. The plate was moved quickly side-to-side and back-and-forth after being placed in an incubator at 37 °C. A full-medium change was performed daily. After 6 days, the NPCs were passaged to a new PLO/Laminin-coated 6-well plate as described above, but at a density of 175.000 cells/cm^2. These cells were designated as NPC passage 1. The medium was changed daily for a week and then passaged to NPC passage 2. When the NPCs were ready for passage 3, they were collected in 15-ml Falcon tubes as normal, but the pellet was resuspended in a new medium, STEMdiff™ Neural Progenitor Medium (Stemcell Technologies) and plated on a PLO/Laminin-coated 6-well plate with a density of 125.000 cells/cm^2.

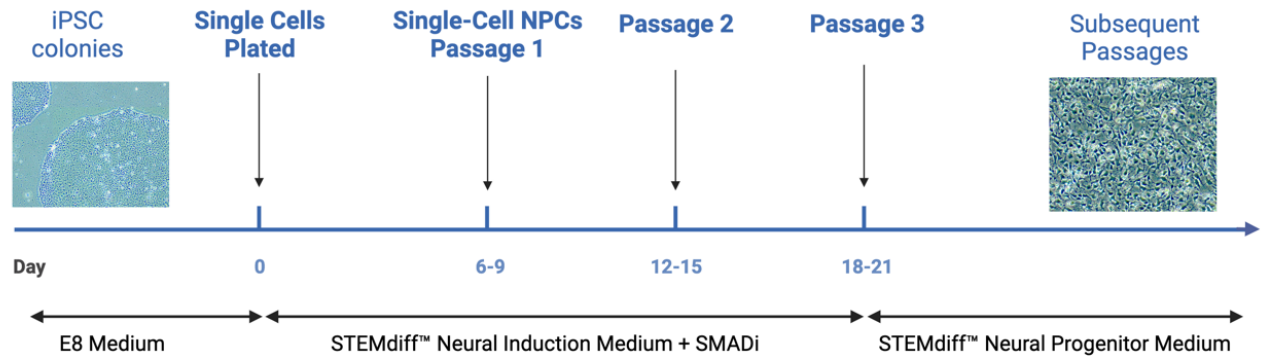

Figure 2.2. A simple timeline for differentiation of NPC from iPSC using the Stemcell Technologies´ NPC Monolayer Protocol (66). *iPSCs are differentiated to NPCs by replacing E8 medium with STEMdiff™ NIM + SMADi (Stemcell Technologies), and eventually switch to STEMdiff™ Neural Progenitor Medium (Stemcell Technologies) to obtain pure NPCs. Figure created using BioRender (https://biorender.com/).*

2.6 Differentiation of Induced Pluripotent Stem Cells to Neural Progenitor Cells using Stemcell Technologies´ NPC Embryoid Bodies Protocol

A second approach from Stemcell Technologies was also tested to generate NPCs from iPSCs (66). This protocol differs from the two protocols described in 2.4 and 2.5 as it generates NPCs from embryoid bodies. An overview of the experiment is shown in figure 2.3. The iPSCs used to generate NPCs with this protocol are listed in table 2.4.

2.6.1 Preparing Plates with Extracellular Matrix

500 µl of Anti-Adherence Rinsing Solution (Stemcell Technologies) was added to each well of an AggreWell™800 24-well plate (Stemcell Technologies). One well was used for each clone. The plate was centrifuged at 1300 x *g* for 5 minutes to get rid of any bubbles in the wells. The Anti-Adherence Rinsing Solution was aspirated, and the wells were washed with 1 ml of DMEM/F12 before 1 ml of warm STEMdiff™ NIM with 10 µM Y-27632 was added to each well of the 24-well plate.

2.6.2 Generating and Passaging Neural Progenitor Cells

Day 0-4: When iPSCs reached 70-80% confluence they were dissociated to single cells and quantified as described in subsection 2.2.2 with the additional step mentioned in subsection 2.5.2. 3 million cells were transferred to a single 15-ml Falcon tube, and the pellet was

resuspended in 1 ml warm STEMdiff™ NIM with 10 µM Y-27632. The cell suspension was transferred to one well of a 24-well plate prepared as described in subsection 2.6.1 to obtain 10.000 cells/microwell. The cell suspension was gently pipetted up and down in the well several times to evenly distribute the cells along the microwells. The plate was centrifuged at 100 x *g* for 3 minutes to capture the cells in the microwells and incubated at 37 °C. 1.5 ml of warm STEMdiff™ NIM was changed daily until day 4.

Day 5-11: A 40 µm Cell Strainer (Corning) was placed upside-down on a 50-ml tube. The EBs in the microwell were dislodged carefully using a 1-ml cut pipette tip and transferred to the strainer on top of a 50-ml tube, to remove the single cells that did not form EBs. The strainer was carefully, but quickly, turned around and placed on top of a new 50-ml tube. 2 ml of STEMdiff™ NIM was added to the strainer to collect the EBs in the new tube. The collected EBs was plated in a well of a Matrigel-coated 6-well plate, and incubated at 37 °C. The plate was moved quickly back-and-forth and side-to-side to distribute the EBs evenly along the well. A full medium change with warm STEMdiff™ NIM was done daily until day 11.

Day 12: The cells were washed once with 1 ml DMEM/F12 and incubated at 37 °C for 1.5 hours with 1 ml of warm STEMdiff™ Neural Rosette Reagent (Stemcell Technologies), a reagent that only allows neural rosettes to detach from the plate. Further, the STEMdiff™ Neural Rosette Reagent was removed and 1 ml of DMEM/F12 was firmly expelled to the well aiming at the rosette clusters to dislodge them from the well. The lifted neural rosettes were added to a 15-ml Falcon tube. This step was repeated several times to collect the remaining neural rosettes. The tube was centrifuged at 350 x *g* for 5 minutes and the pellet was carefully resuspended in 2 ml warm STEMdiff™ NIM. The neural rosette suspension was added to a Matrigel-coated 6-well plate, and incubated at 37 °C. The plate was moved quickly back-and-forth and side-to-side to distribute the rosettes evenly across the surface of the well. A full-medium change with warm STEMdiff™ NIM was performed daily until day 17.

Day 17: The neural rosettes formed an NPC monolayer, and the NPC passage were performed as described for NPC passage 1, and further, in subsection 2.5.2.

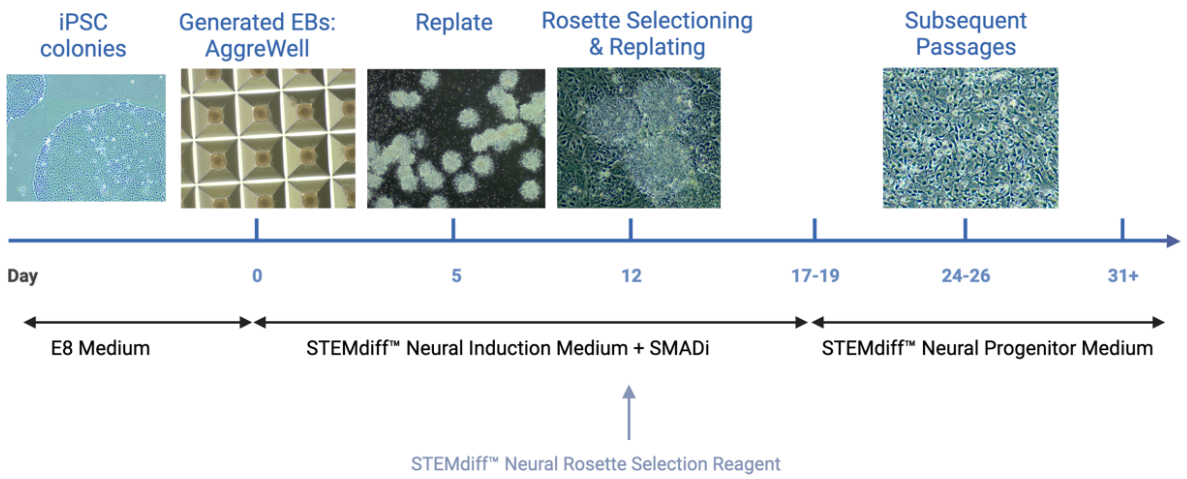

Figure 2.3. Timeline for differentiation of NPC from iPSC using the Stemcell Technologies´ NPC Embryoid Bodies Protocol (66). *iPSCs are grown in suspension to generate embryoid bodies (EB). Subsequently after 5 days, the EBs are transferred to a non-suspension plate to form neural rosette. On day 12 the neural rosettes are selected and replated using STEMdiff™ Neural Rosette Reagent (Stemcell Technologies) to generate pure NPCs. Figure created using BioRender (https://biorender.com/).*

2.7 Cerebral Organoids

Cerebral organoids were generated from iPSCs, using two control clones (AGc1, AGc6) and three patient clones (Bc4, Bc9, Tc3). The organoids were cultured according to the original Lancaster *et al*. protocol (53), with minor modifications.

2.7.1 Generation of Cerebral Organoids

The cerebral organoid protocol consists of five main steps, as illustrated in figure 2.4.

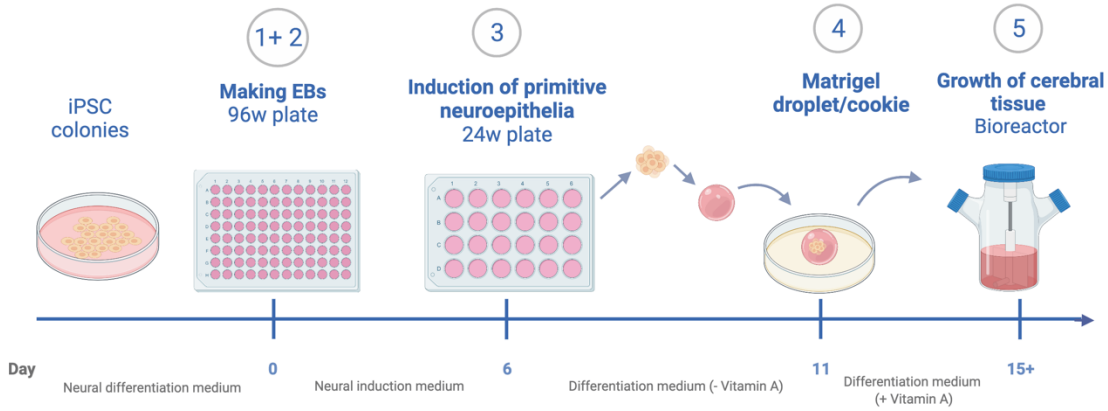

Figure 2.4. Overview of cerebral organoid development*. iPSCs are grown in suspension to form embryoid bodies. On day 5-7 the embryoid bodies are transferred to a 24-well plate for induction of primitive neuroepithelia. 4-5 days later the neural tissue is transferred to Matrigel droplets or cookies. Finally, after 4-5 more days, the tissues form more expanded neuroepithelium and are transferred to a spinning bioreactor to become fully developed cerebral organoids. Figure created using BioRender (https://biorender.com/).*

Step 1: Making embryoid bodies

iPSCs at 70-80% confluence were observed under a microscope to ensure optimal features of pluripotency and no sign of differentiation, as this is an important step to succeed in generating cerebral organoids. The confluent iPSCs with optimal morphology were treated as described for NPCs (subsection 2.2.2), except the cells were resuspended in Neural Differentiation Medium (NDM) with 5 µM Y-27632. Single cells were plated on a 96-well plate with 9.000 cells/well in 150 ml NDM. The plate was centrifuged at 100 x *g* for 5 minutes to center the cells in each well and incubated at 37 °C overnight.

Step 2: Feeding embryoid bodies and initiation of germ layer differentiation

After 24 hours clear borders were observed on the successfully formed EBs. The EBs were cultured for 5-7 days to reach a size of 350-600 µm diameter. During this time, 80 µl of the old medium was carefully replaced with 110 µl of fresh NDM every other day. As the EBs did not form properly in the medium suggested in the Lancaster *et al*. (53) protocol, NDM, modified from Mariani *et al*. (67), was used in the first two steps of generating cerebral organoids.

Step 3: Induction of primitive neuroepithelia

After 5-7 days when the EBs reached approximately 350-600 µm in diameter, they were transferred with a 1-ml cut pipette tip to a 24-well suspension plate at 5-6 EBs per well with 500 µl Neural Induction Medium (NIM) and incubated at 37 °C. Medium was changed 48 hours later and every other day thereafter. 4-5 days later optimal EBs was brighter around the outside, indicating neuroectodermal formation.

Step 4: Transferring neuroepithelial tissues to Matrigel droplets or cookies

When signs of neuroepithelium appeared, the EBs was transferred to Matrigel droplets or cookies, depending on their size.

Matrigel droplets: A parafilm was prepared with a square of 4 x 4 dimples by pressing it onto an empty tip tray and placed into a 100 mm petri dish (SARSTEDT). Each EB was transferred to separate dimples by a 200 µl pipette tip, cut with a sterile scissor to make a 1.5-2.0 mm diameter opening. The excess medium in each dimple was carefully removed without disrupting the tissues, and 30 µl of Matrigel was immediately added. The tissues were positioned at the center of the droplets with a 10 µl pipette tip, following incubation at 37 °C for 30 minutes to polymerize the Matrigel. The Matrigel droplets were removed from the

parafilm sheet by blowing 10 ml Differentiation Medium without Vitamin A (DM -A) directly to the sheet to wash down the droplets and further incubated at 37 °C. After 48 hours the old medium was replaced with 5 ml fresh medium by slightly tilting the dish to allow the droplets to sink and prevent disturbing the organoids.

Matrigel cookies: The smallest EBs got embedded in Matrigel cookies instead of droplets, using a protocol modified from Qian *et al* (68). The EBs were transferred to a 15-ml Falcon tube by using a 5-ml pipette. After the EBs settled, the supernatant was removed and replaced with 1 ml DM -A. When the EBs settled again, a cut 200-µl pipette tip was used to transfer 20-30 EBs in 67 ul medium to an Eppendorf tube. Another cut pipette tip was used to add 100 µl of Matrigel to the Eppendorf tube to get a 3:2 ratio of Matrigel and medium. The solution was mixed well by pipetting up and down multiple times. The mixture was transferred to a 6-well suspension plate in the center of one of the wells to make the ´Matrigel cookie´. The EBs were spread evenly within the cookie to prevent fusion, and the cookie were made with a thickness of more than 1 mm to allow the EBs to fully envelop. The plate was incubated at 37 °C for 30 minutes to polymerize. When the cookies solidified, 3 ml of DM -A was added to the wall of the well to prevent disturbing the neuroepithelial tissue and again placed in the incubator at 37 °C. After 48 hours the medium was changed.

Step 5: Growth of cerebral tissue

After 4-5 days in static culture, the tissues formed more expanded neuroepithelium, and were ready to be transferred to their final destination: a spinning bioreactor or a plate placed in shaking incubator.

Matrigel droplets: The Matrigel droplets were transferred to a spinner flask (Corning) with 100 ml Differentiation Medium with vitamin A (DM +A) using a 5-ml pipette. Maximum 32 organoids were transferred to one bioreactor. The bioreactor was placed on a magnetic stir at 37 °C. Medium change was performed on a weekly basis.

Matrigel cookies: The entire Matrigel cookie was pipetted up and down at least 2-3 times using a 5-ml pipette, until the organoids dissociated from the Matrigel. The organoids together with the medium were transferred to a 15-ml Falcon tube by a 10-ml pipette. When the organoids settled after 1-2 minutes, the supernatant was removed. 10 ml of DM -A was added to the tube from the bottom for resuspension, and when the organoids settled once again, the supernatant was removed. This was done to get rid of the remaining Matrigel to prevent chunks of Matrigel to aggregate in the cerebral tissue culture. The organoids were transferred to a new 6-well suspension plate using a cut 1-ml pipette tip and 3 ml of DM +A was added to the well.

The plate was placed in a shaking incubator at 37 °C. A full medium change was done every 3-4 days.

The organoids generated from both Matrigel droplets and Matrigel cookies continued to grow up until 2 months before stabilizing but could be cultured for up to a year if desired.

2.7.2 Preparation of Cerebral Organoids for Cryosectioning and Immunohistochemistry

The cerebral organoids were collected at 2 weeks, 1 month and 2 months in the shaking incubator or spinning flask. 5-6 organoids were transferred to a 2 ml Eppendorf tube and washed once with 1X PBS. The organoids were fixed by adding 1 ml of 4% PFA in 1X PBS containing 1% sucrose and placed in a rotator at 4 °C overnight. After 24 hours the organoids were washed with 1X PBS and 1 ml of 15% sucrose in 1X PBS was added and incubated for another 24 hours at 4 °C on a rotator. Then, Optimal cutting temperature (OCT) compound (Thermo Fisher Scientific) was used to make a block to store the organoids. While the OCT compound polymerized in -20 °C, single organoids were placed in each well of a 24-well plate and washed once with 1 ml 1X PBS. The PBS was replaced with 700 µl Erythrosine dye (RAL Diagnostics) and removed after 10-15 seconds. 1 ml 1X PBS was added to each well, and 800 µl was then removed. A cut 1-ml pipette tip was used to transfer the organoids onto the polymerized layer of OCT compound in the block. The PBS was removed from the block, and the organoids were positioned in the center. The OCT compound was added on until the organoids were completely covered. The blocks were covered with Parafilm and kept at -80 °C. Slides were prepared by cutting sections of 14-20 µM using Leica CM3050 S Cryostat (Leica Biosystems) with Object Temperature (OT) at -18 °C and Chamber Temperature (CT) at -24 °C and stored at -20 °C.

2.8 Immunostaining

Immunostaining was used to detect protein expression of specific markers in iPSCs, NPCs and the three germ layers with immunocytochemistry (ICC), and in cerebral tissue with immunohistochemistry (IHC).

2.8.1 Immunocytochemistry

The cells were cultured in a 48-well plate, and the cells were washed with 300 µl of 1X PBS. 200 µl of fresh 4% paraformaldehyde in 1X PBS was added and the plate was incubated at room temperature for 10 minutes to fix the cells. Subsequently, cells were washed twice with 300 µl of 1X PBS before permeabilization with 200 µl of 0.1% Triton-X in 1X PBS at room

temperature for 15 minutes. 150 µl of Blocking Buffer (5 % goat gut serum, 5 % bovine serum albumin (BSA), 0.1 % Triton-X/1X PBS) was added and incubated for 30-45 minutes. The primary antibody (Appendix 3, table A.2) was added in a 1:10 dilution of blocking buffer in 1X PBS and incubated overnight at 4 °C. 500 µl of 0.1% Tween-20 in 1X PBS was used to wash the cells 3 times, before adding 150 µl of the secondary antibody (Appendix 3, table A.3) in a 1:10 dilution of Blocking Buffer in 1XPBS and incubated for 1 hour in the dark. The cells were washed 3 times with 0.1% Tween-20 in 1X PBS and 150 µl of DAPI (1:1000 in PBS, Sigma) was added to stain the nucleus for 10 minutes. Subsequently, 500 µl of 1X PBS was added and the plate was kept at 4°C before visualizing the cells using the EVOS® FL Auto Imaging System (Thermo Fisher Scientific).

2.8.2 Immunohistochemistry

Immunohistochemistry was performed on slides of cerebral organoids to characterize different regions of the tissue. The staining procedure were the same as in section 2.8.1, except for some specific steps. Briefly, the slides were kept at room temperature to dry, before a Dako Pen (Agilent) was used to draw circles around the cerebral tissue on the slide to make a hydrophobic barrier. After blocking the samples with Blocking Buffer for 1 hour at room temperature, the primary and secondary antibodies were incubated as described in 2.8.1. 100 µl of ultrapure water (Ambion) was added to rinse the samples and removed to dry them out. ProLong™ Gold antifade reagent with DAPI (Thermo Fisher Scientific) was added and a cover glass (18x18 mm) was placed on top, carefully, to prevent air bubbles. Fluorescent imaging was carried out using the EVOS® FL Auto Imaging System (Thermo Fisher Scientific).

2.9 Characterization of Induced Pluripotent Stem Cells and Neural Progenitor Cells by qPCR

The mRNA in cells was isolated, and reverse transcribed from RNA to cDNA. Following, qPCR was run on the cDNA to quantify cell stage-specific markers at an mRNA level (as illustrated in figure 2.5).

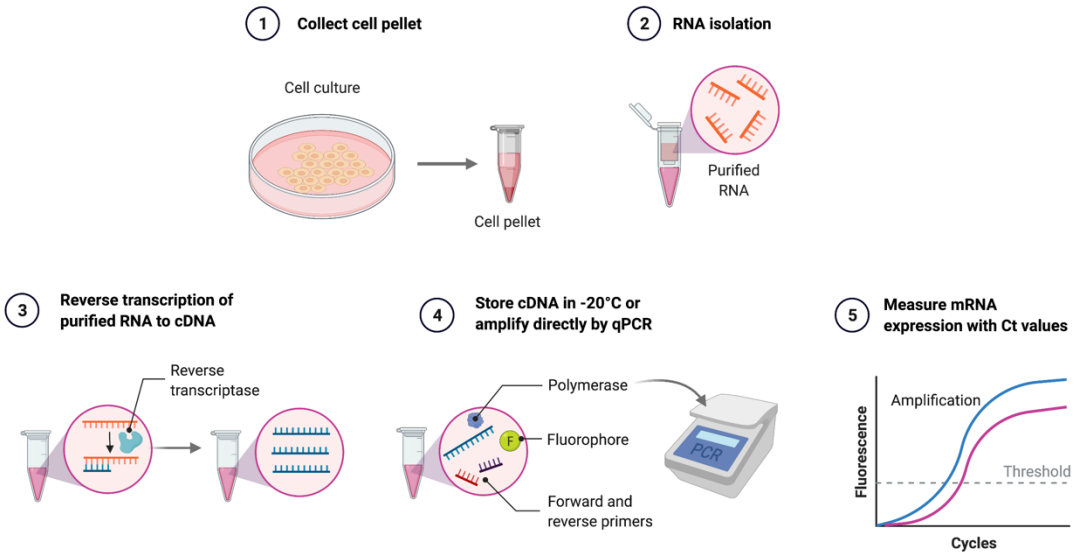

Figure 2.5. *The workflow of collecting cells to perform qPCR for detection of mRNA. Figure created using BioRender (https://biorender.com/).*

This assay was performed on the clones listed in table 2.5.

Table 2.5. The iPSC and NPC clones analyzed by qPCR to quantify gene expression of specific cell stage markers.

	iPSC	**NPC**
Control	AGc1, Agc6, ATc2	Agc1, AGc6
Patient B	Bc4, Bc6, Bc9	Bc4, Bc9
Patient T	Tc3, Tc18	Tc3

2.9.1 RNA Isolation and Purification

Total RNA was isolated from cultured iPSCs and NPCs using RNeasy® Mini Kit (Qiagen) as described in the manufacturer´s protocol. The RNA was quantified using a NanoDrop One^{C} spectrophotometer (Thermo Fisher Scientific).

2.9.2 cDNA Synthesis by Reverse Transcription

1000 ng cDNA was reverse transcribed from 1000 ng RNA with 20 µl total volume for each clone, using the High-Capacity cDNA Reverse Transcription Kit (Thermo Fisher Scientific). Using T100™ Thermal Cycler (Bio-Rad), the samples were run at 25 °C for 10 minutes to anneal primers, and further set to 37 °C for 120 minutes to activate the reverse transcriptase (RT) and for DNA polymerization, before setting to 85 °C for 5 minutes to inactivate RT. The samples were hold at 4 °C overnight, before making a dilution of 10 ng/µl RNA to prepare for qPCR.

2.9.3 Quantitative Polymerase Chain Reaction (qPCR)

A PCR master mix was prepared by mixing 10 µl of 2X Power SYBR® Green Master Mix (Thermo Fisher Scientific), 1 µl of forward and reverse primer (Appendix 4) and 5 µl of RNase free water. 3 ng of the cDNA prepared in 2.9.2 was added to MicroAmp™ Optical 96-Well Reaction Plate (Thermo Fisher Scientific), together with 17 µl of the PCR master mix. The plate was sealed with MicroAmp™ Optical Adhesive Film (Thermo Fisher Scientific), vortexed and centrifuged before running the plate in the StepOnePlus™ Real-Time PCR System (Thermo Fisher Scientific) with StepOne™ Software v2.3 (Thermo Fisher Scientific). The qPCR was run for 2 minutes at 50 °C; 10 minutes at 95 °C; 1 minute at 60 °C and 15 °C minutes at 95 °C for 40 cycles.

2.10 Fluorometric Proteasome 20S Activity Assay

A proteasome 20S activity assay was performed on iPSC and NPC to compare the level of proteasome activity in patients and controls in different differentiation stages. This was done using the Proteasome 20S Activity Assay Kit (Sigma-Aldrich). The iPSCs and NPCs were passaged as described in subsection 2.2.2 and 2.4.2, respectively. 100 µl with 80.000 cells per well was added in duplicates for each clone to a Geltrex-coated 96-well plate. After incubating at 37 °C overnight, 10 µl of a 1 µM stock of the proteasome inhibitor Epoxomicin (MedChemExpress) was added to two additional wells with control cells and incubated at 37 °C for 1 hour. This step was performed to confirm that the activity measured is uniquely related to the proteasome. Following, 100 µl of Proteasome Assay Loading Solution (Sigma-Aldrich) was added to each well and incubated at 37 °C for 4 hours before monitoring the fluorescence intensity with excitatory wavelength at 485 nm and emitter wavelength at 520 nm using FLUOstar® Omega (BMG Labtech) microplate reader. The Proteasome Assay Loading Solution (Sigma-Aldrich) contains the fluorogenic substrate LLVY-R110, which is a target for chymotrypsin-like protease activity associated with the proteasome complex in the cells, generating a strong green, fluorescent signal upon cleavage. Thus, enable a quantification of the proteasome activity across the samples (69).

2.11 Proliferation Assay for Neural Progenitor Cells

Proliferation assays were performed to investigate whether exposure to proteasome inhibitors differentially affects controls- and patients-derived NPCs. Here, NPCs at passage 3 and 4 generated using the standard protocol was passaged as described in subchapter 2.4.2 and plated onto a Geltrex-coated 96-well plate with 10.000 cells in each well with NEM. The experimental set-up is described in Appendix 5. The plate was incubated at 37 °C overnight, the medium was removed, and fresh NEM was added together with the designated concentrations of the proteasome inhibitors MG132 (Sigma-Aldrich), Bortezomib (MedChemExpress) or Epoxomicin (MedChemExpress) as specified in the results part. Cell viability was measured at several time points (different days). Therefore, at the designated time point, 10 µl of PrestoBlue™ (Thermo Fisher Scientific) was added to each well and incubated at 37 °C for 30 minutes. The percentage of live cells was measured using FLUOstar® Omega (BMG Labtech) microplate reader, using an excitation filter at 544 nm and an emission filter at 590 nm. PrestoBlue™ contains the fluorogenic dye resazurin, which is reduced by enzymes present in viable cells, consequently, allowing the quantification of viable cells in culture.

2.12 Flow Cell Cytometry for Neural Progenitor Cells

Flow cell cytometry was performed on NPCs with specific concentrations of proteasome inhibitors after 48 hours, determined by the proliferation assay. NPCs at passage 3 from the standard protocol was passaged as described in subsection 2.4.2. 200.000 NPCs in 1 ml NEM was added to each well of a Geltrex-coated 12-well plate. The plate was incubated at 37 °C for 48 hours to grow. Following, the old medium was replaced with 1 ml fresh NEM together the designated concentrations of proteasome inhibitors. The plate was incubated at 37 °C for another 48 hours. The cells were washed twice with warm D-PBS, and 500 µl of Accutase was added to each well. The plate was incubated at 37 °C for 5-8 minutes. The single cell-suspension in Accutase firmly expelled by pipetting up and down a few times and transferred to separate Eppendorf tubes containing 500 µl DMEM/F12. The tubes were centrifuged at 400 x *g* for 5 minutes, and supernatant was discarded. The pellet was washed by adding 1 ml of 1X PBS and centrifuged once again at 400 x *g* for 5 minutes. The supernatant was discarded, and the pellet was resuspended in 1 ml 1X PBS with 1 µg/ml 7-Aminoactinomycin D (7-AAD), except for one pellet that was only resuspended in PBS to measure the background signal. The tubes were incubated on ice in the dark for 20 minutes, before being analyzed by flow cell cytometry on BD FACSCanto (BD Biosciences). Two biological replicates were included for each sample.

2.13 Liquid Chromatography-Mass spectrometry

Liquid chromatography-mass spectrometry (LC-MS) was used to determine global alterations in protein expression in iPSCs compared to NPCs, and to identify alterations in levels of ubiquitinated proteins and proteins associated with the UPS. An overview of the clones used in this experiment is listed in table 2.6.

Table 2.6. Clones analyzed by LC-MS/MS.

	Replicate Specifications*
AGc1	Control 1
AGc6	Control 2
Bc4	Patient 1, Clone 1
Bc9	Patient 1, Clone 2
Tc3	Patient 2, Clone 1

**Analysis was performed with three biological replicates of each clone.*

2.13.1 Sample Preparation for LC-MS/MS

A modified RIPA buffer (150 mM NaCl, 50 mM Tris-HCl pH 7.4, 1% NP40, 0.5% sodium deoxycholate, 0.1% SDS, 10 mM EGTA and 10mM $MgCl_2$, 1 mM DTT). 10 µl phosphatase inhibitors (Sigma), 20 µl protease inhibitors (Complete, Roche) and 0.5 µl nucleases (Omni cleave, Benzonase, MN, 10 mg/mL RNase) was freshly added to 1 mL RIPA buffer, to resuspend iPSC and NPC pellets on ice.

Cell pellets were lysed by resuspension in 40-80 µl (2X PCV) RIPA buffer and incubation on ice for 1 hour. Following, protein concentrations were measured using the Bio-Rad protein assay: 1-2 µl of cell lysate was added to 1 ml water and 250 µl of the Bio-Rad Protein Assay Dye Reagent (Bio-Rad) and the absorbance of the sample was measured at 595 nm.

25 µg protein was added to 1.5 ml Protein LoBind® tube (Eppendorf) together with 100 mM NH_4HCO_3 (Sigma-Aldrich) to make a final volume of 30 µl. 0.75 µl of tris-(2-carboxyethyl) phosphine (TCEP) was added to the lysate to reduce the cysteine bonds with a final concentration of 5 mM and incubated at room temperature for 30 minutes. 1 µl of 50 mM Iodoacetamide (IAM) (Sigma) was added to the lysate for protein alkylation and prior to incubation in the dark for 30 minutes. To remove reagents that are not compatible with mass spectrometry analysis, such as salts and detergents, proteins were precipitated using a methanol-

chloroform procedure. Briefly, 400 µl of CH_3OH, 100 µl of $CHCl_3$ and 300 µl of H_2O (all reagents HPLC grade from Thermo Fisher) was added to each tube and centrifuged at maximum speed (15.000 rpm) for 2 minutes. The aqueous top layer was removed, and 800 µl of CH_3OH was added. The tube was centrifuged for another 2 minutes at 15.000 rpm. Supernatant was removed and 1 ml of CH_3OH was once again added to the sample and centrifuged with the same settings. The supernatant was removed, and the pellet was resuspended in 0.5 µg trypsin at 1:50 weight-to-weight (w/w) ratio of trypsin and protein, diluted in 100 mM NH_4HCO_3 to a final volume of 50 µl. The samples were incubated overnight at 37 °C in a ThermoMixer® C (Eppendorf, WVR) at 9.000 rpm for digestion. Then, samples were dried out in a SpeedVac (Eppendorf), resuspended in 45 µl of 0.1 % formic acid and incubated in a ThermoMixer® C for 1 hour at 4 ºC. The sample was centrifuged at 13.000 rpm for 30 minutes at 4 °C and 20 µl of the supernatant was added to a 11mm Snap Ring Micro-Vial (Thermo Fisher Scientific), and peptide concentration was measured using NanoDrop One^C spectrophotometer (Thermo Fisher Scientific) at 205 nm with the Scopes method. 1.5 µg peptide was used for the final mass spectrometry analysis.

2.13.2 Mass Spectrometry Analysis

Peptides were analyzed on an LC-MS/MS platform consisting of an Easy-nLC 1000 UHPLC system (Thermo Fisher Scientific) interfaced with an LTQ-Orbitrap Elite hybrid mass spectrometer (Thermo Fisher Scientific) via a nanospray ESI ion source (Proxeon). Peptides were injected into a C-18 trap column (Acclaim PepMap100, 75 µm i.d. × 2 cm, C18, 3 µm, 100 Å, Thermo Fisher Scientific) and further separated on a C-18 analytical column (Acclaim PepMap100, 75 µm i.d. × 50 cm, C18, 2 µm, 100 Å, Thermo Fisher Scientific) using a 180 minutes gradient with buffer A (0.1% formic acid) and buffer B (CH3CN, 0.1% formic acid): From 0 to 2% B in 1 min, 2−25% B in 150 min, 25−95% B in 19 min, and 10 min with 100% A. The flow rate was 250 nL/min. Peptides eluted were analyzed on the LTQ-Orbitrap Elite hybrid mass spectrometer operating in positive ion and data-dependent acquisition mode using the following parameters: electrospray voltage 1.9 kV, CID fragmentation with normalized collision energy 35, and automatic gain control target value of 1E6 for Orbitrap MS and 1E3 for MS/MS scans. Each MS scan (m/z 300−1800) was acquired at a resolution of 120 000 fwhm, followed by 20 MS/MS scans triggered for intensities above 500, at a maximum ion injection time of 200 ms for MS and 120 ms for MS/MS scans.

2.13.3 Analysis of Mass Spectrometry Data

Mass spectrometry data analysis were performed by Animesh Sharma, a senior engineer specialized in computational science, working at the Proteomics and Modomics Core Facility (PROMEC) at NTNU. According to Animesh Sharma, proteins were quantified by processing MS data using MaxQuant v.1.6.17.0 (70) using the following search parameters: enzyme specified as trypsin with a maximum of two missed cleavages allowed; acetylation of protein N-terminal, oxidation of methionine, deamidation of asparagine/glutamine, and phosphorylation of serine/threonine/tyrosine as dynamic post-translational modification. Data was queried against the Human proteome downloaded from Uniprot (71) in October 2020 with point mutations R178Q and A216D in P09936 along with MaxQuant's internal contaminants database using Andromeda built into MaxQuant. For both Protein and peptide identifications false discovery rate (FDR) was set to 1%, only unique peptides with high confidence were used for final protein group identification. Peak abundances were extracted by integrating the area under the peak curve. Each protein group abundance was normalized by the total abundance of all identified peptides for each run and protein by calculated median summing all unique and razor peptide-ion abundances for each protein using LFQ algorithm (72) with minimum peptides ≥ 1. LFQ values for all samples were log-transformed with base 2 and these transformed values representing each condition were subjected to two-sided Student's T-tests (73) as implemented in R (74) in order to check the consistency of change. The amount of change was estimated by subtracting the median of these values representing each group (log2FC) as they are more robust to outliers and extreme variations noticed in observed values within replicates. Directionality of the change is encoded within the sign of log2FC whereby a negative sign reflecting decreased and a positive sign reflecting the increased expression of the respective protein group. Further, to estimate the false-discovery rate (FDR), the T-test P-values were corrected using the Benjamini- Hochberg procedure (75). Differentially-expressed (DE) protein groups were identified at FDR<0.3 and absolute log2FC>0.5. The DE quantified only in one group were checked if their coefficient-of-variation of log2FC was within 5%. The Uniprot accession IDs of these DE were mapped to a volcano-plot using R package ggplot2 (76) and correlation heatmap using R package pheatmap (77). Finally, a group comparison was performed to investigate the significant differences in protein expression profiles of patient iPSCs and NPCs compared to control cells at the same stage of differentiation.

3 Results and Discussion

3.1 Characterization of iPSC

The first aim of this study was to generate and characterize the generated iPSCs, as well as neuronal cells and brain organoids. As for monolayer neuronal cells, iPSCs were characterized by studying their morphology and analyzing the expression of pluripotency markers by qPCR and immunocytochemistry. In addition, evaluation of iPSC ability to differentiate into the three germ layers and karyotypic analysis were performed as quality control measurements prior to further differentiation to NPC or organoids. The following section describes the characterization assays conducted in iPSC.

3.1.1 Morphology of iPSC

Prior to this project, Dr. Wei Wang in our lab has generated iPSC by reprogramming fibroblasts isolated from healthy individuals and UCHL1-patients. The morphology of fibroblasts is quite distinct from iPSC. While fibroblasts display plump spindle shaped morphology with a round or oval nucleus in the center (78) (figure 3.1A), iPSC are round shaped cells with a large nucleus and scant cytoplasm. During this project, the morphology of the reprogrammed cells was evaluated. The generated cells showed EB-like structures with clear edges and similar features described for iPSC, indicating that these cells are indeed iPSCs (figure 3.1B). However, evaluation of morphological features alone is not a reliable method to confirm cell identity. Hence, further characterization at molecular level was performed to confirm the generation of iPSC.

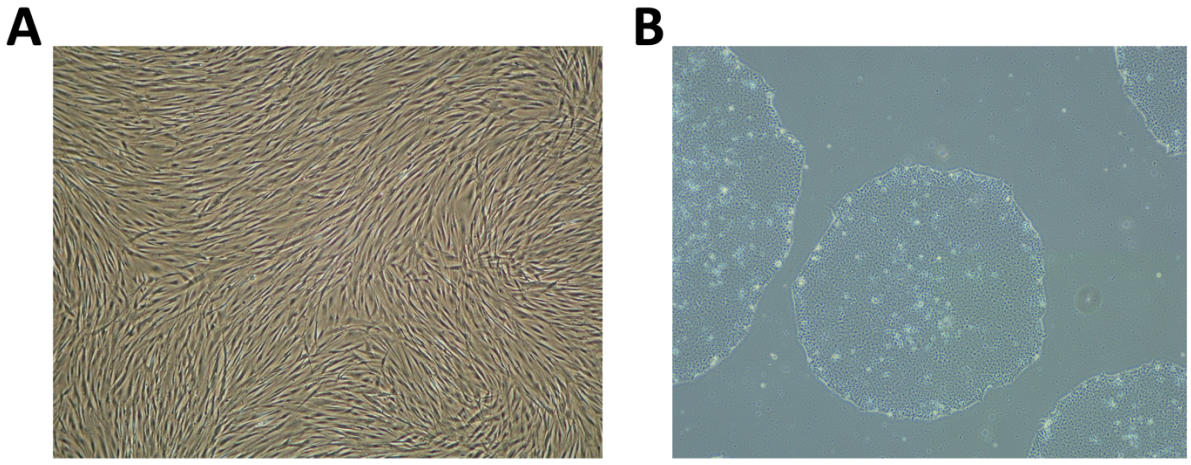

***Figure 3.1**. Phase-contrast images showing the morphology of human fibroblasts (79) (**A**) and a representative of the iPSCs used for experiments in this study (**B**).*

3.1.2 Pluripotency Markers

iPSCs exhibit distinct properties which allows them to be characterized through the detection of marker genes and proteins. Thus, qPCR analyses were performed to quantify the mRNA expression level of pluripotent marker genes in the iPSCs relative to parental fibroblasts. The mRNA expression levels increased around a thousand-fold from parental fibroblasts to iPSCs for both Nanog (figure 3.2A) and Oct4 (figure 3.2B). The mRNA expression level of Sox2 increased around a hundred thousand-fold in iPSCs from fibroblasts (figure 3.2C). The mRNA expression levels in control and patient derived iPSCs are similar for the three marker genes, suggesting that all fibroblast clones were successfully reprogramed to iPSC (figure 3.2A-C).

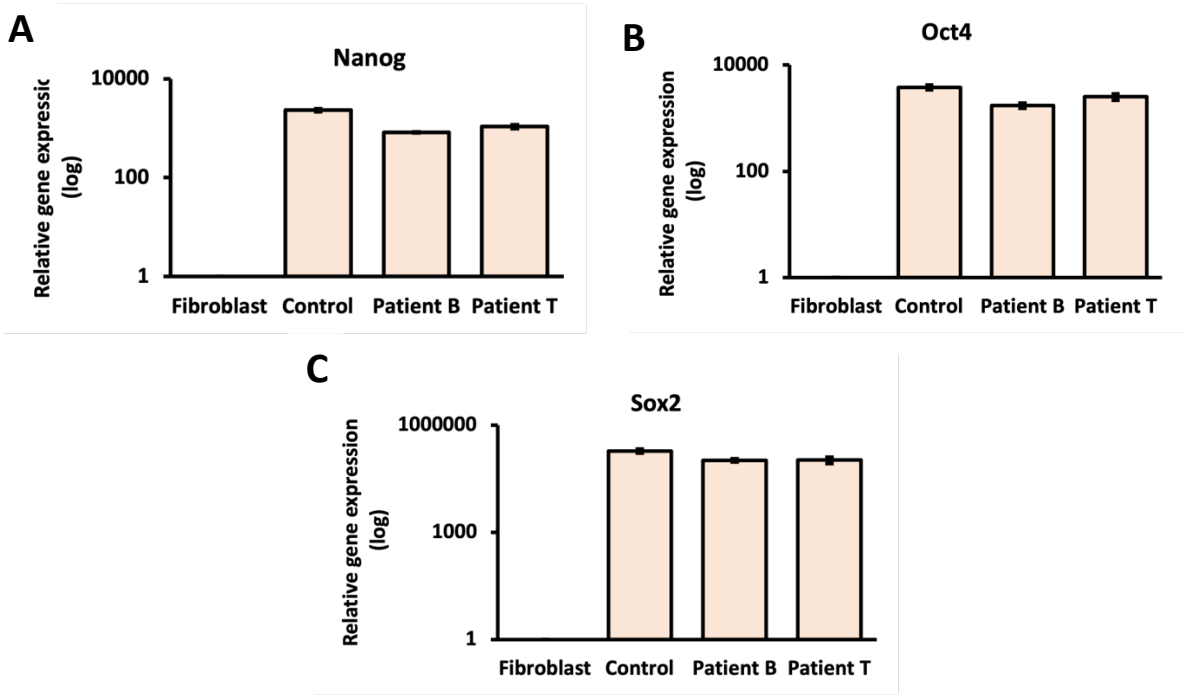

Figure 3.2. *mRNA expression levels of the pluripotency markers Nanog (A), Oct4 (B) and Sox2 (C) in iPSCs of control, patient B and patient T clones. ΔΔCT method was used to normalize the CT-values to the housekeeping gene β-actin, and with fibroblasts as reference (set to 1). Error bars represent the standard deviation of 3 technical replicates.*

Importantly, mRNA levels do not necessarily reflect the presence of the pluripotency marker proteins, as there are many levels of regulation in between an mRNA transcript and the protein end product (80). Thus, to detect the expression of the same pluripotent markers at protein level, and thereby confirm the pluripotency of the reprogrammed iPSCs, ICC was performed. This experiment revealed a presence of all the three pluripotency marker proteins (Nanog, SSEA4 and Oct4) in control and patients iPSCs, further supporting the statement of

successful iPSC generation (figure 3.3). All clones displayed similar expression patterns of marker proteins.

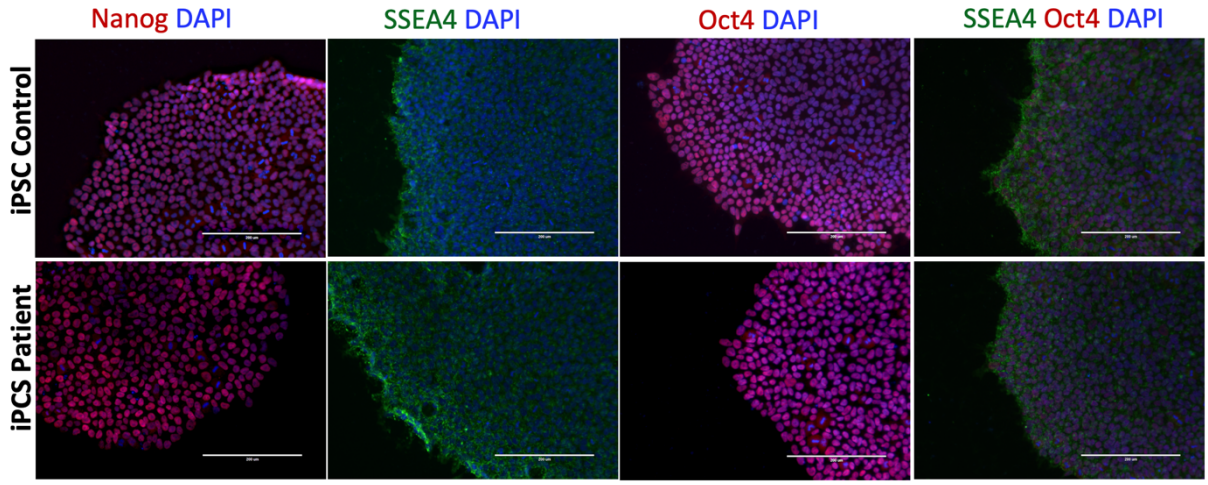

Figure 3.3. *Immunocytochemistry of the pluripotent marker proteins Nanog, SSEA4 and Oct4 in control and patient iPSC. Cell nuclei are stained with DAPI (blue). The two pictures on the right end are stained with both SSEA4, Oct4 and DAPI. One representative is chosen from each genotype. 20X magnification. Scale bars = 200 µm.*

3.1.3 Trilineage Differentiation

To further evaluate the quality and pluripotency of the iPSCs, cells were differentiated into the three germ layers and stained with markers for the designated layer. All of the iPSCs expressed the lineage specific markers (figure 3.4), indicating full potential in their ability to differentiate into the three germ layers.

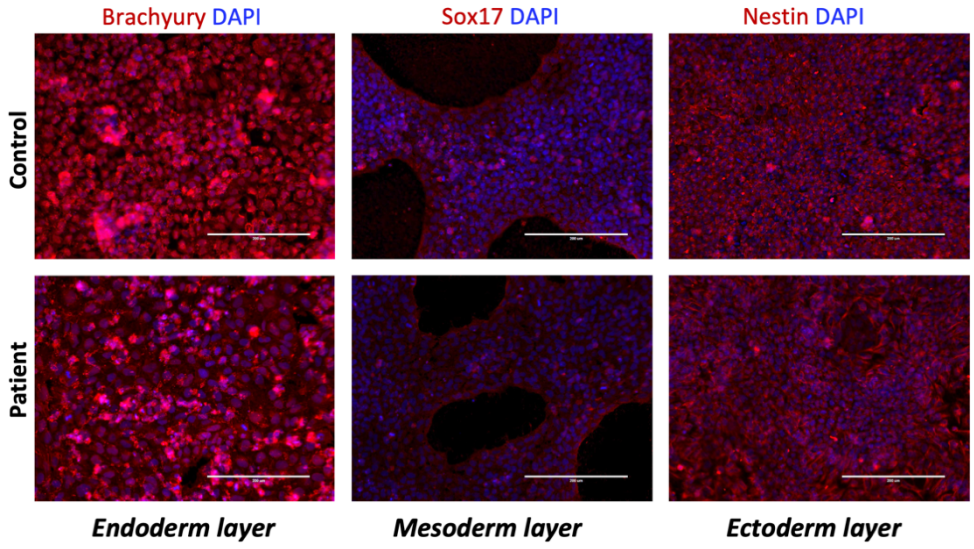

Figure 3.4. *Immunocytochemistry of the lineage marker genes; Brachyury (endoderm), Sox17 (mesoderm) and Nestin (ectoderm), in iPSC controls and patients, with DAPI to stain the nucleus. One representative is chosen from each genotype. 20X magnification. Scale bars = 200 µm.*

3.1.4 Genetic Analysis

A genetic analysis was performed on all the iPSCs listed in table 2.1, except AGc6. This was done to check for karyotypic abnormalities, as iPSCs are predisposed to genetic instability after several passages. The genetic analysis can detect 75% of the karyotypic abnormalities typically observed by cytogenetics. The results from the genetic analysis database, provided by Stemcell Technologies, is shown in figure 3.5. The figure showed no significant change in copy number of the tested loci, thus, indicating no karyotypic abnormalities in the iPSC clones.

Altogether, our data supports that the iPSCs generated from patient and control cells are indeed pure and high-quality iPSC populations.

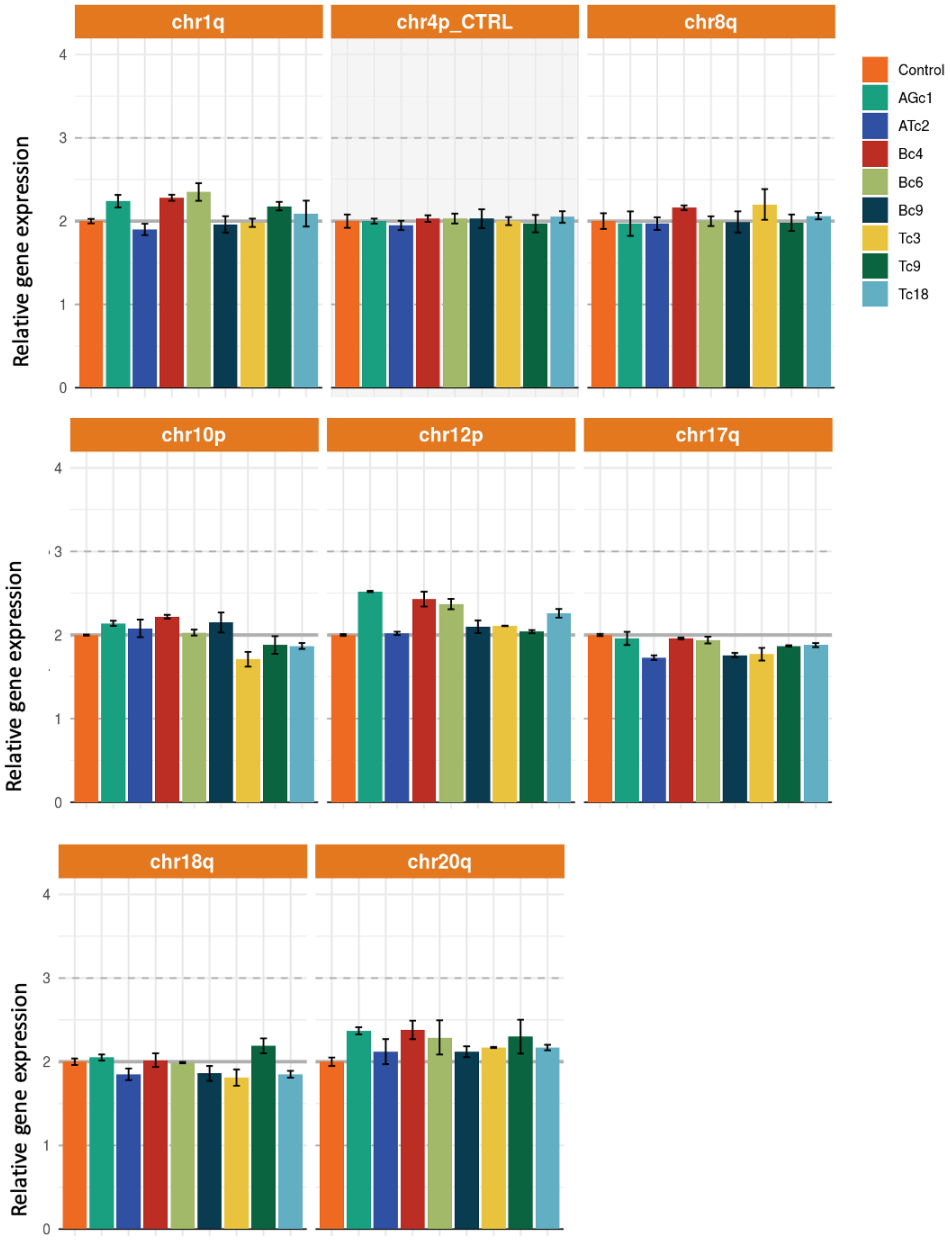

Figure 3.5. *Visual representation of the qPCR results provided by the genetic analysis database of Stemcell Technologies, using their "hPSC Genetic Analysis Kit". CT-values were normalized to Chr4p. Error bars represent the standard deviation of 3 technical replicates.*

3.2 Generation and Characterization of NPC

As the UCHL1-patients struggle with neurodegeneration, it is reasonable to investigate the impact of UCHL1 mutations in neuronal cells. NPC is the intermediate stage of CNS differentiated cells, with neurons being one of the terminal destinations. During this study, iPSC were successfully differentiated to NPC. However, there were persisting problems with the NPC culture, hindering further generation of mature neurons. Three different protocols were employed in an attempt to circumvent the poor survival of NPCs, however, with no success. In

the following section, a detailed description of NPC generation, characterization by studying morphology and presence of NPC markers by qPCR and immunocytochemistry, as well as functional experiments will be presented.

3.2.1 Generation of NPCs Using the Standard Protocol

Throughout the first months of this project, the "Standard Protocol", based on Qian *et al* (68) with minor modifications, was the main method used to generate NPCs from iPSCs. This procedure is based on growing a monolayer of NPCs. The iPSCs clones used for this protocol were the control: AGc1, AGc6, and patient: Bc4, Bc9, Tc3 and Tc9. Because cell differentiation is a dynamic and gradual process with cells in intermediate developmental stages, a purer NPC population is expected to be observed at later passage of the cells. Thus, it was desirable to reach at least passage 4-5, before conducting further experiments on the NPCs and initiating further differentiation to neurons. However, the NPCs never reached passage 5. Using the standard protocol, generated NPCs were healthy and survived until passage 3-4 (figure 3.6). After this point, a progressive increase in the number of dead cells was repeatedly observed for all clones. This led to the decision in switching to a commercial protocol.

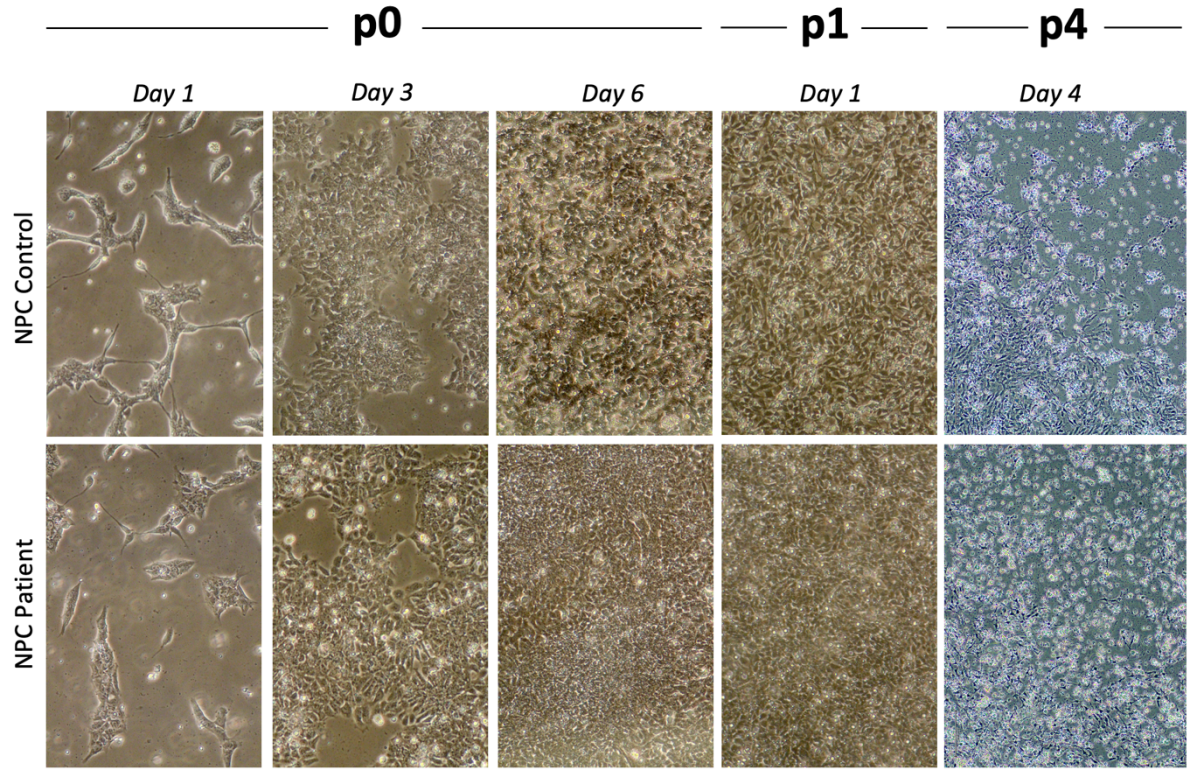

Figure 3.6. *Phase-contrast images of control and patient NPCs using the "Standard Protocol" in different days of passage 0 (p0), passage 1 (p1) and passage 4 (p4) with 10X magnification. The two images on the right end show a timepoint where the NPCs started to die. 4X magnification.*

3.2.2 Generation of NPCs Using the Stemcell Technologies´ Monolayer Protocol

It was reasonable to switch to a commercial protocol that was based on the same principle; iPSCs going directly to an NPC monolayer. In this attempt, we switched some of the iPSC clones to exclude contribution of poor survival due to clonal difference. One control iPSC clone (AGc6) and two patient iPSCs were switched (Bc9 and Tc9) to a new control iPSC: ATc2 and the patient iPSCs: Bc9 and Tc18. Using the Stemcell Technologies´ Monolayer protocol, the iPSCs immediately started to form an NPC monolayer, but rapidly died at the beginning of passage 1. This protocol was performed several times, but with the same outcome every time. Based on suggestions from Stemcell Technologies technical support, modifications on coating, cell density loading, and medium changing were made, but only slightly improved the cell survival (illustrated in figure 3.7). At this stage, it was decided to switch to the Stemcell Technologies´ NPC EB protocol as it is supposed to be a more robust method for fragile cells.

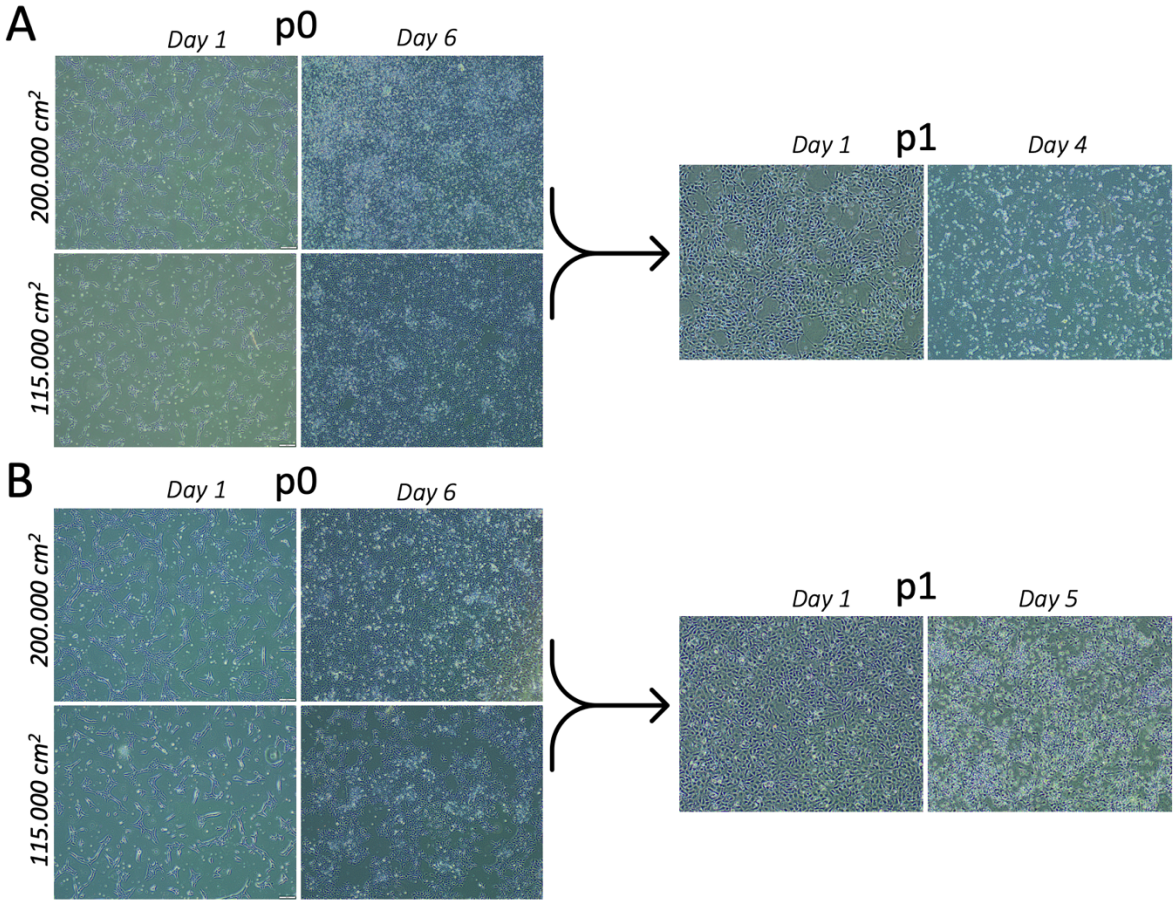

Figure 3.7. *Phase-contrast images of control (**A**) and patient (**B**) NPCs using the "Stemcell Technologies´ Monolayer Protocol" at different days in passage 0 (p0) and passage 1 (p1) with Matrigel coating (PLO/Laminin-coating showed no difference). Two different cell densities were tested from the beginning, specified at the left end of the images. The two images on the right end show initial stages of NPCs death. 4X magnification.*

3.2.3 Generation of NPCs Using the Stemcell Technologies´ EB Protocol

The EB protocol is based on forming EBs of iPSCs, and further plate the EBs to a standard plate to form neural rosettes, which eventually will expand to an NPC monolayer. Most of the EBs formed well-defined edges (figure 3.8A) but some of them were smaller. After multiple trials, only once neural rosette formation was observed (figure 3.8B). During the failed attempts, the replated EBs started to die from the middle (figure 3.8C, D). This problem persisted throughout several attempts, both for control and patient iPSCs.

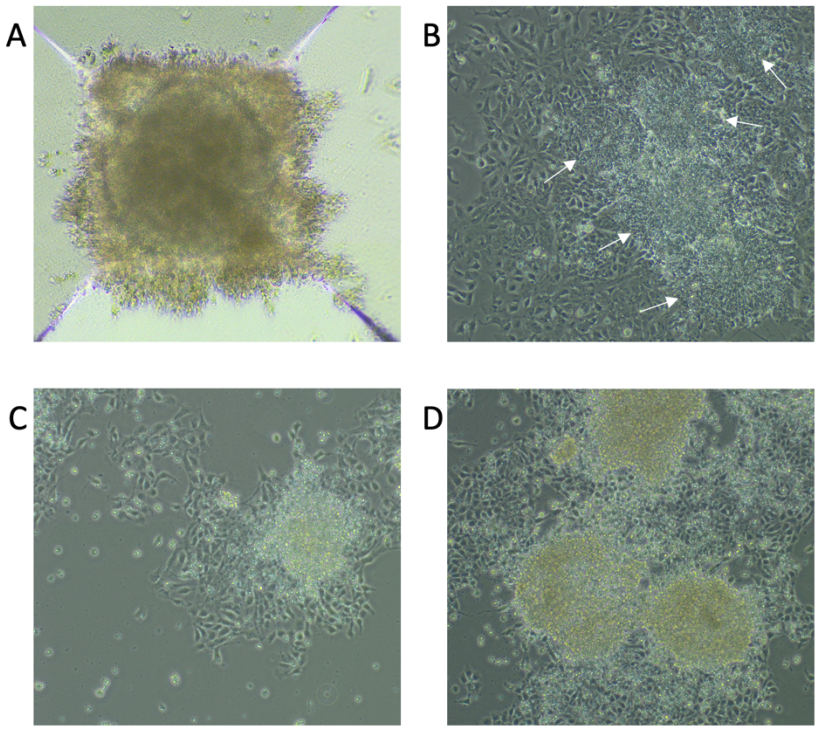

Figure 3.8. *Phase-contrast images from the "Stemcell Technologies´ EB Protocol" showing an embryoid body with clear edges at day 5 (**A**), a successful neural rosette formation (arrows) at day 8 of AGc1 control clone (**B**), and failed rosette formation at day 8 for ATc2 control clone (**C**) and Tc18 patient clone (**D**). Image C and D shows cell death of attached cells starting from the middle of the plate. 10X magnification.*

Previous work on our laboratory has demonstrated the ability of iPSCs to differentiate to at least NPC passage 6 using the "Standard Protocol". Thus, it was not expected that the NPCs would die at passage 3-4, after several attempts with our clones, using the same protocol. Due to time restrictions of this project, it was decided to switch to the Stemcell Technologies´ NPC monolayer protocol, considered to be a promising protocol to acquire good quality NPCs. However, the NPCs only reached early passage 1 before dying. Since neither of the monolayer-based protocols worked optimally, it was decided to optimize the seeding density and changing

the extracellular matrix. This only led to a minor increase in survival. However, the individual clones showed a variation in survival in different seeding densities, suggesting that the individual clones needed to have optimized seeding densities to increase cell survival. This hypothesis was supported by the troubleshooting section of Stemcell Technologies. As optimization of individual clones is outside the scope and feasibility of this project, a NPC differentiation protocol based on the formation of embryoid bodies and suggested to be more robust for cells that are challenging to differentiate, was explored. However, generated EBs were not sufficiently large, hindering the formation of neural rosettes. We also cultured the EBs for a longer period to ensure proper growth, as suggested in the troubleshooting section of Stemcell Technologies, however, with no success. The consisting problem with the NPC survival are still not entirely clear. It should be noted, however, that the E8 medium was used to culture the iPSCs instead of mTeSR™1/mTeSR™-E8™ suggested by the protocol. Alteration in cell media composition can change protein expression patterns contributing to differential responses to developmental stimuli.

Since the two commercial protocols did not improve NPC survival, and there was a time limitation hindering further optimization of each of the three protocols, as well as the exploration of a fourth protocol, we decided to employ the method with highest survival, i.e., the "Standard Protocol". Thus, NPCs generated via the Standard Protocol at earlier passages, where cells were usually still healthy, where used to perform functional assays.

As the problems with the NPC culture consisted, no neurons were generated. Bianchi *et al.* (81) and Grigor'eva *et al.* (82) each describes a protocol that generates motor neurons and GABAergic striatal neurons, respectively, directly from iPSCs without the need of generating NPCs as an intermediate stage. These protocols could serve as an alternative route to obtain mature neurons. The protocols also describe a time-frame shorter than the protocols used in this study.

3.2.4 Expression of NPC Markers

NPCs were characterized using qPCR and ICC to detect the expression levels of neuronal markers. qPCR was performed to detect the mRNA expression level of the NPC markers; Pax6, DcX, Nestin and Sox1. The pluripotency marker Nanog was also used to verify the level of undifferentiated cells in the NPC population. The qPCR analysis revealed high levels of mRNA expression of the Pax6 and Dcx in NPCs relative to the iPSCs (figure 3.9A, B). There were also observed higher levels of Nestin and Sox1 in NPCs than iPSCs (figure 3.9C, D), only revealing minor differences between the cell types. Furthermore, the pluripotent

marker Nanog was expressed in high levels in iPSCs, but not in the NPCs, indicating that the cells no longer had pluripotent features (figure 3.9E). No significant genotypic difference was observed.

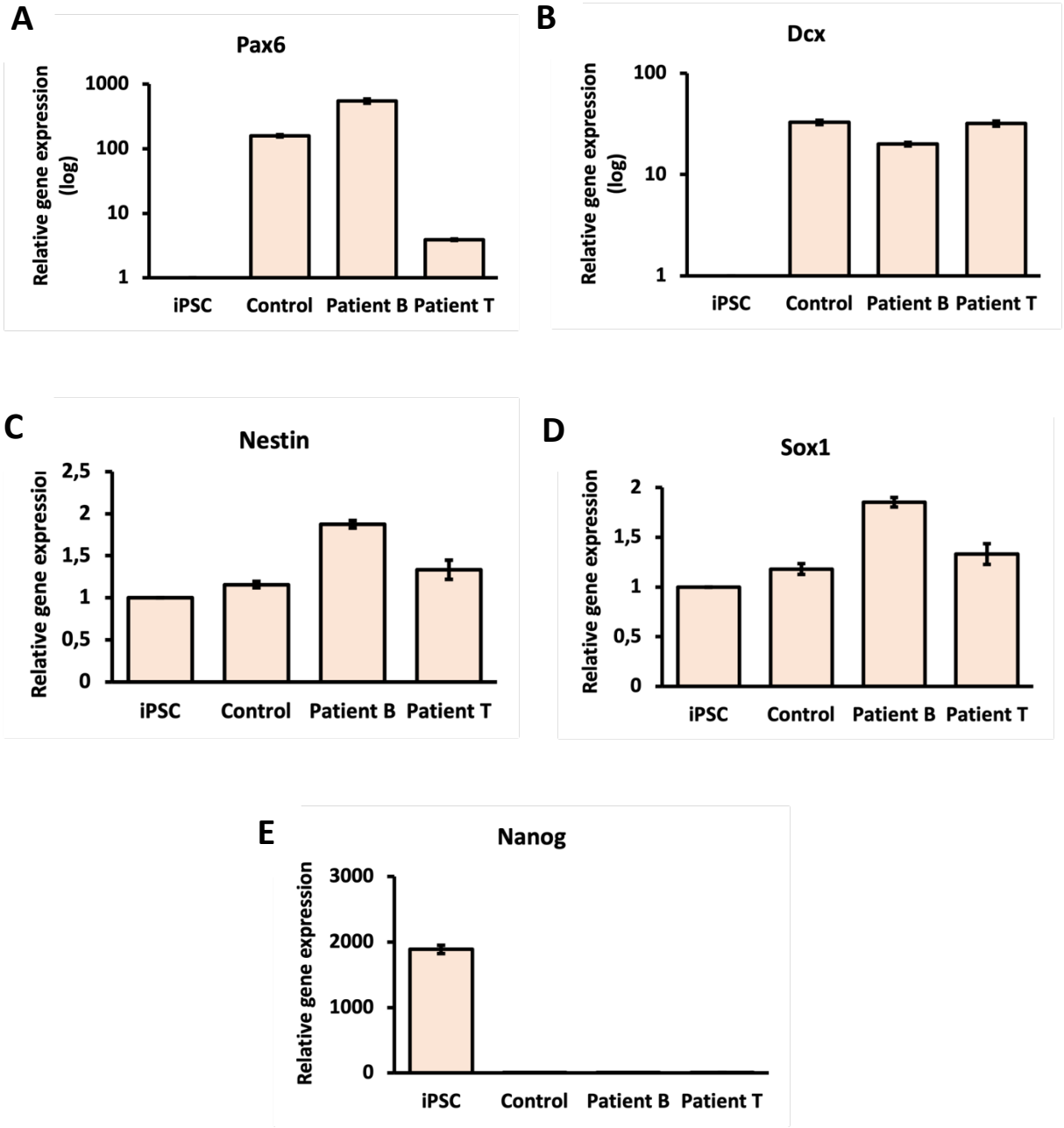

Figure 3.9. *mRNA expression levels of the neural cell markers Pax6 (**A**), DcX (**B**), Nestin (**C**) and Sox1 (**D**) in iPSC of a control clone, and NPCs of control and patient clones. Nanog (**E**) was used as a pluripotency marker. ΔΔCT method was used to normalize the CT-values to the housekeeping gene β-actin, and with iPSCs as reference (set to 1) except for Nanog. Error bars represent the standard deviation of 3 technical replicates.*

ICC was performed to confirm the existence of neural proteins in the cells (figure 3.10). Both MSI1 and Nestin were expressed in controls and patients NPCs, with no clear genotypic difference. Sox2 were only expressed in the patients NPCs.

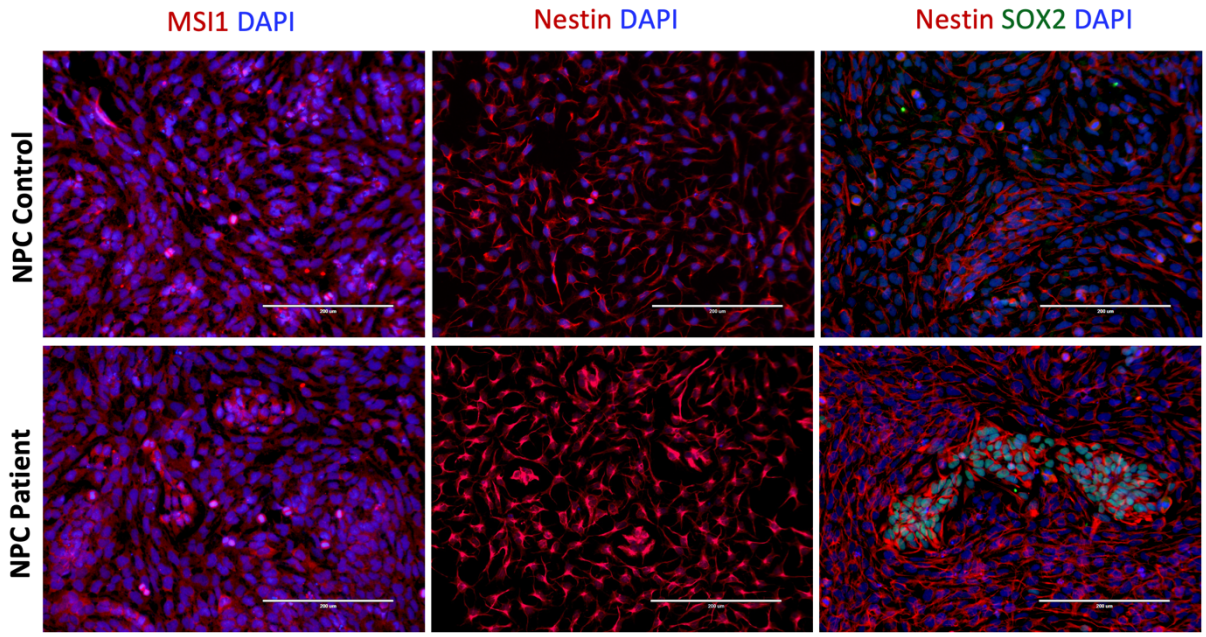

Figure 3.10. *Immunocytochemistry of the multipotency marker protein Sox2 and the neural marker proteins; MSI1 and Nestin in NPC controls and patients, with DAPI to stain the nucleus. One representative is chosen from each genotype. 20X magnification. Scale bars = 200 µm.*

Expectedly, the qPCR data show that the mRNA expression of the NPC makers Pax6 and DcX increased substantially in NPCs compared to the iPSCs. However, the Sox1 and Nestin expression only slightly increased in the NPCs. A possible reason for this could be due to spontaneous differentiation of the iPSCs to the ectoderm layer, thus also expressing the NPC markers in a higher level than expected. Nevertheless, the mRNA expression of the pluripotency marker Nanog was significant low in the NPCs, suggesting that the generated cells have differentiated and are no longer iPSCs. At protein level, both the neural markers MSI1 and Nestin were detected in control and patient NPC, while SOX2, was detected only in the patient-derived NPCs. The latter could be explained by the fact that the NPCs are heterogenous, thus, existing in different stages of their path to become a pure NPC population. Additionally, pluripotent markers were not detected in NPCs (data not shown). Taken together, our morphological, qPCR and ICC data reveals that the generated cells are in fact NPCs.

3.3 Generation and Characterization of Cerebral Organoid

To investigate whether the altered UCHL1 was associated with neurodegenerative disorders in the patients, we aimed at generating brain organoids from control and patient-derived iPSCs using the Lancaster *et al*. protocol (53). To successfully form cerebral tissue, it was sufficient to choose iPSCs with optimal morphology and no sign of differentiation.

3.3.1 Generation of Cerebral Organoids

The optimal iPSCs are round and have well-defined edges (figure 3.11A). Already after 24 hours the iPSCs formed embryoid bodies. The growth of the EBs varied greatly, with some growing up to 4-500 μM in diameter showing optimal morphology with a well-defined border and brighten (figure 3.11B), while others growing at slower rate, only up to 1-200 μM in diameter, displaying a darker shade (figure 3.11C). The optimal EBs got transferred to new medium for induction of neuroectodermal formation.

Signs of neural induction were observed when the EBs formed radial organization of pseudostratified epithelium, exhibiting the neuroepithelium, which is translucent and develops on the outer surface (figure 3.11D). Some of the EBs never became translucent and had a consistent dark shade, indicating failed neural induction (figure 3.11E). The EBs with neural induction were embedded in Matrigel to enhance growth of neuroepithelial buds and general expansion as seen in figure 3.11G. However, some tissues failed to develop neuroepithelial buds, and instead showed signs of direct neural differentiation (figure 3.11F). The embedded organoids were transferred to a spinning flask or shaker, which allowed for further growth and development of the cerebral organoid. After the transfer, it was observed that the suboptimal organoids started to dissolve and die (figure 3.11H). Conversely, the optimal organoids continued to grow showing more complex structure (figure 3.11I, J). After a few weeks pigmented regions of the organoids was observed with the naked eye, possibly indicating retinal region development.

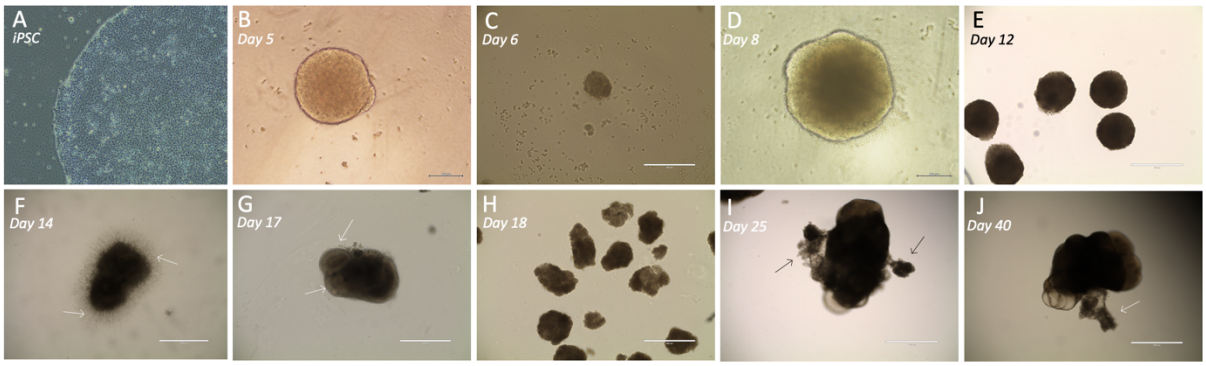

Figure 3.11. *Development of cerebral organoids from control and patient iPSCs, showing optimal (A, B, D, G, I and J) and suboptimal (C, E, F and H) morphology.* ***(A)*** *An optimal iPSC colony showing clear edges with no sign of differentiation.* ***(B)*** *Optimal EB at day 5 brightened around the surface with smooth edges. 400 µM in diameter.* ***(C)*** *A small EB at day 6 with some cell debris and lacking a clear, bright edge. 200 µM in diameter.* ***(D)*** *EB at day 8 showing signs of neuroectodermal differentiation with translucent radial pseudostratified neuroepithelium. 600 µM in diameter.* ***(E)*** *EBs at day 12 lacking translucent edges and have a darker shade, indicating failed neural induction.* ***(F)*** *An organoid at day 14 which failed to form neuroepithelial buds, and instead display direct neural differentiation signs (arrows).* ***(G)*** *An ideal organoid at day 17 that has formed neural epithelial buds surrounding a visible lumen (arrows).* ***(H)*** *Organoids that failed the neural induction and dissolving.* ***(I, J)*** *A healthy organoid at day 25 and day 40, respectively, revealing neural tissue that has greatly expanded. Non-neuroepithelial cells that have escaped the neural induction, often fibroblast-like cells (arrows). These cells typically migrate away from the organoid, appearing to promote neuroepithelial bud outgrowth. Scale bars = 200 µm (B, D), 400 µm (C, E, G) and 1000 µm (F, I, J).*

3.3.2 Characterization of Cerebral Organoids

To identify regions of the brain organoids throughout its development, immunohistochemistry analysis was performed on slides of organoids at three different time points: 2 weeks, 1 month and 2 months after moving the organoid to its final destination for growth and expansion in suspension (figure 3.12). After growing for 2 weeks in suspension, Pax6 expression was detected around ventricle-like cavities indicating expanding neuroepithelium (figure 3.12A). Nestin and Sox2 expression were observed mainly at the edges while Tuj1 levels were quite low, indicating only occasional neuronal differentiation (figure 3.12A, B). About 1-2 months after moving to the suspension culture, the organoids expressed more of NPCs, marked by expression of Nestin (figure 3.12C) and of Sox2 (figure 3.12D-E, G), marking the expression of radial glias (RGs) at the ventricular zone (VZ), forming the pseudostratified layer of neuroepithelium. In addition, higher levels of Tuj1 were detected, indicating more neurons formed at 1 month and 2 months, surrounding the ventricular zone (VZ) (figure 3.12D, E). At 2 months the SOX2 expression was observed mainly on the outer

surface of the organoid, while the Tuj1 expression was evenly distributed across the organoid (figure 3.12F).

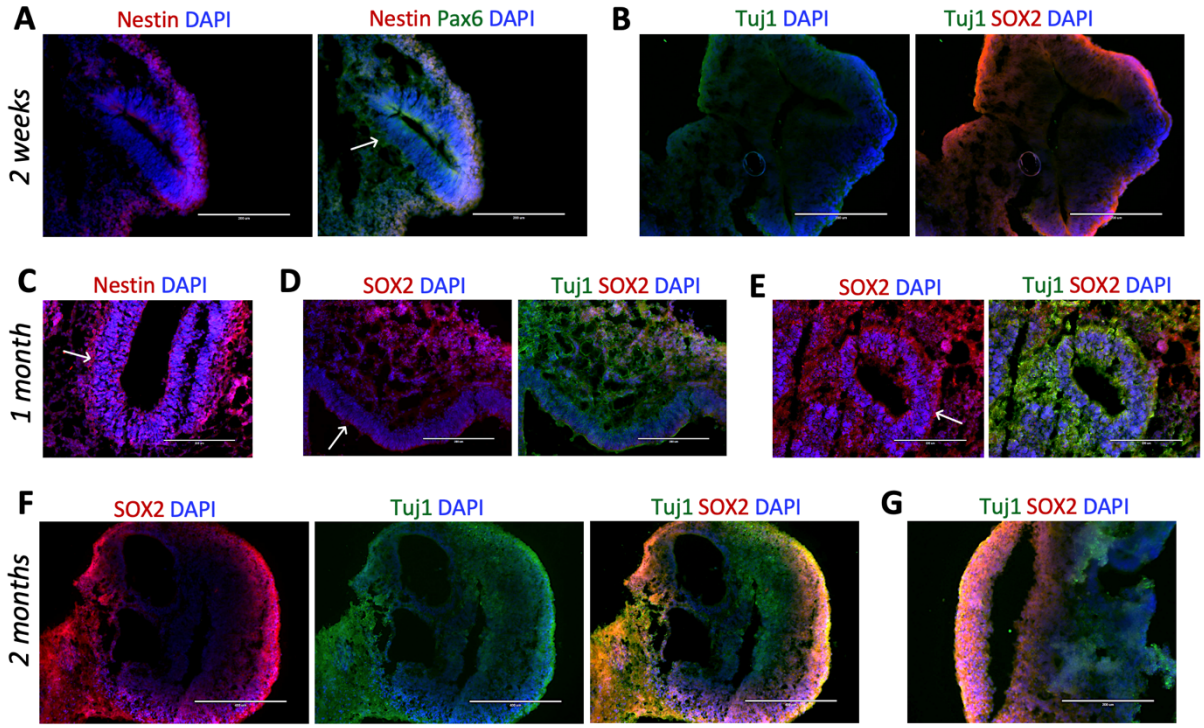

Figure 3.12. Immunohistochemical characterization of growing cerebral organoids at several time points. (A) *Detection of expanding neuroepithelium using Pax6 (green, second panel) and NPCs via Nestin (red) in organoids cultured for 2 weeks; (**B**) Weak staining of neurons, stained byTuj1, and RGs marked with SOX2 (red, second panel) in 2-week-old organoids. (**C**) Detection of NPCs (Nestin) in 1-month-old organoids. (**D, E**) Staining for RGs, SOX2, and neurons, Tuj1, in 1-month old organoid and (**F, G**) and 2-month-old organoids. Arrows indicate the ventricle-like cavities with pseudostratified neuroepithelium. Scale bars = 200 µm (**A-E, G**) and 400 µm (**F**).*

Patient-specific cerebral organoids provide a great tool for studying brain development and neurological disorders. This is a relatively new technology; thus, many of the current existing protocols have potential for improvements.

When following the Lancaster *et al*. protocol (53), we experienced problems with forming EBs. However, by switching to another medium from a study by Mariani *et al*. (67) we observed major improvements. We also experienced poor growth of EBs, and lack of neural induction. According to the troubleshooting section in the Lancaster *et al*. protocol (53) it is essential that the iPSCs are of high quality and have no karyotypic abnormalities. Additionally, EBs should not be transferred too early – nor too late, from the first plate where they grow. As a great amount of EBs was generated at the same time, and the neural induction timing varied highly amongst the EBs, it would be challenging and time-consuming to match the timing for each of the EBs, individually. Over several batches, the lack of neural induction in the EBs was

especially consistent within the patient organoids. Thus, only cerebral organoids from control iPSCs were successfully generated, confirmed by ICC. It might be that the patient-derived cells need specific conditions to successfully generate organoids. Alternatively, as there are no reports on the generation of cerebral organoids from UCHL1-patient cells, we cannot rule out that UCHL1 alteration may be a major contributor for the lack of success in growing patient-derived brain organoid.

As the Lancaster *et al*. paper states (53), the generated brain organoids lack the meninges; a three-layered membrane along the surface of the brain (83), and vascularization; blood vessels within the brain tissue, which limits the growth of the organoids. This further contributes to a stochastic growth pattern of the neural tissue, which is among other things dependent on the access of nutrients. For this reason, there is a significant variability between the organoids, especially between organoids cultured in different dishes and time points.

Nonetheless, the cerebral organoid protocols are constantly evolving and improving (84). Very recently, Shi *et al*. (85) introduced a new method that overcomes the issue of vascularization, namely by transplanting the organoids into a mouse cortex.

3.4 Viability Assay in Response to Drug Modulation and Enzymatic Assays

The major goal of this part of the study was to determine whether exposure to drugs that modulate the UPS affects differently the survival of control- and patient-derived NPCs. To this end, cells were treated with the proteasome inhibitors: MG132, Bortezomib and Epoxomicin.

3.4.1 Cell Proliferation Assay

To determine appropriate concentrations of the three different proteasome inhibitors, multiple attempts were done with a large range of concentrations at 24 hours. The goal was to determine drug concentrations that affected cell growth without immediately killing the cells. The final steps of this fine-tuning process are shown in figure 3.13.

Notably, the initial number of cells varied greatly between the NPC clones, demonstrated by the values without drug exposure. While the control clones in this experiment displayed initial cell number like observed in previous assays with healthy NPCs, the patient clones showed a significantly lower initial number of cells. In fact, the initial values of Tc3 are similar to background levels, indicating that these cells were likely dead. The precise reasons for these variations are not entirely understood.

It should be noted that the initial cell number was fine from the start (0 hours), and that the variations were not observed until after 24 hours. This indicates that the cell number variation is not due to poor counting of cells. However, as the cells were in passage 4, a time point preceding the often-observed progressive cell death, it might be that patient cells were more sensitive and had already initiated the cell death process at the time of the experiment.

Nevertheless, as healthy control cells are considered the normal state, and therefore, the standard, appropriated drug concentration ranges were selected based on the response observed in control clones. Thus, for MG132 a dose between 62.5-125 nM (100 nM), as well as 7.5 nM Bortezomib and 10 nM Epoxomicin were selected as suitable doses to investigate a long-term effect in cell viability.

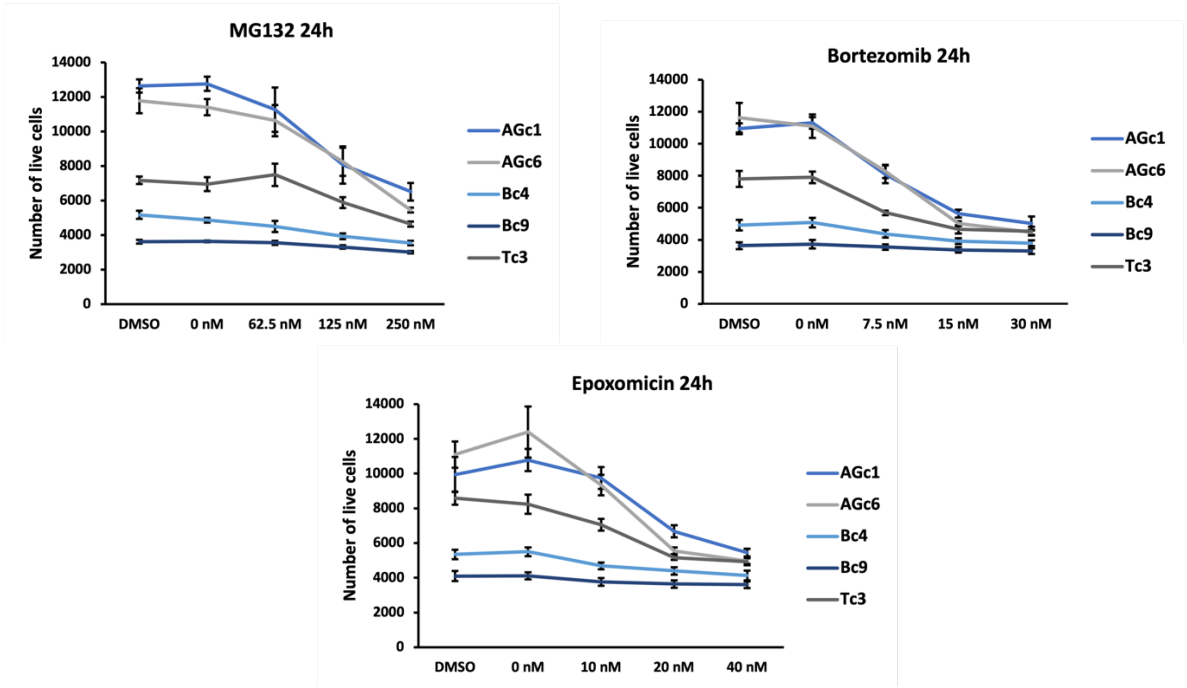

Figure 3.13. *24-hour survival assay to investigate the control and patient NPCs at passage 4 in response to the proteasome inhibitors: MG132, Bortezomib and Epoxomicin. The error bars represent the standard deviation of six technical replicates.*

Cells were then treated with the selected doses and cell viability was monitored at four different time points between 0-72 hours (figure 3.14). The goals of this assay were to confirm that the selected doses were appropriated, to investigate whether control and patient NPCs are differentially affected by the drugs in long-term and to identify a suitable time point to validate the observed drug responses by flow cytometry. However, none of the patient clones survived during the experiment and were therefore not included in figure 3.14. And once again, as control

cells reflect the standard conditions, this experiment was used to delineate optimal drug doses and time point for further evaluation of survival by flow cytometry.

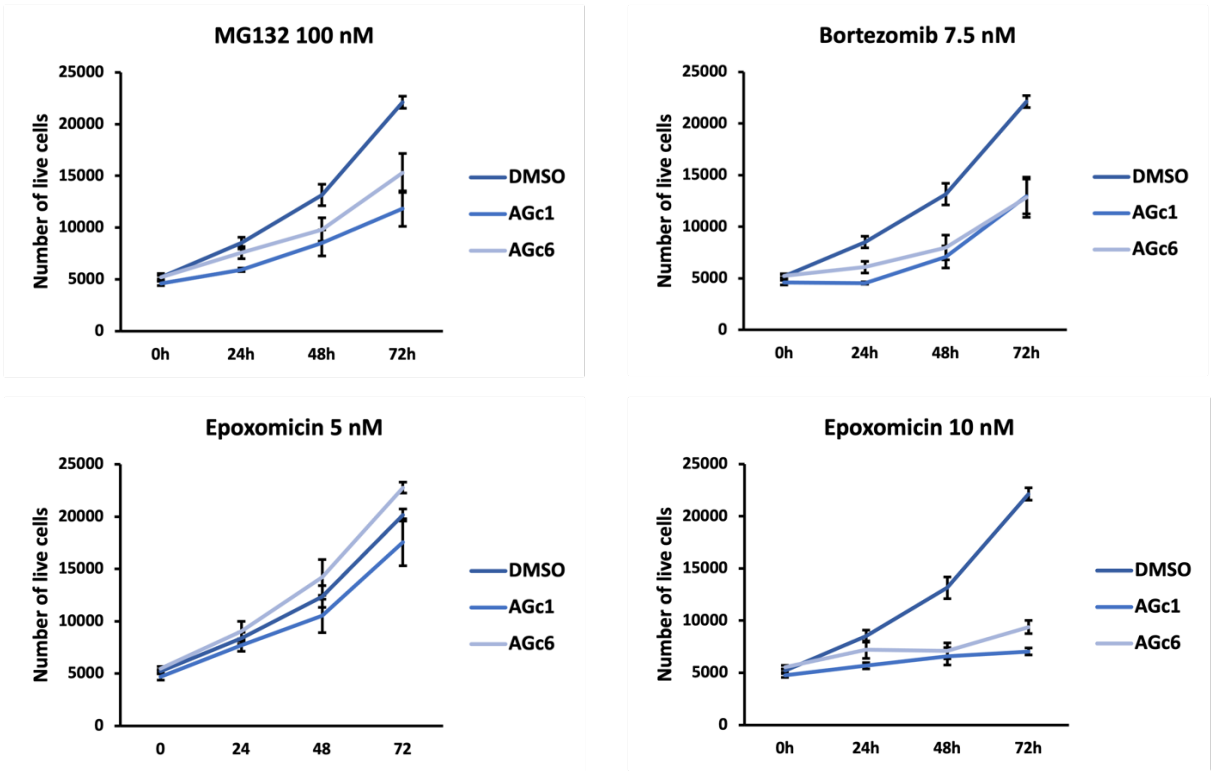

Figure 3.14. *Proliferation assay of control NPCs at passage 3 in response to the proteasome inhibitors MG132, Bortezomib and Epoxomicin. The error bars represent the standard deviation of six technical replicates.*

The results in figure 3.14 confirmed that appropriate proteasome inhibitor concentrations are 100 nM for MG132, 7.5 nM for Bortezomib and somewhere between 5-10 nM for Epoxomicin. In addition, a clearer effect on cell survival was observed at 48 hours compared to 24 hours. It was observed an even greater response at 72 hours, but as there was observed sudden cell death at 72 hours in previous experiments, 48 hours was selected as the optimal time point for further tests.

3.4.2 Flow Cell Cytometry

The differentiation of iPSCs to NPCs is a dynamic process, in which the NPCs are composed of subpopulations of early, intermediate, and mature NPCs, in other words, is a heterogenous population with cells at different stages of differentiation. The different clones presumably have a different distribution of the NPC subpopulations, that could respond differently to the drugs. For this reason, flow cell cytometry was performed with the drug

concentrations and time point delineated on the proliferation assay in figure 3.13. Additionally, flow cytometry would provide a more accurate picture between live and dead cells, as this method is more sensitive compared to the PrestoBlue™ quantification, used for the viability and proliferation assay. Hence, an experiment including control and patient NPCs was designed and samples were prepared for flow cytometry analysis, which was performed by the senior engineer Nina-Beate Liabakk at IKOM, NTNU. However, according to the data analysis, 90% cell death was observed across all samples, both treated and untreated NPCs (not shown).

The enormous number of dead cells was not expected, but unfortunately, we were unable to investigate the underlying reason due to the limit of time. Thus, this experiment was performed only once.

3.4.3 Proteasome 20S Activity Assay

To investigate the basal level of proteasome activity in control and patient iPSCs and NPCs, the 20S proteasomal activity was measured using the Proteasome 20S Activity Assay Kit (Sigma-Aldrich). The iPSC proteasomal activity between the controls and patients in iPSCs is shown in figure 3.15. Cells treated with Epoxomicin are included as negative control, since their proteasomal activity is expected to be fully inhibited. As illustrated in figure 3.15, no clear differences in proteasome activity were observed between controls and patients of the iPSCs.

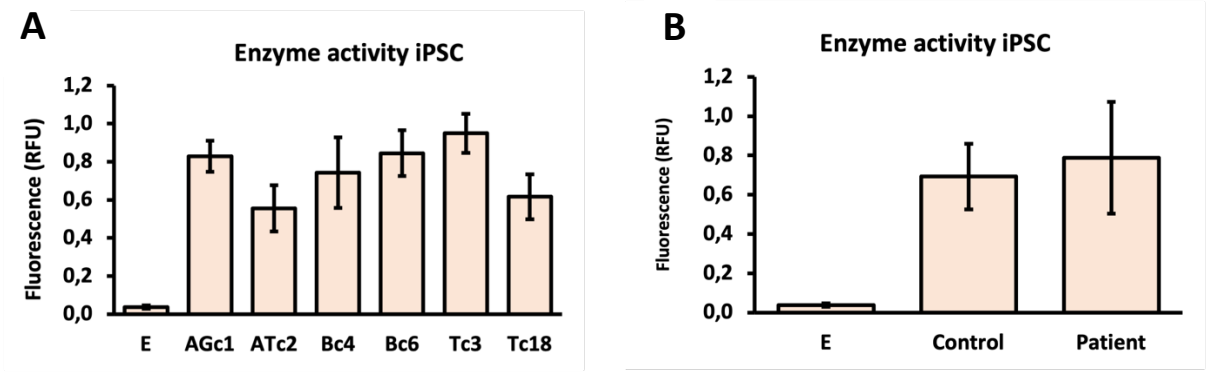

Figure 3.15. *Detection of basal proteasome activity in control and patient iPSCs. (**A**) Illustrating the measurement of each of the iPSC clones. (**B**) Illustrating the measurement in control and patient groups. Ex/Em = 485/520. The error bars represent the standard deviation of 2 technical replicates.*

The basal proteasomal activity measured in the different clones of NPCs at passage 3 is shown in figure 3.16A. The result showed a huge variation between the clones, and also had some negative values. The signal from medium without cells was measured and subtracted from the corresponding values of NPC clones, to decrease background signals that were not specific for the proteasome activity and could account for the negative values in samples where the

activity lies within the detection limit. The experiment was repeated to check its reproducibility (figure 3.16B). This time, negative signal was observed in all the samples after background subtraction, suggesting that the signal in the samples with cells was lower than the signal from the sample without cells. Together with the results from the previous experiment, it seemed like the NPC medium signal highly contributed to unspecific fluorescent signal, disturbing the signal specifically measured from the substrate.

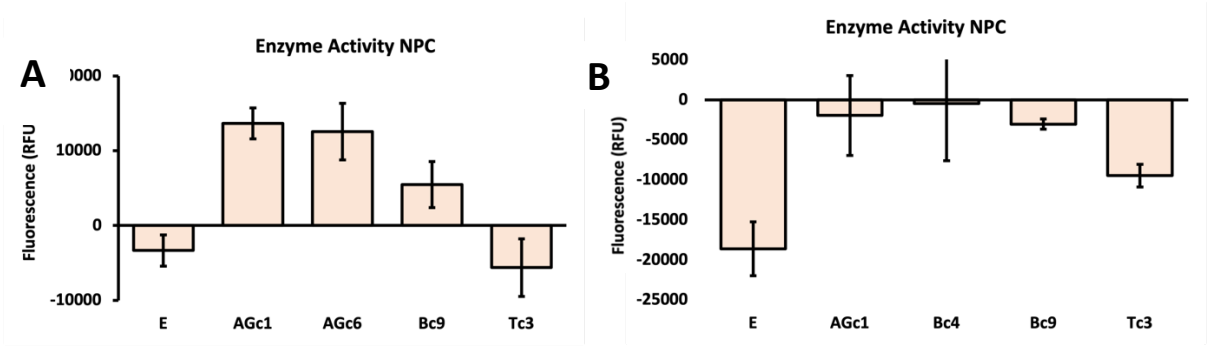

Figure 3.16. *Detection of basal proteasome activity in control and patient NPCs at passage 3 the first time (**A**) and second time (**B**). Ex/Em = 485/520. The error bars represent the standard deviation of 3 technical replicates.*

A new experiment was set up without any cells or the specific fluorophore to measure the proteasome activity, only leaving the medium inside. The two main components of the NPC medium (Neurobasal and DMEM/F12) were tested separately and together, as well as a new possible candidate for this experiment, MEM, which is transparent in contrast to the other two (figure 3.17). In addition, the healthy control NPC with the fluorophore in the NPC medium (dark blue bars) was added to the diagram as a comparison. Both 100 µl and 50 µl was tested to verify if the signals were specific, and therefore, decrease by about half in the 50 µl samples. There was approximately 50 µl of Neurobasal and 50 µl of DMEM/F12 together in one sample run of NPCs. The results showed that the NPC medium had a higher signal than the sample with NPCs and the fluorophore. For Neurobasal and DMEM/F12 alone, the Neurobasal had approximately a signal as high as the NPCs for 100 µl, corresponding to nearly half the signal for 50 µl. The DMEM/F12 had substantially lower signal than the Neurobasal, along with the MEM.

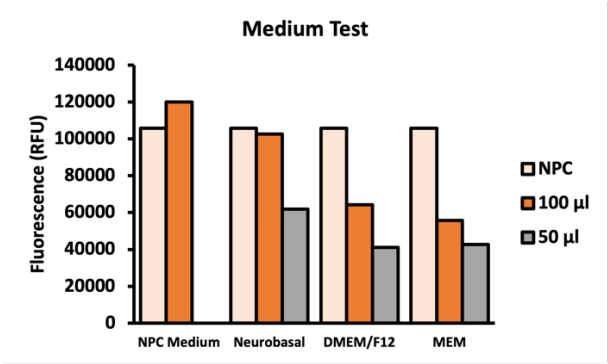

Figure 3.17. *Detection of background fluorescence in different media for NPCs compared to NPCs with the fluorophore (dark blue bars) included to reflect its proteasomal activity. Ex/Em = 485/520.*

This data supports the hypothesis that the NPC medium has a higher fluorescence signal than the specific signal coming from the NPC proteasomal activity. Stadtfeld *et al*. (86), along with several other studies, have previously demonstrated that phenol red contributes to increased levels of background fluorescence. As both Neurobasal and DMEM/F12 contain this component, it is reasonable to think that this is what explains the high level of background signal. This is further supported by MEM having lower fluorescence signal, as this does not contain any phenol red, but is a transparent medium. If more time was provided, the next step would be to measure the NPC proteasome activity in MEM instead of the NPC medium.

3.5 Mass Spectrometry Analysis

Mass spectrometry analysis was performed to determine global alterations in protein expression profiles, as well as in levels of proteins associated with the UPS, in control and patient derived cells at two different developmental stages: iPSCs and NPCs.

3.5.1 Group Comparison of Patient and Control iPSC

A group comparison analysis between patient and control iPSCs identified 4017 proteins. To identify proteins that are significantly changed between the groups, a cut-off of Benjamini-Hochberg adjusted p-values (Corrected P-value BH)≤0.3 was adopted, resulting in only 14 proteins (see table 3.1 & figure 3.18). The first three proteins mentioned in the table are downregulated in the patient iPSC, and the ones below are upregulated in patients relative to the control iPSCs.

Table 3.1. *Proteins identified in a group comparison of patient and control iPSCs from mass spectrometry within a criteria of corrected p-value BH<0.3.*

UniProt Code	Protein Name	Gene	Fold change	Corrected P-Value BH	T test P-value	Log2 Median Change
Q86XZ4	Spermatogenesis-associated serine-rich protein 2	SPAS2	0,53	0,28	0,00407	-0,92
Q04727	Transducin-like enhancer protein 4	TLE4	0,78	0,28	0,00407	-0,36
Q7Z4S6	Kinesin-like protein KIF21A	KI21A	0,79	0,11	0,00133	-0,35
Q9BRT6	Protein LLP homolog	LLPH	1,17	0,25	0,00330	0,23
P62081	40S ribosomal protein S7	RS7	1,20	0,22	0,00278	0,26
Q8NFH4	Nucleoporin Nup37	NUP37	1,22	0,26	0,00356	0,29
P53701	Cytochrome c-type heme lyas	CCHL	1,25	0,03	0,00031	0,32
P35249	Replication factor C subunit 4	RFC4	1,28	0,28	0,00408	0,36
P80365	Corticosteroid 11-beta-dehydrogenase isozyme 2	DHI2	1,44	0,05	0,00055	0,53
Q5SSJ5	Heterochromatin protein 1-binding protein 3	HP1B3	1,48	0,28	0,00416	0,57
O96005	Cleft lip and palate transmembrane protein 1	CLPT1	1,50	0,17	0,00205	0,59
Q14696	LRP chaperone MESD	MESD	1,51	0,17	0,00199	0,60
P52630	Signal transducer and activator of transcription 2	STAT2	1,67	0,20	0,00243	0,74
Q9UHI5	Large neutral amino acids transporter small subunit 2	LAT2	2,17	0,24	0,00312	1,11

A second selection based on fold change was performed, and only proteins with a fold change ≥ 2 were considered. The only protein that fulfilled this requirement is marked in blue in table 3.1, namely, LAT2, and marked in purple (figure 3.18).

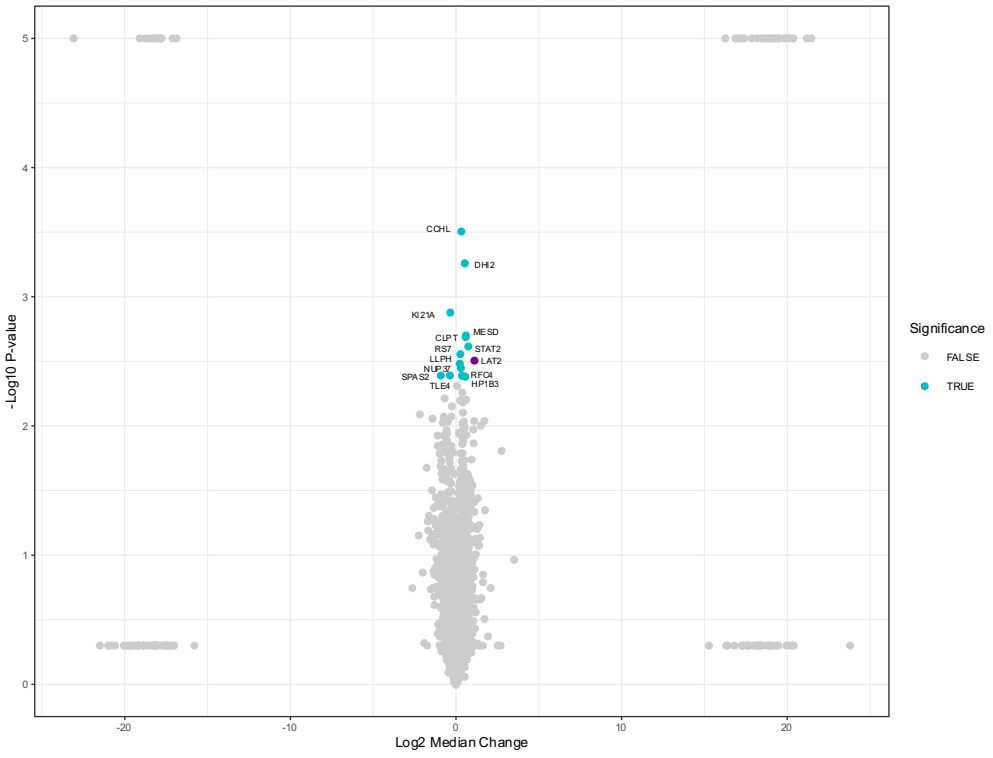

Figure 3.18. *Volcano plot highlighting the significant proteins based on corrected P-value BH<0.3 (blue dots), when comparing patient and control iPSC groups quantified by mass spectrometry analysis. Labels are given as gene names. The only protein with a P-value BH<0.3 and fold change ≥ 2 is marked in purple.*

Not surprisingly, the majority of quantified proteins showed similar levels in control and patients at the iPSC stage. A longer list of up- and down-regulated proteins is expected to be observed at later developmental stages, such as at the mature neuron/forebrain neurons. At mature developmental stages, phenotypes are fully established, and the cell proteome reflects in higher magnitude the alterations/dysregulations in molecular networks that characterize a disease. Nevertheless, the MS data pinpoints alterations in LAT2 in patient-derived cells already at the iPSC stage.

Large amino transporter 2, LAT2, function as transporter and exchanger of neutral amino acids when associated with SLC3A2/4F2hc. High expression of LAT2 is seen in kidney, and moderate expression is reported in placenta and brain, followed by other tissues (87). A study by Kido *et al*. (88) indicated that LAT2 function as an amino acid transporter at the blood-brain barrier. Another study by Zielinska *et al*. (89) suggests that upregulation of LAT2 leads to increased efflux of arginine in exchange of extracellular glutamine, which is linked to an altered nitric oxide/cGMP pathway. cGMP, a second messenger molecule important in the brain (90), modulates several downstream effects, such as retinal phototransduction and neurotransmission (91). Nitric oxide (NO) upregulation of cGMP has been associated with several effects, like improved cognitive function (90). This is interesting, as both visual loss and improved cognitive function is observed in the UCHL1-patients.

3.5.2 Group Comparison of Patient and Control NPC

Interestingly, the group comparison of patient and control NPCs at passage 3 also resulted in 4017 identified proteins. After the same cut-off based on the corrected p-value-BH as for iPSCs, 17 proteins were identified (see table 3.2 & figure 3.19). In the table, the eight first proteins are downregulated in the patient NPCs, while the next nine proteins are upregulated compared to the control NPCs.

Table 3.2. *An overview over the proteins identified in a group comparison of patient and control NPCs at passage 3 from mass spectrometry within the criteria of corrected p-value-BH ≤ 0.3.*

UniProt Code	Protein Name	Gene	Fold change	Corrected P Value BH	T test P value	Log2 Median Change
P09936	Ubiquitin carboxyl-terminal hydrolase isozyme L1	UCHL1	0,43	0,12	0,00140	-1,22
Q99653	Calcineurin B homologous protein 1	CHP1	0,45	0,24	0,00325	-1,15
O43602	Neuronal migration protein doublecortin	DCX	0,46	0,02	0,00026	-1,11
Q96IR7	4-hydroxyphenylpyruvate dioxygenase-like protein	HPDL	0,55	0,22	0,00292	-0,87
P54652	Heat shock-related 70 kDa protein 2	HSP72	0,65	0,29	0,00426	-0,62

Q6UVK1	Chondroitin sulfate proteoglycan 4	CSPG4	0,68	0,29	0,00423	-0,55
P38606	V-type proton ATPase catalytic subunit A	VATA	0,85	0,29	0,00400	-0,24
P53621	Coatomer subunit alpha	COPA	0,96	0,05	0,00053	-0,06
Q12824	Isoform B of SWI/SNF-related matrix-associated actin-dependent regulator of chromatin subfamily B member 1	SNF5	1,09	0,14	0,00164	0,13
Q16658	Fascin	FSCN1	1,11	0,03	0,00030	0,15
P49736	DNA replication licensing factor MCM2	MCM2	1,13	0,15	0,00193	0,17
Q99816	Tumor susceptibility gene 101 protein	TS101	1,21	0,18	0,00225	0,27
Q6Y7W6	GRB10-interacting GYF protein 2	GGYF2	1,27	0,02	0,00025	0,34
Q13085	Acetyl-CoA carboxylase 1	ACACA	1,27	0,28	0,00378	0,35
Q9Y2R5	28S ribosomal protein S17, mitochondrial	RT17	1,34	0,11	0,00125	0,43
Q5HYK3	2-methoxy-6-polyprenyl-1,4-benzoquinol methylase, mitochondrial	COQ5	1,44	0,14	0,00168	0,53
P07197	Neurofilament medium polypeptide	NFM	4,13	0,29	0,00428	2,05

In the NPC group comparison, four proteins had a fold change ≥ 2. Namely the blue-marked proteins in the table; UCHL1, CHP1, DCX and NFM. The proteins are marked in purple in the volcano plot (figure 3.19).

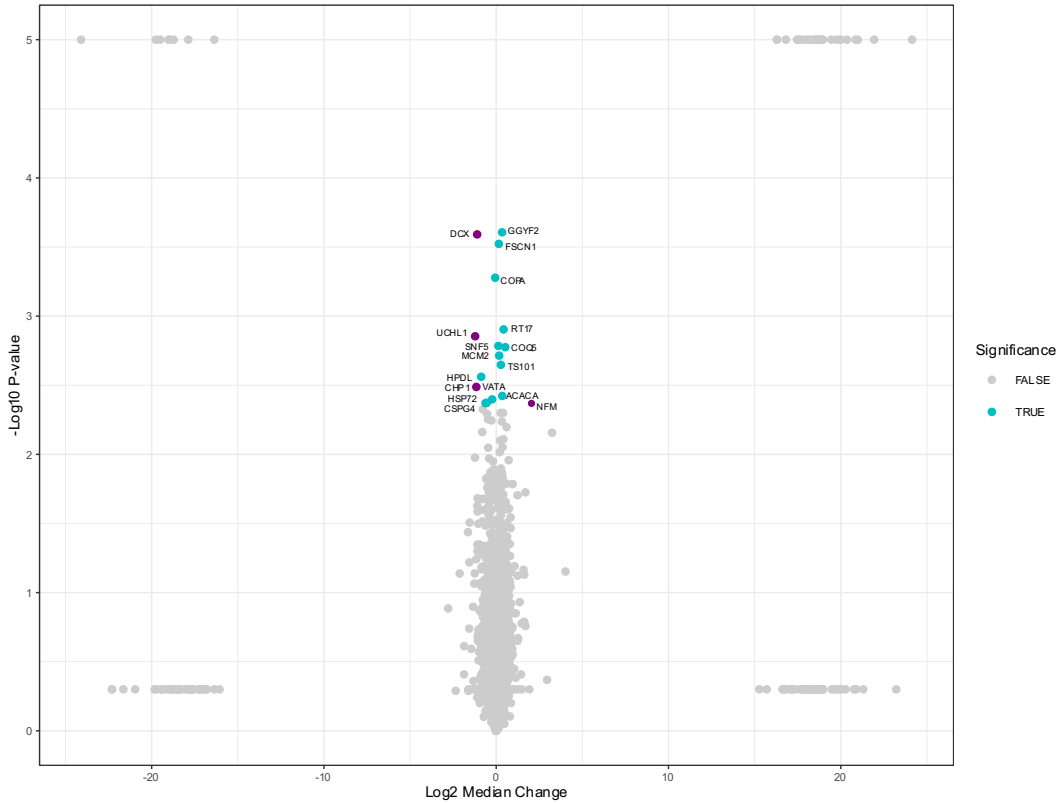

Figure 3.19. *Volcano plot highlighting the significant proteins based on corrected P-value BH<0.3 (blue dots), when comparing patient and control NPC groups quantified by mass spectrometry analysis. Labels are given as gene names. Proteins with P-value BH<0.3 and fold change ≥ 2 are marked in purple.*

Markedly, UCHL1 was the most downregulated protein (about 2 times) in the patient derived NPCs. A 4-fold decrease in UCHL1 levels has been previously reported in fibroblasts from the same patients (1). Lower levels of UCHL1 already at the NPC stage could be an early sign of a progressively decrease in the enzyme levels in fully differentiated brain cells. Due to the high levels of UCHL1 in normal brain, it would not be surprising if this enzyme plays more important roles in brain cells compared to its roles in, for example, fibroblasts. It would have been quite interesting to determine whether the UCHL1 levels in patient-derived mature brain cells are further down-regulated and whether the levels vary in distinct brain regions.

The second-most downregulated protein in the patient NPCs, compared to control cells is the Calcineurin B homologous protein 1, Chp1, which is a Calcium-binding protein involved in processes such as the Na^+/H^+ exchanging on the plasma membrane (92). It has later been identified as an ARCA-causing gene in humans (93). ARCA is short for autosomal recessive cerebellar ataxia and comprises of rare neurological disorders mainly related to the central and peripheral nervous system (94). Downregulation of CHP1 (as seen in the patient NPCs in this study) causes an impaired NHE1 (Na^+/H^+ exchanger 1) which is an important regulator of intracellular ions and pH homeostasis. This leads to an impaired ion homeostasis in the cell, that in the end result in Purkinje neuron degeneration and ataxia (93, 95). Purkinje neurons are located in the cerebral cortex and plays a fundamental role in coordination, control and movement (96). Chp1 depletion is also seen to directly cause ataxia in mouse (95). Chp1 depletion in zebrafish causes movement disorder and motor axon abnormalities (97). This is a very interesting finding, as ataxia is one of the symptoms in the UCHL1-patients.

The neuronal migration protein doublecortin, DcX, was the third downregulated protein identified with a fold change greater than 2 in the patient NPCs and is a microtubule-associated phosphoprotein. It is expressed in neurons, and in this study, it was used as a neural marker for immunostaining. DcX is required for the neuronal distribution and migration to its final destination in the developing cerebral cortex. It is thought to participate in a Ca^{2+}-dependent signal transduction pathway that is important for neuronal interaction when migrating (98).

The only upregulated protein in patient derived NPCs with a fold change of above 2 was the NFM, neurofilament medium protein. It is one of three type IV intermediate filament proteins in neurofilaments, which is composed of neurofilament light chain, heavy chain and medium chain, the last one is encoded by NFM. Neurofilaments make up the cytoskeleton in axons, and their function involves maintaining the axon stability and radial growth. NFM is discussed as a biomarker in neurological disease. Mutations on NFM have been associated with increased susceptibility to neurological diseases like familial PD (99).

3.5.3 Protein Alterations in the UPS

To evaluate if there were any alterations in levels of ubiquitinated proteins and proteins associated with the UPS, a search was performed on the words: “ubiquitin” and “proteasome”, in the iPSC and NPC group comparisons.

In the list of identified proteins in iPSC samples, 82 proteins contained the word “ubiquitin” in their name and 41 proteins contained “proteasome” in their name. However, they did not fulfil the statistical requirements and, therefore, were not considered significantly altered when comparing patient and control samples. Lists of the identified proteins associated with Ubiquitin or Proteasome are provided in Appendix 6, table A.5 and A.6, respectively. Similarly, 83 proteins containing “ubiquitin” and 41 proteins containing “proteasome” were identified in the NPC samples, respectively (Appendix 6, table A.7 and A.8). However, as for iPSC, differences in their levels between the two groups were not statistically significant.

To sum up, the protein profiles of patient and control samples are quite similar at iPSC and NPC levels. However, quantitative MS pinpointed up-regulation of LAT2 in patient cells at iPSC stage and down-regulation of UCHL1, Chp1 and DcX, as well as up-regulation of NFM in patient derived-NPCs.

Since upregulation of LAT2 is associated with an altered NO/cGMP pathway, that further modulates retinal phototransduction, it would be interesting to investigate if this could be connected to the visual impairment seen in the UCHL1-patients. Additionally, upregulation of the NO/cGMP pathway has been associated with improved cognitive function, thus, could also be investigated as a potential reason for the patients improved memory and IQ. As downregulation of CHP1 has been indirectly associated with ataxia through an impaired NHE1, it would also be interesting to investigate if this could be related to the patient’s ataxia.

Most definitely, it would be quite valuable to investigate the protein profiles of mature neurons and verify whether the levels of the mentioned proteins would be further altered, along with novel protein targets associated with the clinical features of the disease. No proteins known to be associated with the UPS were significantly altered in the iPSC and NPC group comparisons. Their impact could potentially be uncovered if analyzing mature neurons. More specifically forebrain or motor neurons would be the most relevant 2D models to further investigate these findings, as the most severe clinical features of UCHL1-patients are related to impaired motor functions.

4 Conclusion and Future Perspectives

In this study iPSCs and NPCs were successfully generated from patients and healthy controls. Furthermore, cerebral organoids were generated and characterized only from healthy controls. As, to our knowledge, there are no reports of successfully generated cerebral organoids from patients harboring mutations on the UCHL1 gene, it is possible that the UCHL1 mutations contributed to the lack of success in growing patient-derived brain organoids. Further attempts in optimizing the protocol to the individual cell clones may improve the outcomes. Accordingly, optimizing of individual cell clones can potentially aid in overcoming the challenges faced during NPC culture, as generation of stable NPCs are essential for further differentiation into mature neurons. Alternatively, switching to protocols which is based on direct generation of mature neurons from the iPSCs without using NPCs as an intermediate stage, could be an alternative to explore.

Although we experienced challenges related to the survival of NPCs in culture, appropriate concentrations of proteasome inhibitors, as well as suitable drug exposure time points were determined via viability and proliferation assays using healthy control NPCs. This information will be valuable for further investigations on the response of control and UCHL1-deficient NPCs in response to proteasome inhibitors. Moreover, measurements of the basal 20S proteasome activity shows no difference between controls- and patients-derived iPSC. Additionally, we demonstrated that the standard NPC culture medium displays high background signal, masking the signal originated from basal levels of proteasome activity, and that MEM can potentially be used as an alternative culture medium in this experiment. However, how culturing NPC in MEM during this assay will impact NPC survival or activate stress-response pathways that can affect proteasomal function needs to be elucidated.

Proteome analysis of control and UCHL1-patient iPSCs and NPCs revealed changes in levels of interesting proteins associated with neurodegenerative disease. Further experiments in mature neuron are paramount to determine whether the levels of these proteins are further affected in advanced stages of development. As more alterations in protein profiles are expected in fully differentiated cells compared to progenitor and stem cells, analysis of mature neurons may unravel new pathomechanisms associated with UCHL1 dysfunction as well as novel targets for therapy for diseases caused by imbalance in ubiquitin homeostasis.

6 References

1. Rydning SL, Backe PH, Sousa MML, Iqbal Z, Øye AM, Sheng Y, et al. Novel UCHL1 mutations reveal new insights into ubiquitin processing. Hum Mol Genet. 2017;26(6):1031-40.
2. Kleiger G, Mayor T. Perilous journey: a tour of the ubiquitin-proteasome system. Trends Cell Biol. 2014;24(6):352-9.
3. Rape M. Ubiquitylation at the crossroads of development and disease. Nat Rev Mol Cell Biol. 2018;19(1):59-70.
4. Hegde AN, Smith SG, Duke LM, Pourquoi A, Vaz S. Perturbations of Ubiquitin-Proteasome-Mediated Proteolysis in Aging and Alzheimer's Disease. Front Aging Neurosci. 2019;11:324.
5. Wang B, Cai W, Ai D, Zhang X, Yao L. The Role of Deubiquitinases in Vascular Diseases. J Cardiovasc Transl Res. 2020;13(2):131-41.
6. Matuszczak E, Tylicka M, Komarowska MD, Debek W, Hermanowicz A. Ubiquitin carboxy-terminal hydrolase L1 - physiology and pathology. Cell Biochem Funct. 2020;38(5):533-40.
7. Bax M, McKenna J, Do-Ha D, Stevens CH, Higginbottom S, Balez R, et al. The Ubiquitin Proteasome System Is a Key Regulator of Pluripotent Stem Cell Survival and Motor Neuron Differentiation. Cells. 2019;8(6).
8. Sun L, Chen ZJ. The novel functions of ubiquitination in signaling. Current Opinion in Cell Biology. 2004;16(2):119-26.
9. Lata S, Mishra R, Banerjea AC. Proteasomal Degradation Machinery: Favorite Target of HIV-1 Proteins. Frontiers in Microbiology. 2018;9(2738).
10. Day IN, Thompson RJ. UCHL1 (PGP 9.5): neuronal biomarker and ubiquitin system protein. Prog Neurobiol. 2010;90(3):327-62.
11. Bishop P, Rocca D, Henley JM. Ubiquitin C-terminal hydrolase L1 (UCH-L1): structure, distribution and roles in brain function and dysfunction. Biochem J. 2016;473(16):2453-62.
12. Tramutola A, Di Domenico F, Barone E, Perluigi M, Butterfield DA. It Is All about (U)biquitin: Role of Altered Ubiquitin-Proteasome System and UCHL1 in Alzheimer Disease. Oxidative Medicine and Cellular Longevity. 2016;2016:2756068.

13. Lee Y-TC, Hsu S-TD. Familial Mutations and Post-translational Modifications of UCH-L1 in Parkinson's Disease and Neurodegenerative Disorders. bioRxiv. 2016:094953.
14. Das Bhowmik A, Patil SJ, Deshpande DV, Bhat V, Dalal A. Novel splice-site variant of UCHL1 in an Indian family with autosomal recessive spastic paraplegia-79. J Hum Genet. 2018;63(8):927-33.
15. Bilguvar K, Tyagi NK, Ozkara C, Tuysuz B, Bakircioglu M, Choi M, et al. Recessive loss of function of the neuronal ubiquitin hydrolase UCHL1 leads to early-onset progressive neurodegeneration. Proc Natl Acad Sci U S A. 2013;110(9):3489-94.
16. Takahashi K, Yamanaka S. Induction of Pluripotent Stem Cells from Mouse Embryonic and Adult Fibroblast Cultures by Defined Factors. Cell. 2006;126(4):663-76.
17. Thomson JA, Itskovitz-Eldor J, Shapiro SS, Waknitz MA, Swiergiel JJ, Marshall VS, et al. Embryonic Stem Cell Lines Derived from Human Blastocysts. Science. 1998;282(5391):1145-7.
18. Wilmut I, Schnieke AE, McWhir J, Kind AJ, Campbell KHS. Viable offspring derived from fetal and adult mammalian cells. Nature. 1997;385(6619):810-3.
19. Tada M, Takahama Y, Abe K, Nakatsuji N, Tada T. Nuclear reprogramming of somatic cells by in vitro hybridization with ES cells. Current biology : CB. 2001;11(19):1553-8.
20. Alberts B, Johnson A, Lewis J, Morgan D, Raff M, Roberts K, et al. Molecular biology of the cell. 2017.
21. Panopoulos AD, Yanes O, Ruiz S, Kida YS, Diep D, Tautenhahn R, et al. The metabolome of induced pluripotent stem cells reveals metabolic changes occurring in somatic cell reprogramming. Cell Research. 2012;22(1):168-77.
22. Doege CA, Inoue K, Yamashita T, Rhee DB, Travis S, Fujita R, et al. Early-stage epigenetic modification during somatic cell reprogramming by Parp1 and Tet2. Nature. 2012;488(7413):652-5.
23. Takahashi K, Tanabe K, Ohnuki M, Narita M, Ichisaka T, Tomoda K, et al. Induction of Pluripotent Stem Cells from Adult Human Fibroblasts by Defined Factors. CELL. 2007;131(5):861-72.
24. Robinton DA, Daley GQ. The promise of induced pluripotent stem cells in research and therapy. Nature. 2012;481(7381):295-305.
25. Chambers I, Colby D, Robertson M, Nichols J, Lee S, Tweedie S, et al. Functional Expression Cloning of Nanog, a Pluripotency Sustaining Factor in Embryonic Stem Cells. Cell. 2003;113(5):643-55.

26. Henderson JK, Draper JS, Baillie HS, Fishel S, Thomson JA, Moore H, et al. Preimplantation Human Embryos and Embryonic Stem Cells Show Comparable Expression of Stage-Specific Embryonic Antigens. STEM CELLS. 2002;20(4):329-37.
27. Showell C, Binder O, Conlon FL. T-box genes in early embryogenesis. Developmental Dynamics. 2004;229(1):201-18.
28. Niakan KK, Ji H, Maehr R, Vokes SA, Rodolfa KT, Sherwood RI, et al. Sox17 promotes differentiation in mouse embryonic stem cells by directly regulating extraembryonic gene expression and indirectly antagonizing self-renewal. Genes Dev. 2010;24(3):312-26.
29. Suzuki S, Namiki J, Shibata S, Mastuzaki Y, Okano H. The Neural Stem/Progenitor Cell Marker Nestin Is Expressed in Proliferative Endothelial Cells, but Not in Mature Vasculature. Journal of Histochemistry & Cytochemistry. 2010;58(8):721-30.
30. Stemcell Technologies. Anti-PAX6 Antibody: stemcell.com; 2015.
31. Ebert AD, Yu J, Rose FF, Jr., Mattis VB, Lorson CL, Thomson JA, et al. Induced pluripotent stem cells from a spinal muscular atrophy patient. Nature. 2009;457(7227):277-80.
32. Stemcell Technologies. Modeling Human Neurological Disease with Induced Pluripotent Stem Cells: stemcell.com; [Available from: https://www.stemcell.com/modeling-neurological-disease.html.
33. Martínez-Cerdeño V, Noctor SC. Neural Progenitor Cell Terminology. Frontiers in Neuroanatomy. 2018;12(104).
34. Stemcell Technologies. Neural Stem Cells: stemcell.com; [Available from: https://www.stemcell.com/technical-resources/area-of-interest/neuroscience-research/neural-stem-cells/overview.html.
35. Li W, Sun W, Zhang Y, Wei W, Ambasudhan R, Xia P, et al. Rapid induction and long-term self-renewal of primitive neural precursors from human embryonic stem cells by small molecule inhibitors. Proceedings of the National Academy of Sciences. 2011;108(20):8299-304.
36. Choi W-Y, Hwang J-H, Lee J-Y, Cho A-N, Lee AJ, Jung I, et al. Chromatin Interaction Changes during the iPSC-NPC Model to Facilitate the Study of Biologically Significant Genes Involved in Differentiation. Genes. 2020;11(10):1176.
37. Zhao X, Moore DL. Neural stem cells: developmental mechanisms and disease modeling. Cell Tissue Res. 2018;371(1):1-6.
38. Stemcell Technologies. Neural Induction for Human Pluripotent Stem Cells (hPSCs) using Monolayer Culture: stemcell.com; [Available from:

https://www.stemcell.com/technical-resources/methods-library/cell-culture/ectodermal-cells/neural-cell-culture/neural-induction-for-human-pluripotent-stem-cells-hpscs-using-monolayer-culture.html.
39. Stemcell Technologies. hPSC-Derived Neural Cell Research: stemcell.com; [Available from: https://www.stemcell.com/product-portfolios/hpsc-derived-neural-cell-research/characterization.html#more.
40. Kan L, Jalali A, Zhao L-R, Zhou X, McGuire T, Kazanis I, et al. Dual function of Sox1 in telencephalic progenitor cells. Developmental Biology. 2007;310(1):85-98.
41. Kaneko Y, Sakakibara S, Imai T, Suzuki A, Nakamura Y, Sawamoto K, et al. Musashi1: an evolutionally conserved marker for CNS progenitor cells including neural stem cells. Dev Neurosci. 2000;22(1-2):139-53.
42. Rao MS, Shetty AK. Efficacy of doublecortin as a marker to analyse the absolute number anddendritic growth of newly generated neurons in the adult dentate gyrus. European Journal of Neuroscience. 2004;19(2):234-46.
43. Jiang YQ, Oblinger MM. Differential regulation of beta III and other tubulin genes during peripheral and central neuron development. J Cell Sci. 1992;103 (Pt 3):643-51.
44. Consortium Hi. Induced pluripotent stem cells from patients with Huntington's disease show CAG-repeat-expansion-associated phenotypes. Cell Stem Cell. 2012;11(2):264-78.
45. Kondo T, Asai M, Tsukita K, Kutoku Y, Ohsawa Y, Sunada Y, et al. Modeling Alzheimer's disease with iPSCs reveals stress phenotypes associated with intracellular Aβ and differential drug responsiveness. Cell Stem Cell. 2013;12(4):487-96.
46. Yuan F, Fang KH, Cao SY, Qu ZY, Li Q, Krencik R, et al. Efficient generation of region-specific forebrain neurons from human pluripotent stem cells under highly defined condition. Sci Rep. 2015;5:18550.
47. Bell S, Hettige N, Silveira H, Peng H, Wu H, Jefri M, et al. Differentiation of Human Induced Pluripotent Stem Cells (iPSCs) into an Effective Model of Forebrain Neural Progenitor Cells and Mature Neurons. BIO-PROTOCOL. 2019;9.
48. Stemcell Technologies. STEMdiff™ Forebrain Neuron Differentiation Kit STEMdiff™ Forebrain Neuron Maturation Kit. stemcell.com; 2020.
49. Hettige NC, Ernst C. FOXG1 Dose in Brain Development. Front Pediatr. 2019;7:482.
50. Lancaster MA, Renner M, Martin C-A, Wenzel D, Bicknell LS, Hurles ME, et al. Cerebral organoids model human brain development and microcephaly. Nature Nature. 2013;501(7467):373-9.

51. Kaushik G, Ponnusamy MP, Batra SK. Concise Review: Current Status of Three-Dimensional Organoids as Preclinical Models. Stem Cells. 2018;36(9):1329-40.
52. Li M, Izpisua Belmonte JC. Organoids - Preclinical Models of Human Disease. N Engl J Med. 2019;380(6):569-79.
53. Lancaster MA, Knoblich JA. Generation of cerebral organoids from human pluripotent stem cells. Nature Protocols. 2014;9(10):2329-40.
54. Ho BX, Pek NMQ, Soh BS. Disease Modeling Using 3D Organoids Derived from Human Induced Pluripotent Stem Cells. Int J Mol Sci. 2018;19(4).
55. Tramontin AD, García-Verdugo JM, Lim DA, Alvarez-Buylla A. Postnatal Development of Radial Glia and the Ventricular Zone (VZ): a Continuum of the Neural Stem Cell Compartment. Cerebral Cortex. 2003;13(6):580-7.
56. Li X, Wang W, Chen J. Recent progress in mass spectrometry proteomics for biomedical research. Sci China Life Sci. 2017;60(10):1093-113.
57. Paulo JA, Kadiyala V, Banks PA, Steen H, Conwell DL. Mass spectrometry-based proteomics for translational research: a technical overview. Yale J Biol Med. 2012;85(1):59-73.
58. Shen X, Shen S, Qu J. Labeling and Label-Free Shotgun Proteomics Quantification in the Research of Cardiovascular Diseases. In: Agnetti G, Lindsey ML, Foster DB, editors. Manual of Cardiovascular Proteomics. Cham: Springer International Publishing; 2016. p. 247-74.
59. Zhu W, Smith JW, Huang C-M. Mass Spectrometry-Based Label-Free Quantitative Proteomics. Journal of Biomedicine and Biotechnology. 2010;2010:840518.
60. Sap K, Demmers J. Labeling Methods in Mass Spectrometry Based Quantitative Proteomics. 2012.
61. University EC. What is LC-MS proteomics? : Edith Cowan University; 2020 [Available from: https://www.ecu.edu.au/schools/science/research-activity/research-support/proteomics/what-is-lc-ms-proteomics.
62. Lindoso RS, Kasai-Brunswick TH, Monnerat Cahli G, Collino F, Bastos Carvalho A, Campos de Carvalho AC, et al. Proteomics in the World of Induced Pluripotent Stem Cells. Cells. 2019;8(7).
63. Technologies S. Functional assay kit to assess pluripotency by directed differentiation of human ES and iPS cells to all three germ layers [Document]: stemcell.com; 2021.

64. Stemcell Technologies. hPSC Genetic Analysis Kit: stemcell.com; 2021 [Available from: https://www.stemcell.com/hpsc-genetic-analysis-kit.html.
65. Perriot S, Mathias A, Perriard G, Canales M, Jonkmans N, Merienne N, et al. Human Induced Pluripotent Stem Cell-Derived Astrocytes Are Differentially Activated by Multiple Sclerosis-Associated Cytokines. Stem Cell Reports. 2018;11(5):1199-210.
66. Stemcell Technologies. Generation and Culture of Neural Progenitor Cells Using the STEMdiff™ Neural System [Technical Manual]: stemcell.no; 2021.
67. Mariani J, Coppola G, Zhang P, Abyzov A, Provini L, Tomasini L, et al. FOXG1-Dependent Dysregulation of GABA/Glutamate Neuron Differentiation in Autism Spectrum Disorders. Cell. 2015;162(2):375-90.
68. Qian X, Jacob F, Song MM, Nguyen HN, Song H, Ming GL. Generation of human brain region-specific organoids using a miniaturized spinning bioreactor. Nat Protoc. 2018;13(3):565-80.
69. Sigma-Aldrich. Proteasome 20S Activity Assay Kit [Product Information]: sigma-aldrich.com; 2014.
70. Tyanova S, Temu T, Cox J. The MaxQuant computational platform for mass spectrometry-based shotgun proteomics. Nature Protocols. 2016;11(12):2301-19.
71. UniProt. Proteomes - Homo sapiens (Human): uniprot.org; [Available from: https://www.uniprot.org/proteomes/UP000005640.
72. Cox J, Hein MY, Luber CA, Paron I, Nagaraj N, Mann M. Accurate Proteome-wide Label-free Quantification by Delayed Normalization and Maximal Peptide Ratio Extraction, Termed MaxLFQ*. Molecular & Cellular Proteomics. 2014;13(9):2513-26.
73. Student. The Probable Error of a Mean. Biometrika. 1908;6(1):1-25.
74. The R Project for Statistical Computing: r-project.org; 2021 [Available from: https://www.r-project.org/.
75. Benjamini Y, Hochberg Y. Controlling the False Discovery Rate: A Practical and Powerful Approach to Multiple Testing. Journal of the Royal Statistical Society Series B (Methodological). 1995;57(1):289-300.
76. Wickham H. ggplot2. Elegant Graphics for Data Analysis. 1st ed: Springer-Verlag New York; 2009.
77. pheatmap: Pretty Heatmaps. 1.0.12 ed: Kolde, Ravio; 2019.
78. Ravikanth M, Soujanya P, Manjunath K, Saraswathi TR, Ramachandran CR. Heterogenecity of fibroblasts. J Oral Maxillofac Pathol. 2011;15(2):247-50.

79. CELLnTEC Advanced Cell Systems AG. PRIMARY HUMAN DERMAL FIBROBLASTS: cellntec.com; 2021 [Available from: https://cellntec.com/products/mesenchyme/fibroblast-cells/.
80. Song P, Yang F, Jin H, Wang X. The regulation of protein translation and its implications for cancer. Signal Transduction and Targeted Therapy. 2021;6(1):68.
81. Bianchi F, Malboubi M, Li Y, George JH, Jerusalem A, Szele F, et al. Rapid and efficient differentiation of functional motor neurons from human iPSC for neural injury modelling. Stem Cell Research. 2018;32:126-34.
82. Grigor'eva EV, Malankhanova TB, Surumbayeva A, Pavlova SV, Minina JM, Kizilova EA, et al. Generation of GABAergic striatal neurons by a novel iPSC differentiation protocol enabling scalability and cryopreservation of progenitor cells. Cytotechnology. 2020;72(5):649-63.
83. Smirniotopoulos JG, Murphy FM, Rushing EJ, Rees JH, Schroeder JW. Patterns of Contrast Enhancement in the Brain and Meninges. RadioGraphics. 2007;27(2):525-51.
84. Zhang S, Wan Z, Kamm RD. Vascularized organoids on a chip: strategies for engineering organoids with functional vasculature. Lab on a Chip. 2021;21(3):473-88.
85. Shi Y, Sun L, Wang M, Liu J, Zhong S, Li R, et al. Vascularized human cortical organoids (vOrganoids) model cortical development in vivo. PLoS Biology. 2020;18(5).
86. Stadtfeld M, Varas F, Graf T. Fluorescent protein-cell labeling and its application in time-lapse analysis of hematopoietic differentiation. Methods in molecular medicine. 2005;105:395-412.
87. Pineda M, Fernández E, Torrents D, Estévez R, López C, Camps M, et al. Identification of a membrane protein, LAT-2, that Co-expresses with 4F2 heavy chain, an L-type amino acid transport activity with broad specificity for small and large zwitterionic amino acids. J Biol Chem. 1999;274(28):19738-44.
88. Kido Y, Tamai I, Uchino H, Suzuki F, Sai Y, Tsuji A. Molecular and functional identification of large neutral amino acid transporters LAT1 and LAT2 and their pharmacological relevance at the blood-brain barrier. Journal of Pharmacy and Pharmacology. 2001;53(4):497-503.
89. Zielińska M, Ruszkiewicz J, Hilgier W, Fręśko I, Albrecht J. Hyperammonemia increases the expression and activity of the glutamine/arginine transporter y+ LAT2 in rat cerebral cortex: implications for the nitric oxide/cGMP pathway. Neurochem Int. 2011;58(2):190-5.

90. García-Osta A, Cuadrado-Tejedor M, García-Barroso C, Oyarzábal J, Franco R. Phosphodiesterases as therapeutic targets for Alzheimer's disease. ACS Chem Neurosci. 2012;3(11):832-44.
91. Tolone A, Belhadj S, Rentsch A, Schwede F, Paquet-Durand F. The cGMP Pathway and Inherited Photoreceptor Degeneration: Targets, Compounds, and Biomarkers. Genes (Basel). 2019;10(6).
92. Lin X, Barber DL. A calcineurin homologous protein inhibits GTPase-stimulated Na-H exchange. Proc Natl Acad Sci U S A. 1996;93(22):12631-6.
93. Mendoza-Ferreira N, Coutelier M, Janzen E, Hosseinibarkooie S, Löhr H, Schneider S, et al. Biallelic CHP1 mutation causes human autosomal recessive ataxia by impairing NHE1 function. Neurol Genet. 2018;4(1):e209.
94. Palau F, Espinós C. Autosomal recessive cerebellar ataxias. Orphanet J Rare Dis. 2006;1:47.
95. Liu Y, Zaun HC, Orlowski J, Ackerman SL. CHP1-mediated NHE1 biosynthetic maturation is required for Purkinje cell axon homeostasis. J Neurosci. 2013;33(31):12656-69.
96. Kano M, Watanabe M. Chapter 4 - Cerebellar circuits. In: Rubenstein J, Rakic P, Chen B, Kwan KY, editors. Neural Circuit and Cognitive Development (Second Edition): Academic Press; 2020. p. 79-102.
97. Saito R, Hara N, Tada M, Honma Y, Miyashita A, Onodera O, et al. Novel CHP1 mutation in autosomal-recessive cerebellar ataxia: autopsy features of two siblings. Acta Neuropathol Commun. 2020;8(1):134.
98. Slepak TI, Salay LD, Lemmon VP, Bixby JL. Dyrk kinases regulate phosphorylation of doublecortin, cytoskeletal organization, and neuronal morphology. Cytoskeleton (Hoboken). 2012;69(7):514-27.
99. Khalil M, Teunissen CE, Otto M, Piehl F, Sormani MP, Gattringer T, et al. Neurofilaments as biomarkers in neurological disorders. Nature Reviews Neurology. 2018;14(10):577-89.

Appendices

Appendix 1: Culture Media

E8 Medium

Component	Amount	Supplier	Cat. no
DMEM/F-12, HEPES	250 ml	Thermo Fisher Scientific	11330032
Absorbic acid 2-phosphate	64 mg/L	Sigma-Aldrich	A8960
Sodium selenite	14 µg/L	Sigma-Aldrich	S5261
$NAHCO_3$	543 mg/L	Sigma-Aldrich	S6014
Insulin	20 mg/L	Sigma-Aldrich	I9278
Transferrin human	10.7 mg/L	Sigma-Aldrich	T3705
bFGF2	100 µg/L	PeproTech	100-18B
TGFB1	2 µg/L	PeproTech	100-21C
Essential 8™ Basal Medium	250 ml	Thermo Fisher Scientific	A1517001

NPC(+) Medium

Component	Amount	Supplier	Cat. no
DMEM/F-12, HEPES	25 ml	Thermo Fisher Scientific	11330032
Neurobasal™ Medium	25 ml	Thermo Fisher Scientific	21103049
GLUTAMAX™ Supplement	250 µl	Thermo Fisher Scientific	11574466
Bovine Serum Albumin	50 µg/ml	Sigma	05470-1G
N-2 Supplement (100X)	500 µl	Thermo Fisher Scientific	17502048
B-27™ Supplement (50X), minus vitamin A	1 ml	Thermo Fisher Scientific	12587010
Recombinant Human LIF (100 µg)	10 ng/ml	PeproTech	300-05
CHIR99021	4 µM	Stemcell Technologies	72054
SB431542	3 µM	Stemcell Technologies	72232
Compound E (1 mg)	0.1 µM	R&D Systems	6476/1

Neural Progenitor Medium, NEM

Component	Amount	Supplier	Cat. no
DMEM/F-12, HEPES	25 ml	Thermo Fisher Scientific	11330032
Neurobasal™ Medium	25 ml	Thermo Fisher Scientific	21103049
GLUTAMAX™ Supplement	250 µl	Thermo Fisher Scientific	11574466
N-2 Supplement (100X)	500 µl	Thermo Fisher Scientific	17502048
B-27™ Supplement (50X), minus vitamin A	1 ml	Thermo Fisher Scientific	12587010
Laminin	1 µg/ml	Sigma-Aldrich	L2020-1MG
Recombinant Human FGF-basic (154 a.a.) (1mg)	10 ng/ml	PeproTech	100-18B
Human EGF	10 ng/ml	R&D Systems	236-EG-200
Recombinant Human/Murine/Rat BDNF (50 µg)	20 ng/ml	PeproTech	450-02

Neural Differentiation Medium, NDM

Component	Amount	Supplier	Cat. no
DMEM/F-12, HEPES	50 ml	Thermo Fisher Scientific	11330032
B-27™ Supplement (50X), minus vitamin A	1 ml	Thermo Fisher Scientific	12587010
N-2 Supplement (100X)	500 µl	Thermo Fisher Scientific	17502048
2-Mercaptoethanol (50 mM)	50 µl	Thermo Fisher Scientific	31350010
Recombinant Human Noggin (250 µg)	100 ng/ml	PeproTech	120-10C

Lancaster EB Medium

Component	Amount	Supplier	Cat. no
DMEM/F-12, HEPES	40 ml	Thermo Fisher Scientific	11330032
Knockout Serum Replacement	10 ml	Thermo Fisher Scientific	10828028
Embryonic stem-cell FBS, qualified	1.5 ml	Thermo Fisher Scientific	10439016
MEM-NEAA	500 µl	Thermo Fisher Scientific	11140050
bFGF	200 ng	Thermo Fisher Scientific	13256029
2-Mercaptoethanol	50 µM	Sigma-Aldrich	805740

Neural Induction Medium, NIM

Component	Amount	Supplier	Cat. no
DMEM/F-12, HEPES	50 ml	Thermo Fisher Scientific	11330032
MEM-NEAA	500 µl	Thermo Fisher Scientific	11140050
N-2 Supplement (100X)	500 µl	Thermo Fisher Scientific	17502048
Heparin	5 µg/ml	Sigma-Aldrich	H3149

DM-A/+A

Component	Amount	Supplier	Cat. no
DMEM/F-12, HEPES	25 ml	Thermo Fisher Scientific	11330032
Neurobasal™ Medium	25 ml	Thermo Fisher Scientific	21103049
GLUTAMAX™ Supplement	250 µl	Thermo Fisher Scientific	11574466
N-2 Supplement (100X)	250 µl	Thermo Fisher Scientific	17502048
B-27™ Supplement (50X), minus vitamin A*	500 µl	Thermo Fisher Scientific	12587010
B-27™ Supplement (50X), serum free**	500 µl	Thermo Fisher Scientific	17504044
MEM-NEAA	250 µl	Thermo Fisher Scientific	11140050
Insulin	2.5 µg/ml	Sigma-Aldrich	I9278-5ML
2-Mercaptoethanol (50 mM)	17.5 µl	Thermo Fisher Scientific	31350010

*** Only in DM(-A)**

**** Only in DM(+A)**

Appendix 2: Analysis of the qPCR Results using the ΔΔCT Method

The ΔΔCT method was used to analyze the qPCR results in this study. Ct stands for cycle threshold and is defined as the number of cycles required for the fluorescent signal of a sample to exceed the background noise. When the Ct level is low, only a few cycles of amplification is necessary to give a signal higher than the background, and vice versa. The Ct value is inversely proportional with the amount of the target gene. Ct < 30 is seen as a strong positive for the target gene. A housekeeping gene is included in the qPCR to have something to normalize against, see table A.1.

Table A.1. *Housekeeping genes used as reference gene to calculate ΔCt.*

qPCR Experiment	**Housekeeping gene**
iPSC Karyotyping	Chr 4p
iPSC and NPC Characterization	β-actin

The ΔΔCT method was calculated doing the following:

1. The mean Ct value was calculated for each sample.
2. ΔCt was normalized by subtracting the mean housekeeping gene from the mean target gene, see equation 1.

$$\Delta Ct = Ct\ (target\ gene) - Ct\ (housekeeping\ gene) \quad (1)$$

3. ΔΔCT was found by comparing the Ct value in a specific cell to ΔCt in the reference cell, equation 2.

$$\Delta\Delta\mathrm{Ct} = \Delta\mathrm{Ct} - \ \Delta\mathrm{Ct}\ (\text{reference cell}) \quad (2)$$

4. The final fold change of gene expression was found using equation 3.

$$2^{-\Delta\Delta\mathrm{Ct}} \quad (3)$$

Appendix 3: Antibodies for ICC

Table A.2. *Primary antibodies used for detecting cell-stage specific protein markers.*

Primary antibodies	Host	Dilution	Supplier	Cat. no
Anti-Musashi-1 (pAb)	Rabbit	1:200	Sigma-Aldrich	AB5977
Anti-Nestin (pAb)	Rabbit	1:200	Sigma-Aldrich	ABD69
anti-Pax6 (mAb)	Mouse	1:200	BioLegend®	862001
Brachyury (pAb)	Goat	1:500	R&D Systems	AF2085
Nanog (D73G4) XP® (mAb)	Rabbit	1:200	Cell Signaling Technology	4903T
Neuron-specific β-III Tubulin (TuJ-1) (mAb)	Mouse	1:200	R&D Systems	MAB1195
Oct4A (C30A3) (mAb)	Rabbit	1:200	Cell Signaling Technology	2840T
Sox17 (pAb)	Goat	1:200	R&D Systems	AF1924
Sox2 (20G5) (mAb)	Mouse	1:200	Thermo Fisher Scientific	MA1-014
Sox2 (D6D9) XP® (mAb)	Rabbit	1:200	Cell Signaling Technology	3579T
SSEA4 (MC813) (mAb)	Mouse	1:200	Cell Signaling Technology	4755T

Table A.3. *Secondary antibodies used for detecting cell-stage specific protein markers.*

Secondary antibodies	Dilution	Supplier	Cat. no
Donkey anti-Goat IgG (H+L), Alexa Fluor 594	1:500	Thermo Fisher Scientific	A-11058
Goat anti-Mouse IgG (H+L), Alexa Fluor Plus 488	1:500	Thermo Fisher Scientific	A32723
Goat anti-Rabbit IgG (H+L), Alexa Fluor 488	1:500	Thermo Fisher Scientific	A-11008
Goat anti-Rabbit IgG (H+L), Alexa Fluor Plus 594	1:500	Thermo Fisher Scientific	A32740

Appendix 4: qPCR Primers

Table A.4. *qPCR Primers used for detection of cell-stage specific markers of mRNA.*

Target gene	**Forward primer sequence**	**Reverse primer sequence**
DcX	TCAGGGAGTGCGTTACATTTAC	GTTGGGATTGACATTCTTGGTG
Nanog	TGCGTCACACCATTGCTATTTTC	AATACCTCAGCCTCCAGCAATG
Nestin	GGCGCACCTCAAGATGTCC	CTTGGGGTCCTGAAAGCTG
Oct4	GTACTCCTCGGTCCCTTTCC	CAAAAACCCTGGCACAAACT
Pax6	GCCCTCACAAACACCTACAG	TCATAACTCCGCCCATTCAC
Sox1	TACAGCCCCATCTCCAACTC	GCTCCGACTTCACCAGAGAG
Sox2	GCCGAGTGGAAACTTTTGTCG	GGCAGCGTGTACTTATCCTTCT
β-Actin	GTTACAGGAAGTCCCTTGCCATCC	CACCTCCCCTGTGTGGACTTGGG

Appendix 5: Viability and Proliferation Assay Set-Up

Figure A.1 shows how the viability and proliferation assays were set up. The outer wells were not used due to chance of evaporation. For viability assays different drug concentrations was tested at one time point. 96-well plates were divided in two, where each cell clone was added to half of the wells. Then, each column had a different drug concentration added as illustrated in figure A.1A. For proliferation assays, different drug concentrations were tested at multiple time points. For this experiment one cell clone was added to a 96-well plate which was divided in three different drugs. Three different concentrations were added to the individual columns for each drug, illustrated in figure A.1B.

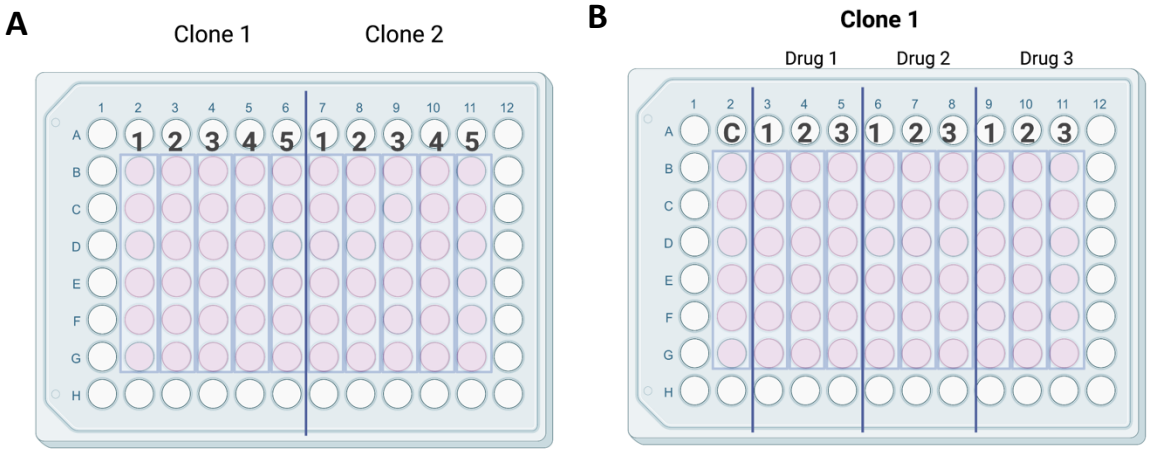

Figure A.1. *Viability (**A**) and proliferation (**B**) assay set-up. C = Control. 1-5 = Different drug concentrations. Figure created using BioRender (https://biorender.com/).*

Appendix 6: Proteins Identified by Mass Spectrometry Associated with "Ubiquitin" or "Proteasome"

Table A.5. *An overview over the proteins identified in a group comparison of patient and control iPSCs from mass spectrometry with "ubiquitin" in their names.*

UniProt Code	Protein Name	Gene	Fold change	Corrected P Value BH	T test P value	Log2 Median Change
O14933	Ubiquitin/ISG15-conjugating enzyme E2 L6	UB2L6	100	0,00	0,376	20,15
A0AVT1	Ubiquitin-like modifier-activating enzyme 6	UBA6	0,72	0,74	0,191	-0,48
Q9H1B7	Probable E3 ubiquitin-protein ligase IRF2BPL	I2BPL	0,43	0,75	0,721	-1,23
P46934	Isoform 4 of E3 ubiquitin-protein ligase NEDD4	NEDD4	0,81	0,76	0,045	-0,30
Q14258	E3 ubiquitin/ISG15 ligase TRIM25	TRI25	0,45	0,76	0,762	-1,14
P09936	Ubiquitin carboxyl-terminal hydrolase isozyme L1	UCHL1	0,41	0,80	0,000	-1,28
P62979	Ubiquitin-40S ribosomal protein S27a	RS27A	0,63	0,80	0,790	-0,66
Q96T88	E3 ubiquitin-protein ligase UHRF1	UHRF1	1,38	0,82	0,617	0,47
P22314	Ubiquitin-like modifier-activating enzyme 1	UBA1	0,44	0,82	0,000	-1,18
Q96RU2	Ubiquitin carboxyl-terminal hydrolase 28	UBP28	0,39	0,83	0,997	-1,34
P62877	E3 ubiquitin-protein ligase RBX1	RBX1	1,04	0,84	0,142	0,06
Q9Y2X8	Ubiquitin-conjugating enzyme E2 D4	UB2D4	0,77	0,85	0,840	-0,39
Q93009	Ubiquitin carboxyl-terminal hydrolase 7	UBP7	0,80	0,85	0,068	-0,33
O95071	E3 ubiquitin-protein ligase UBR5	UBR5	1,41	0,87	0,998	0,49
Q9BSY9	Deubiquitinase DESI2	DESI2	0,86	0,87	0,177	-0,21
Q14157	Ubiquitin-associated protein 2-like	UBP2L	1,15	0,89	0,343	0,20
P68036	Ubiquitin-conjugating enzyme E2 L3	UB2L3	0,76	0,89	0,895	-0,39
Q13356	RING-type E3 ubiquitin-protein ligase PPIL2	PPIL2	0,78	0,89	0,814	-0,36
Q5T6F2	Ubiquitin-associated protein 2	UBAP2	0,59	0,89	0,913	-0,75
Q8NBM4	Ubiquitin-associated domain-containing protein 2	UBAC2	1,25	0,89	0,454	0,33
P61960	Ubiquitin-fold modifier 1	UFM1	0,74	0,90	0,673	-0,44
Q96PU4	E3 ubiquitin-protein ligase UHRF2	UHRF2	0,87	0,91	0,886	-0,21
Q99496	E3 ubiquitin-protein ligase RING2	RING2	0,78	0,91	0,011	-0,36
Q99942	E3 ubiquitin-protein ligase RNF5	RNF5	1,12	0,92	0,257	0,16
P54578	Ubiquitin carboxyl-terminal hydrolase 14	UBP14	0,82	0,92	0,865	-0,29
Q9UPN9	Isoform Beta of E3 ubiquitin-protein ligase TRIM33	TRI33	1,28	0,92	0,749	0,36
Q9Y508	E3 ubiquitin-protein ligase RNF114	RN114	0,84	0,92	0,627	-0,25
Q8N806	Putative E3 ubiquitin-protein ligase UBR7	UBR7	2,21	0,92	0,506	1,14
O95155	Ubiquitin conjugation factor E4 B	UBE4B	1,38	0,92	0,095	0,47
P62253	Ubiquitin-conjugating enzyme E2 G1	UB2G1	0,67	0,92	0,302	-0,57
Q14669	Isoform 4 of E3 ubiquitin-protein ligase TRIP12	TRIPC	1,25	0,92	0,804	0,32
Q16186	Proteasomal ubiquitin receptor ADRM1	ADRM1	0,87	0,92	0,625	-0,21
Q9Y5K5	Ubiquitin carboxyl-terminal hydrolase isozyme L5	UCHL5	0,85	0,92	0,524	-0,24
Q9P0J7	E3 ubiquitin-protein ligase KCMF1	KCMF1	1,38	0,92	0,783	0,46
P60604	Ubiquitin-conjugating enzyme E2 G2	UB2G2	0,81	0,92	0,011	-0,30
A0A087X1S3	E3 ubiquitin-protein ligase HUWE1 (Fragment)	A0A087X1S3	0,82	0,93	0,643	-0,29

Q7Z6Z7	E3 ubiquitin-protein ligase HUWE1	HUWE1	0,77	0,93	0,000	-0,38
Q96FW1	Ubiquitin thioesterase OTUB1	OTUB1	0,89	0,93	0,546	-0,16
Q16763	Ubiquitin-conjugating enzyme E2 S	UBE2S	1,04	0,93	0,410	0,05
Q5VTR2	E3 ubiquitin-protein ligase BRE1A	BRE1A	0,88	0,94	0,111	-0,19
P61086	Ubiquitin-conjugating enzyme E2 K	UBE2K	0,82	0,94	0,328	-0,29
P61088	Ubiquitin-conjugating enzyme E2 N	UBE2N	0,84	0,94	0,377	-0,25
Q8WVD3	E3 ubiquitin-protein ligase RNF138	RN138	0,81	0,95	0,913	-0,31
O00762	Ubiquitin-conjugating enzyme E2 C	UBE2C	1,28	0,95	0,398	0,36
Q969T4	Ubiquitin-conjugating enzyme E2 E3	UB2E3	0,83	0,95	0,677	-0,27
P51784	Ubiquitin carboxyl-terminal hydrolase 11	UBP11	0,67	0,95	0,861	-0,58
Q96K76	Ubiquitin carboxyl-terminal hydrolase 47	UBP47	0,72	0,95	0,075	-0,48
Q8IYM9	E3 ubiquitin-protein ligase TRIM22	TRI22	0,80	0,96	0,284	-0,32
Q92890	Ubiquitin recognition factor in ER-associated degradation protein 1	UFD1	0,94	0,96	0,414	-0,09
Q9ULT8	E3 ubiquitin-protein ligase HECTD1	HECD1	1,03	0,96	0,082	0,04
P45974	Ubiquitin carboxyl-terminal hydrolase 5	UBP5	0,90	0,96	0,118	-0,15
Q8WVY7	Ubiquitin-like domain-containing CTD phosphatase 1	UBCP1	1,18	0,96	0,266	0,24
Q9Y4X5	E3 ubiquitin-protein ligase ARIH1	ARI1	0,89	0,96	0,924	-0,17
Q93008	Probable ubiquitin carboxyl-terminal hydrolase FAF-X	USP9X	0,85	0,97	0,946	-0,23
Q15819	Ubiquitin-conjugating enzyme E2 variant 2	UB2V2	0,88	0,97	0,372	-0,18
O95376	E3 ubiquitin-protein ligase ARIH2	ARI2	0,80	0,97	0,242	-0,31
Q9NT62	Ubiquitin-like-conjugating enzyme ATG3	ATG3	0,77	0,97	0,208	-0,38
Q05086	Ubiquitin-protein ligase E3A	UBE3A	1,14	0,97	0,575	0,19
Q13404	Ubiquitin-conjugating enzyme E2 variant 1	UB2V1	0,87	0,98	0,580	-0,19
Q14694	Ubiquitin carboxyl-terminal hydrolase 10	UBP10	1,05	0,98	0,032	0,06
Q86UV5	Ubiquitin carboxyl-terminal hydrolase 48	UBP48	0,90	0,98	0,491	-0,14
Q8N6M0	Deubiquitinase OTUD6B	OTU6B	1,12	0,98	0,108	0,17
P22681	E3 ubiquitin-protein ligase CBL	CBL	1,04	0,98	0,420	0,06
Q9C0C9	(E3-independent) E2 ubiquitin-conjugating enzyme	UBE2O	0,93	0,99	0,496	-0,10
Q5T4S7	E3 ubiquitin-protein ligase UBR4	UBR4	1,05	0,99	0,667	0,07
Q2Q1W2	E3 ubiquitin-protein ligase TRIM71	LIN41	0,98	0,99	0,779	-0,03
P61077	Ubiquitin-conjugating enzyme E2 D3	UB2D3	0,95	0,99	0,047	-0,07
O43164	E3 ubiquitin-protein ligase Praja-2	PJA2	1,06	0,99	0,059	0,08
P15374	Ubiquitin carboxyl-terminal hydrolase isozyme L3	UCHL3	0,93	0,99	0,213	-0,11
Q9GZZ9	Ubiquitin-like modifier-activating enzyme 5	UBA5	1,05	0,99	0,994	0,06
P63165	Small ubiquitin-related modifier 1	SUMO1	1,01	0,99	0,553	0,01
O75150	E3 ubiquitin-protein ligase BRE1B	BRE1B	1,01	1,00	0,029	0,01
Q96JP5	E3 ubiquitin-protein ligase ZFP91	ZFP91	1,00	0	0,475	0
C9JWE6	E3 ubiquitin-protein ligase PDZRN3 (Fragment)	C9JWE6	1,00	0	0,216	0
E9PJ93	Ubiquitin carboxyl-terminal hydrolase 48 (Fragment)	E9PJ93	1,00	0	0,634	0
Q96K19	Isoform 3 of E3 ubiquitin-protein ligase RNF170	RN170	0,01	0	0,689	-17,60
Q9UPN9	E3 ubiquitin-protein ligase TRIM33	TRI33	2,06	0	0,796	1,04
Q9UNE7	E3 ubiquitin-protein ligase CHIP	CHIP	1,00	0	0,000	0
O00507	Probable ubiquitin carboxyl-terminal hydrolase FAF-Y	USP9Y	1,00	0	0,734	0

Q5JRR6	Ubiquitin-like modifier-activating enzyme 1	Q5JRR6	1,00	0	0,875	0
Q9UHP3	Ubiquitin carboxyl-terminal hydrolase 25	UBP25	1,00	0	0,754	0
Q9NPD8	Ubiquitin-conjugating enzyme E2 T	UBE2T	6,46	0	0,000	2,69

Table A.6. *An overview over the proteins identified in a group comparison of patient and control iPSCs from mass spectrometry with "proteasome" in their names.*

UniProt Code	Protein Name	Gene	Fold change	Corrected P Value BH	T test P value	Log2 Median Change
P49720	Proteasome subunit beta type-3	PSB3	0,66	0,80	0,735	-0,60
P49721	Proteasome subunit beta type-2	PSB2	0,77	0,84	0,095	-0,37
O75832	26S proteasome non-ATPase regulatory subunit 10	PSD10	0,60	0,85	0,281	-0,74
P28072	Proteasome subunit beta type-6	PSB6	0,79	0,85	0,606	-0,33
P28066	Proteasome subunit alpha type-5	PSA5	0,90	0,86	0,000	-0,16
P51665	26S proteasome non-ATPase regulatory subunit 7	PSMD7	0,90	0,86	0,585	-0,15
P28070	Proteasome subunit beta type-4	PSB4	0,88	0,87	0,126	-0,18
O00487	26S proteasome non-ATPase regulatory subunit 14	PSDE	0,71	0,90	0,618	-0,49
P25789	Proteasome subunit alpha type-4	PSA4	0,84	0,90	0,536	-0,25
Q13200	26S proteasome non-ATPase regulatory subunit 2	PSMD2	0,90	0,90	0,000	-0,16
P61289	Proteasome activator complex subunit 3	PSME3	0,88	0,91	0,738	-0,19
P43686	26S proteasome regulatory subunit 6B	PRS6B	0,85	0,92	0,893	-0,23
O43242	26S proteasome non-ATPase regulatory subunit 3	PSMD3	0,83	0,92	0,219	-0,27
P48556	26S proteasome non-ATPase regulatory subunit 8	PSMD8	0,87	0,92	0,794	-0,21
P55036	26S proteasome non-ATPase regulatory subunit 4	PSMD4	0,85	0,92	0,374	-0,23
P62191	26S proteasome regulatory subunit 4	PRS4	0,92	0,92	0,155	-0,12
P62195	26S proteasome regulatory subunit 8	PRS8	0,89	0,92	0,849	-0,17
Q16186	Proteasomal ubiquitin receptor ADRM1	ADRM1	0,87	0,92	0,326	-0,21
Q5VYK3	Proteasome adapter and scaffold protein ECM29	ECM29	0,71	0,93	0,652	-0,49
P25786	Proteasome subunit alpha type-1	PSA1	0,91	0,93	0,253	-0,14
Q15008	26S proteasome non-ATPase regulatory subunit 6	PSMD6	0,86	0,93	0,679	-0,21
O00232	26S proteasome non-ATPase regulatory subunit 12	PSD12	0,88	0,94	0,000	-0,19
Q9UNM6	26S proteasome non-ATPase regulatory subunit 13	PSD13	0,88	0,94	0,246	-0,19
P60900	Proteasome subunit alpha type-6	PSA6	0,91	0,96	0,810	-0,14
Q9UL46	Proteasome activator complex subunit 2	PSME2	0,92	0,96	0,370	-0,12
F5H4Z3	Proteasome inhibitor PI31 subunit (Fragment)	F5H4Z3	1,07	0,97	0,774	0,09
P62333	26S proteasome regulatory subunit 10B	PRS10	0,91	0,98	0,889	-0,13
P25787	Proteasome subunit alpha type-2	PSA2	0,94	0,98	0,120	-0,10
P20618	Proteasome subunit beta type-1	PSB1	0,92	0,98	0,021	-0,12
P28074	Proteasome subunit beta type-5	PSB5	0,95	0,98	0,215	-0,07
Q99460	26S proteasome non-ATPase regulatory subunit 1	PSMD1	0,94	0,98	0,000	-0,09
O00233	26S proteasome non-ATPase regulatory subunit 9	PSMD9	1,08	0,98	0,000	0,11
R4GNH3	26S proteasome regulatory subunit 6A	R4GNH3	1,04	0,98	0,000	0,06
P35998	26S proteasome regulatory subunit 7	PRS7	0,94	0,98	0,814	-0,09

O95456	Proteasome assembly chaperone 1	PSMG1	1,03	0,98	0,259	0,04
Q16401	26S proteasome non-ATPase regulatory subunit 5	PSMD5	1,03	0,99	0,559	0,05
O00231	26S proteasome non-ATPase regulatory subunit 11	PSD11	0,95	0,99	0,622	-0,07
O14818	Proteasome subunit alpha type-7	PSA7	0,99	0,99	0,720	-0,02
P25788	Proteasome subunit alpha type-3	PSA3	0,98	0,99	0,548	-0,02
Q06323	Proteasome activator complex subunit 1	PSME1	0,96	0,99	0,371	-0,05
Q99436	Proteasome subunit beta type-7	PSB7	0,99	1,00	0,670	-0,01

Table A.7. *An overview over the proteins identified in a group comparison of patient and control NPCs at passage 3 from mass spectrometry with "ubiquitin" in their names.*

UniProt Code	Protein Name	Gene	Fold change	Corrected P Value BH	T test P value	Log2 Median Change
P09936	Ubiquitin carboxyl-terminal hydrolase isozyme L1	UCHL1	0,43	0,12	0,887	-1,22
P54578	Ubiquitin carboxyl-terminal hydrolase 14	UBP14	0,87	0,56	0,384	-0,20
P22314	Ubiquitin-like modifier-activating enzyme 1	UBA1	0,57	0,67	0,121	-0,81
Q9NT62	Ubiquitin-like-conjugating enzyme ATG3	ATG3	1,54	0,68	0,791	0,62
Q96FW1	Ubiquitin thioesterase OTUB1	OTUB1	0,82	0,85	0,353	-0,29
Q9UPN9	Isoform Beta of E3 ubiquitin-protein ligase TRIM33	TRI33	1,44	0,85	0,000	0,53
Q9BSY9	Deubiquitinase DESI2	DESI2	1,44	0,86	0,575	0,52
Q99942	E3 ubiquitin-protein ligase RNF5	RNF5	1,37	0,88	0,319	0,46
P68036	Ubiquitin-conjugating enzyme E2 L3	UB2L3	0,74	0,89	0,730	-0,43
Q16186	Proteasomal ubiquitin receptor ADRM1	ADRM1	1,45	0,92	0,539	0,54
Q93009	Ubiquitin carboxyl-terminal hydrolase 7	UBP7	0,87	0,93	0,808	-0,20
Q2Q1W2	E3 ubiquitin-protein ligase TRIM71	LIN41	1,36	0,93	0,197	0,44
Q8N806	Putative E3 ubiquitin-protein ligase UBR7	UBR7	1,24	0,93	0,000	0,31
P45974	Ubiquitin carboxyl-terminal hydrolase 5	UBP5	0,90	0,94	0,000	-0,16
P61960	Ubiquitin-fold modifier 1	UFM1	0,59	0,94	0,000	-0,77
Q9H1B7	Probable E3 ubiquitin-protein ligase IRF2BPL	I2BPL	0,77	0,95	0,167	-0,37
Q05086	Ubiquitin-protein ligase E3A	UBE3A	0,89	0,95	0,944	-0,16
A0AVT1	Ubiquitin-like modifier-activating enzyme 6	UBA6	1,38	0,96	0,280	0,46
Q14694	Ubiquitin carboxyl-terminal hydrolase 10	UBP10	1,14	0,96	0,512	0,18
Q9Y2X8	Ubiquitin-conjugating enzyme E2 D4	UB2D4	0,83	0,98	0,958	-0,27
Q8N6M0	Deubiquitinase OTUD6B	OTU6B	0,86	0,98	0,000	-0,21
Q96JP5	E3 ubiquitin-protein ligase ZFP91	ZFP91	1,28	0,98	0,345	0,36
P63165	Small ubiquitin-related modifier 1	SUMO1	0,89	0,98	0,191	-0,16
E9PJ93	Ubiquitin carboxyl-terminal hydrolase 48 (Fragment)	E9PJ93	1,18	0,98	0,912	0,24
Q96K19	Isoform 3 of E3 ubiquitin-protein ligase RNF170	RN170	0,75	0,98	0,319	-0,42
P51784	Ubiquitin carboxyl-terminal hydrolase 11	UBP11	0,77	0,98	0,000	-0,37
O43164	E3 ubiquitin-protein ligase Praja-2	PJA2	1,17	0,98	0,000	0,23
O95155	Ubiquitin conjugation factor E4 B	UBE4B	0,75	0,98	0,000	-0,42
P15374	Ubiquitin carboxyl-terminal hydrolase isozyme L3	UCHL3	0,80	0,98	0,000	-0,33
P62253	Ubiquitin-conjugating enzyme E2 G1	UB2G1	0,85	0,98	0,860	-0,23

Q13356	RING-type E3 ubiquitin-protein ligase PPIL2	PPIL2	0,71	0,98	0,472	-0,50
Q15819	Ubiquitin-conjugating enzyme E2 variant 2	UB2V2	0,90	0,98	0,348	-0,15
Q16763	Ubiquitin-conjugating enzyme E2 S	UBE2S	1,31	0,98	0,646	0,39
Q5T4S7	E3 ubiquitin-protein ligase UBR4	UBR4	1,19	0,98	0,125	0,25
Q86UV5	Ubiquitin carboxyl-terminal hydrolase 48	UBP48	1,11	0,98	0,793	0,15
Q93008	Probable ubiquitin carboxyl-terminal hydrolase FAF-X	USP9X	0,72	0,98	0,121	-0,46
Q9P0J7	E3 ubiquitin-protein ligase KCMF1	KCMF1	2,18	0,98	0,861	1,13
Q9Y4X5	E3 ubiquitin-protein ligase ARIH1	ARI1	0,71	0,98	0,018	-0,49
Q14669	Isoform 4 of E3 ubiquitin-protein ligase TRIP12	TRIPC	1,35	0,99	0,947	0,43
Q96T88	E3 ubiquitin-protein ligase UHRF1	UHRF1	1,04	0,99	0,623	0,05
P61077	Ubiquitin-conjugating enzyme E2 D3	UB2D3	0,90	0,99	0,514	-0,15
Q9ULT8	E3 ubiquitin-protein ligase HECTD1	HECD1	1,07	0,99	0,944	0,10
Q13404	Ubiquitin-conjugating enzyme E2 variant 1	UB2V1	0,94	0,99	0,431	-0,08
Q5T6F2	Ubiquitin-associated protein 2	UBAP2	1,54	0,99	0,237	0,63
Q9C0C9	(E3-independent) E2 ubiquitin-conjugating enzyme	UBE2O	1,17	0,99	0,943	0,23
Q5VTR2	E3 ubiquitin-protein ligase BRE1	BRE1A	0,93	0,99	0,860	-0,11
A0A087X1S3	E3 ubiquitin-protein ligase HUWE1 (Fragment)	A0A087X1S3	1,07	0,99	0,803	0,10
Q9Y508	E3 ubiquitin-protein ligase RNF114	RN114	1,02	0,99	0,177	0,03
P22681	E3 ubiquitin-protein ligase CBL	CBL	0,94	0,99	0,375	-0,10
Q969T4	Ubiquitin-conjugating enzyme E2 E3	UB2E3	1,05	0,99	0,833	0,07
Q14258	E3 ubiquitin/ISG15 ligase TRIM25	TRI25	0,92	0,99	0,910	-0,13
O95071	E3 ubiquitin-protein ligase UBR5	UBR5	0,95	0,99	0,732	-0,08
Q8WVD3	E3 ubiquitin-protein ligase RNF138	RN138	1,36	0,99	0,707	0,45
O00762	Ubiquitin-conjugating enzyme E2 C	UBE2C	1,20	0,99	0,229	0,26
P62877	E3 ubiquitin-protein ligase RBX1	RBX1	0,98	0,99	0,643	-0,03
P62979	Ubiquitin-40S ribosomal protein S27a	RS27A	0,92	0,99	0,027	-0,13
Q9Y5K5	Ubiquitin carboxyl-terminal hydrolase isozyme L5	UCHL5	0,97	0,99	0,082	-0,04
Q8WVY7	Ubiquitin-like domain-containing CTD phosphatase 1	UBCP1	0,94	0,99	0,655	-0,09
Q96K76	UMAN Ubiquitin carboxyl-terminal hydrolase 47	UBP47	0,94	0,99	0,019	-0,10
P46934	Isoform 4 of E3 ubiquitin-protein ligase NEDD4	NEDD4	0,94	0,99	0,785	-0,08
P61088	Ubiquitin-conjugating enzyme E2 N	UBE2N	1,01	0,99	0,268	0,02
Q7Z6Z7	E3 ubiquitin-protein ligase HUWE1	HUWE1	1,02	0,99	0,532	0,03
Q96RU2	Ubiquitin carboxyl-terminal hydrolase 28	UBP28	0,95	0,99	0,598	-0,07
Q14157	Ubiquitin-associated protein 2-like	UBP2L	0,89	0,99	0,279	-0,16
O14933	Ubiquitin/ISG15-conjugating enzyme E2 L6	UB2L6	0,98	0,99	0,391	-0,03
Q9NPD8	Ubiquitin-conjugating enzyme E2 T	UBE2T	0,93	0,99	0,447	-0,11
O75150	E3 ubiquitin-protein ligase BRE1B	BRE1B	1,01	1,00	0,932	0,02
O95376	E3 ubiquitin-protein ligase ARIH2	ARI2	1,00	1,00	0,512	-0,01
P61086	Ubiquitin-conjugating enzyme E2 K	UBE2K	1,00	1,00	0,578	0,01
Q8NBM4	Ubiquitin-associated domain-containing protein 2	UBAC2	1,01	1,00	0,863	0,02
Q92890	Ubiquitin recognition factor in ER-associated degradation protein 1	UFD1	0,99	1,00	0,000	-0,02
Q99496	E3 ubiquitin-protein ligase RING2	RING2	0,99	1,00	0,102	-0,01

Q9GZZ9	Ubiquitin-like modifier-activating enzyme 5	UBA5	0,99	1,00	0,331	-0,01
Q8IYM9	E3 ubiquitin-protein ligase TRIM22	TRI22	1,00	0,00	0,172	0,00
C9JWE6	E3 ubiquitin-protein ligase PDZRN3 (Fragment)	C9JWE6	1,00	0,00	0,723	0,00
Q9UPN9	E3 ubiquitin-protein ligase TRIM33	TRI33	1,00	0,00	0,671	0,00
Q9UNE7	E3 ubiquitin-protein ligase CHIP	CHIP	1,00	0,00	0,046	0,00
O00507	Probable ubiquitin carboxyl-terminal hydrolase FAF-Y	USP9Y	1,00	0,00	0,919	0,00
P60604	Ubiquitin-conjugating enzyme E2 G2	UB2G2	0,61	0,00	0,084	-0,71
Q5JRR6	Ubiquitin-like modifier-activating enzyme 1	Q5JRR6	1,00	0,00	0,483	0,00
Q9UHP3	Ubiquitin carboxyl-terminal hydrolase 25	UBP25	1,00	0,00	0,851	0,00
Q96PU4	E3 ubiquitin-protein ligase UHRF2	UHRF2	0,73	0,00	0,541	-0,46

Table A.8. *An overview over the proteins identified in a group comparison of patient and control NPCs at passage 3 from mass spectrometry with "proteasome" in their names.*

UniProt Code	Protein Name	Gene	Fold change	Corrected P Value BH	T test P value	Log2 Median Change
P62195	26S proteasome regulatory subunit 8	PRS8	1,17	0,44	0,965	0,23
P61289	Proteasome activator complex subunit 3	PSME3	1,15	0,84	0,000	0,21
P25789	Proteasome subunit alpha type-4	PSA4	0,93	0,86	0,471	-0,10
Q13200	26S proteasome non-ATPase regulatory subunit 2	PSMD2	0,94	0,88	0,164	-0,09
Q16186	Proteasomal ubiquitin receptor ADRM1	ADRM1	1,45	0,92	0,539	0,54
Q9UL46	Proteasome activator complex subunit 2	PSME2	0,67	0,93	0,054	-0,57
Q16401	26S proteasome non-ATPase regulatory subunit 5	PSMD5	1,17	0,93	0,712	0,23
F5H4Z3	Proteasome inhibitor PI31 subunit (Fragment)	F5H4Z3	1,22	0,94	0,617	0,29
P48556	26S proteasome non-ATPase regulatory subunit 8	PSMD8	1,22	0,95	0,000	0,29
Q06323	Proteasome activator complex subunit 1	PSME1	0,93	0,95	0,442	-0,10
Q5VYK3	Proteasome adapter and scaffold protein ECM29	ECM29	0,84	0,96	0,550	-0,24
O75832	26S proteasome non-ATPase regulatory subunit 10	PSD10	0,54	0,98	0,000	-0,88
O00231	26S proteasome non-ATPase regulatory subunit 11	PSD11	1,14	0,98	0,169	0,19
O00487	26S proteasome non-ATPase regulatory subunit 14	PSDE	0,75	0,98	0,062	-0,42
O14818	Proteasome subunit alpha type-7	PSA7	0,93	0,98	0,166	-0,11
P20618	Proteasome subunit beta type-1	PSB1	0,89	0,98	0,933	-0,16
P28070	Proteasome subunit beta type-4	PSB4	0,96	0,98	0,271	-0,05
P28072	Proteasome subunit beta type-6	PSB6	1,09	0,98	0,738	0,13
P55036	26S proteasome non-ATPase regulatory subunit 4	PSMD4	0,92	0,98	0,561	-0,11
O95456	Proteasome assembly chaperone 1	PSMG1	1,36	0,99	0,723	0,44
P25788	Proteasome subunit alpha type-3	PSA3	1,08	0,99	0,108	0,11
P60900	Proteasome subunit alpha type-6	PSA6	1,06	0,99	0,938	0,09
P62191	26S proteasome regulatory subunit 4	PRS4	0,94	0,99	0,039	-0,09
P25787	Proteasome subunit alpha type-2	PSA2	1,03	0,99	0,663	0,04
P62333	26S proteasome regulatory subunit 10B	PRS10	1,03	0,99	0,370	0,04
O00232	26S proteasome non-ATPase regulatory subunit 12	PSD12	1,04	0,99	0,702	0,06
O43242	UMAN 26S proteasome non-ATPase regulatory subunit 3	PSMD3	0,99	0,99	0,616	-0,01

P25786	Proteasome subunit alpha type-1	PSA1	0,96	0,99	0,621	-0,06
P28066	Proteasome subunit alpha type-5	PSA5	0,94	0,99	0,899	-0,09
P28074	Proteasome subunit beta type-5	PSB5	0,95	0,99	0,715	-0,07
P43686	26S proteasome regulatory subunit 6B	PRS6B	1,04	0,99	0,158	0,06
P49720	Proteasome subunit beta type-3	PSB3	0,87	0,99	0,556	-0,19
Q9UNM6	26S proteasome non-ATPase regulatory subunit 13	PSD13	0,94	0,99	0,984	-0,09
R4GNH3	26S proteasome regulatory subunit 6A	R4GNH3	0,90	0,99	0,114	-0,15
O00233	26S proteasome non-ATPase regulatory subunit 9	PSMD9	0,92	0,99	0,783	-0,12
P35998	26S proteasome regulatory subunit 7	PRS7	0,99	0,99	0,000	-0,02
Q15008	26S proteasome non-ATPase regulatory subunit 6	PSMD6	1,03	0,99	0,937	0,04
Q99436	Proteasome subunit beta type-7	PSB7	1,03	0,99	0,242	0,04
P51665	26S proteasome non-ATPase regulatory subunit 7	PSMD7	0,99	1,00	0,809	-0,01
Q99460	26S proteasome non-ATPase regulatory subunit 1	PSMD1	0,99	1,00	0,364	-0,02
P49721	Proteasome subunit beta type-2	PSB2	1,00	1,00	0,546	0,00

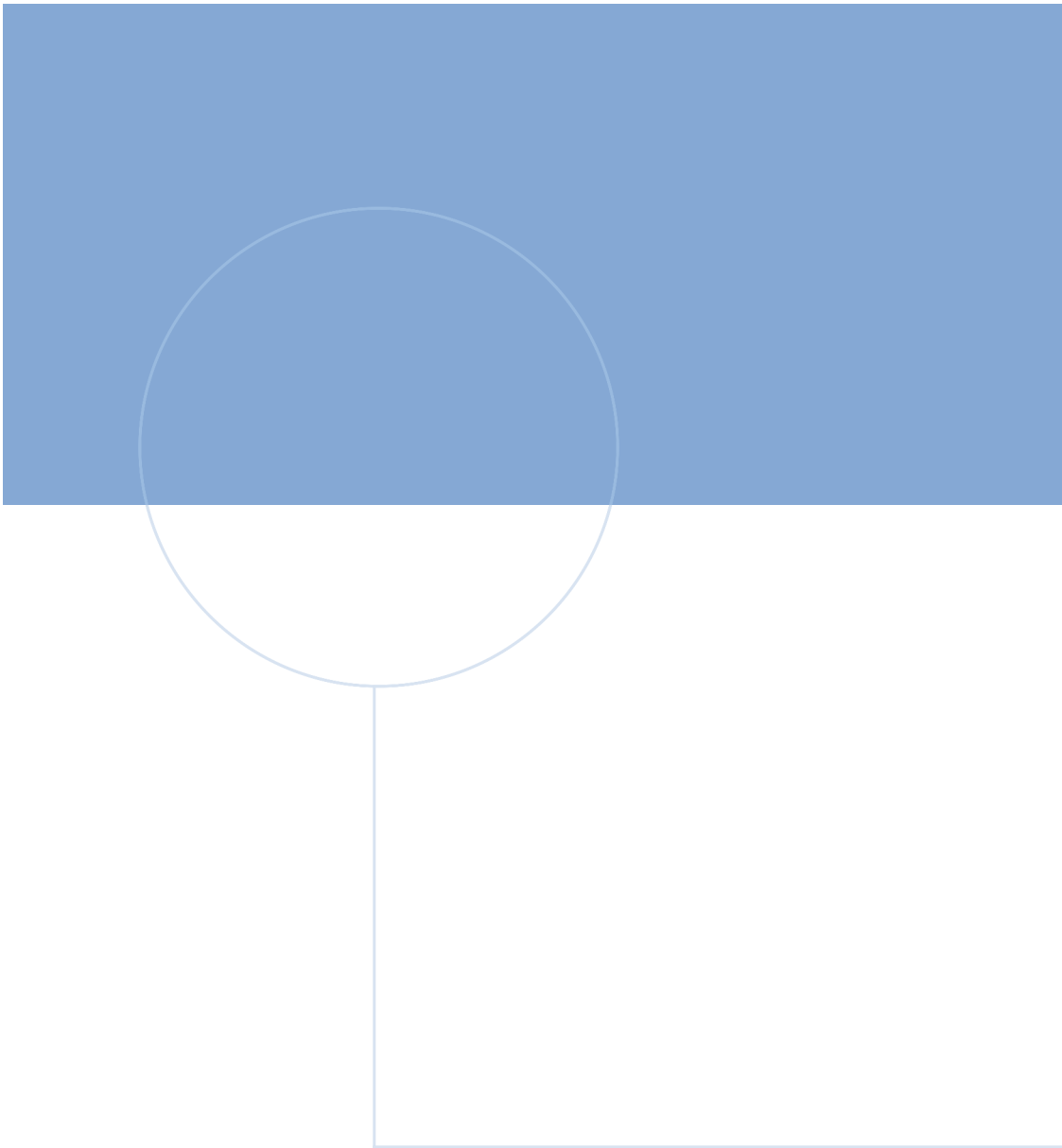

NTNU

Norwegian University of
Science and Technology